Deciphering the gene regulatory network underlying successful neuronal regeneration

Mac Gillavry, H.D.

2010

document version
Publisher's PDF, also known as Version of record

DECIPHERING THE GENE REGULATORY NETWORK UNDERLYING SUCCESSFUL NEURONAL REGENERATION

The work described in this thesis was performed at the department of Molecular and Cellular Neurobiology, Center for Neurogenomics and Cognitive Research (CNCR), VU University, Amsterdam and the laboratory for Neuroregeneration, Netherlands Institute for Neuroscience (NIN), Amsterdam, The Netherlands. This work received financial support from the Dutch Ministry of Economic Affairs (SenterNovem grant ISO52022) and from the Center for Medical Systems Biology (CMSB) in the framework of the Netherlands Genomics Initiative (NGI).

The publication of this thesis was financially supported by:
Vrije Universiteit Amsterdam
Center for Neurogenomics and Cognitive Research
Laboratory for Neuroregeneration, NIN, Amsterdam
J. E. Jurriaanse Stichting

About the cover
Starlings generally move in large flocks, which display complex, synchronous movements. It has been thought that one 'leader' guides the movements of the flock. However, it has now been recognized that individual starlings simply follow the movements of their close neighbors. Thus, the collective behavior of a flock is the result of the movements of individuals. This type of decentralized, self-organizing behavior can also be found in many types of biological (gene) networks, where individual components react in response to their close environment.

photo
Harry van Rhoon http://www.vanrhoon.nl/

print
Ipskamp Drukkers, Enschede

VRIJE UNIVERSITEIT

Deciphering the gene regulatory network underlying successful neuronal regeneration

ACADEMISCH PROEFSCHRIFT

ter verkrijging van de graad Doctor aan
de Vrije Universiteit Amsterdam,
op gezag van de rector magnificus
prof.dr. L.M. Bouter,
in het openbaar te verdedigen
ten overstaan van de promotiecommissie
van de faculteit der Aard- en Levenswetenschappen
op dinsdag 5 oktober 2010 om 13.45 uur
in de aula van de universiteit,
De Boelelaan 1105

door

Harold Duncan Mac Gillavry

geboren te Gouda

promotoren:	prof.dr. A.B. Smit prof.dr. J. Verhaagen
copromotor:	dr. R.E. van Kesteren

Table of contents

Scope and outline of this thesis

Accidents or tumor formation in the spinal cord can lead to damage of the nerve fiber tracts that run through the spinal cord. These types of spinal cord injury (SCI), often result in loss of motor and sensory function below the site of the injury. Depending on the level and severity of the injury, it can lead to paralysis of the arms and legs, bowel and bladder dysfunction, breathing problems, sexual dysfunction and neuropathic pain. Unfortunately, adequate treatments aimed at the regrowth of damaged nerve fibers and the subsequent restoration of motor and sensory functions are not available. Whereas injury to neurons in the central nervous system (CNS) is mostly irreversible, injured neurons in the peripheral nervous system (PNS) have the ability to regenerate their axons over long distances and to restore functional connections. This difference in regenerative potential can be attributed to the environment of the neurons and to the intrinsic capacity of a neuron to regrow its axon. To successfully regenerate axons over long distances, coordinated changes in gene expression, protein synthesis, post-translational modification and protein localization are required.

Gene expression is controlled by transcription factors (TF), which can physically bind *cis*-regulatory DNA elements in gene promoters or enhancer regions and activate or repress transcription. The complex of interactions between TFs and their target genes is referred to as a transcriptional regulatory network. Knowledge of the transcriptional regulatory network or modules therein, provides a systematic insight into the principles that govern gene expression. In order to understand transcriptional regulatory networks, or the smaller building blocks of regulatory modules, it is of critical importance to identify the key molecular components and their mutual interrelationships. In **Chapter 1**, I will discuss the strategies that are used to unravel transcriptional networks, and how these approaches can be applied to study the transcriptional control of axon regeneration. First, I will describe the general principles of the regulation of gene expression. Subsequently, I will discuss the emerging molecular and computational methods that are instrumental to define the interactions between TFs and their target genes. Finally, I will discuss what we know about neuronal regeneration as a starting point to decipher the transcriptional regulatory networks that govern successful neuronal regeneration.

In my thesis project I focus on the intrinsic ability of neurons to regenerate their axons. Specifically, I use the different approaches, discussed in this chapter, to start to unravel the transcriptional regulatory network that underlies successful axon regeneration. I have undertaken a systematic approach in which I combined gene expression analysis, high-throughput functional screening, computational analysis and TF-target gene interaction analysis to get a complete view on which TFs regulate regenerative neurite outgrowth and how these TFs interact in transcriptional regulatory modules. **Chapter 2** describes how we used gene expression data to select a set of differentially regulated TFs that was then functionally tested using high-throughput cellular screening meth-

ods. This chapter also describes experiments on one of the newly identified outgrowth-modulating TFs, namely NFIL3 (nuclear factor, interleukin 3 regulated). Paradoxically, we find a significant upregulation of NFIL3 in injured neurons during successful regeneration, while it repressed neurite outgrowth. This chapter describes experiments that show that NFIL3 acts as a feed-forward repressor of the CREB-induced transcriptional response. This is the first example of a transcriptional module that regulates neuronal regeneration. In **Chapter 3** we describe the design and *in vivo* application of a dominant-negative form of NFIL3 in an attempt to enhance neuronal regeneration. Specifically, we use an adeno-associated viral vector to transduce adult rat dorsal root ganglion (DRG) neurons with dominant-negative NFIL3 and evaluate the effect on sciatic nerve regeneration after nerve crush. In **Chapter 4** we applied ChIP-chip technology to identify direct NFIL3 and CREB target genes to study the NFIL3/CREB transcriptional feed-forward loop in more detail. We identified approximately 500 NFIL3 targets genes, a subset of which is regulated by cAMP and CREB. **Chapter 5** describes the development of a new computational method, LLM3D (log-linear modeling of 3D contingency tables) that identifies overrepresented transcription factor binding sites (TFBSs) in functional groups of genes. We applied this method to genome-wide, temporal gene expression data on rat DRGs after either sciatic nerve or dorsal root crush, confirming and expanding our previous gene expression study. LLM3D predicted the involvement of the TF PPARγ (peroxisome proliferator activator receptor γ), which we experimentally confirm in *in vitro* models of neurite outgrowth. Finally, **Chapter 6** gives an overview of the literature on regeneration-associated genes and discusses how new developments and the results in this thesis will aid to unravel the regeneration-associated transcriptional network.

Chapter 1

General introduction: reconstructing the transcriptional regulatory network that underlies successful neuronal regeneration

Regulation of gene expression: a brief introduction

In eukaryotes, genes are transcribed into RNA due to the concerted action of hundreds of proteins, termed transcription factors (TFs). Gene transcription is initiated at the core promoter upstream of a gene's transcription start site (TSS) (Figure 1). The core promoter usually consists of a short DNA sequence, called the TATA-box, which is recognized by the TATA-box binding protein (TBP). TBP itself is a component of the general transcription factor (GTF) TFIID. After TFIID binding, the other GTFs (TFIIA, TFIIB, TFIIE, TFIIF, TFIIH) and RNA polymerase II are assembled into the so-called pre-initiation complex (PIC). Although the formation of this complex is sufficient to drive a very low, or basal level of transcription, the rate of transcription is regulated by TFs that bind specific *cis*-regulatory DNA elements, or transcription factor binding sites (TFBSs) in proximal gene promoters or in further upstream enhancer regions. TFs stimulate or repress gene transcription by influencing the recruitment, formation or activity of the PIC. Some TFs can directly interact with the PIC, but most TFs require co-regulator proteins that have no DNA sequence-specificity but bridge the regulatory TF and the basal transcription machinery. Another type of co-regulators affects the accessibility of promoter DNA sequences, either by covalently modifying chromatin (chromatin modifiers), or by changing nucleosome position (chromatin remodellers). Both chromatin modifiers and remodellers change the chromatin architecture and can either expose *cis*-regulatory sequences allowing TF binding, or make promoter regions less accessible for TFs. Most steps in gene regulation, from the assembly of the core complex to the recruitment of regulatory TFs, are rate limiting and thus points of control that can be used to regulate gene transcription in response to developmental or environmental signals.

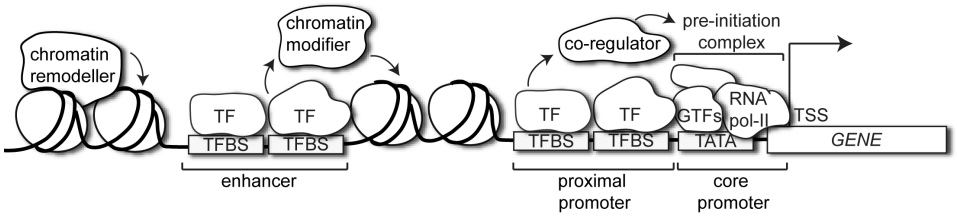

Figure 1. Transcriptional regulation.
Eukaryotic gene transcription is initiated by the formation of the so-called pre-initiation complex (PIC) at the core promoter or TATA box. The PIC consists of general transcription factors (GTFs) and the RNA polymerase II holoenzyme. Binding of TFs to the proximal promoter region of a gene is mediated by specific DNA sequences, or transcription factor binding sites (TFBSs). Bound TFs can then either directly, or indirectly via co-regulators, influence the activity of the PIC. TFs are also recruited to more upstream promoter regions, or enhancers. Finally, chromatin modifiers and remodellers can regulate gene transcription by modulating chromatin structure and architecture.

Transcriptional regulatory networks

The combinatorial interaction of *cis*-regulatory sequences and the regulatory proteins that bind to them dictate the temporal and spatial expression pattern of a gene. The interactions of TFs and their target genes can be described and modeled in so-called transcriptional regulatory networks, in which the regulatory TFs and target genes form the nodes, which are connected by edges describing the interaction of the TF with its target genes (Figure 2A). Recent developments in molecular biology and bioinformatics have made it possible to identify the relevant nodes in the network and to predict and verify regulator-target interactions, or edges, in the network. Together, this information enables the accurate reconstruction of transcriptional regulatory networks. High-throughput methods, including microarray technology, chromatin immunoprecipitation (ChIP) and RNA interference combined with high-content cellular screening make it possible to systematically identify regulators and cognate target genes. This integrated analysis yields large data sets, and their analysis and predictive value heavily depend on computational methods. Figure 2B shows a schematic overview of how a combination of computational and biological methods allows the identification of key TFs and their cognate target genes in a transcriptional regulatory network that controls a biological

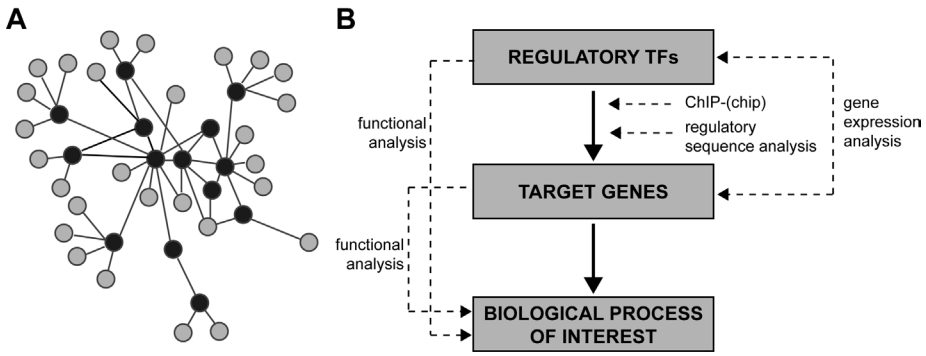

Figure 2. Constructing transcriptional regulatory networks.

(A) Transcriptional regulatory networks describe the interaction between TFs and target genes. The nodes are formed by the TFs (dark grey circles) and target genes (light grey circles) and the edges describe their connections. An edge can thus represent an interaction between one or more TFs and/or interactions between a TF and a gene. (B) The construction of transcriptional regulatory networks requires different complementary methods. First, the nodes that form the transcriptional network are identified by gene expression analysis. Genes identified by gene expression analysis include target genes, but can also include regulated TFs. The functions of these genes in the process of interest are tested by functional analysis using loss-of-function or gain-of-function biological assays. The interactions between TFs and their target genes can then be predicted using computational regulatory sequence analysis algorithms. TF-target gene interactions are biologically tested using ChIP(-chip) analysis. Detailed descriptions of the different techniques can be found in the text.

process of interest. In the following sections I will describe how this workflow is applied to contribute to the construction of transcriptional regulatory networks.

Reconstructing gene regulatory networks: molecular and computational methods to fill in the nodes and edges

Identifying the nodes: gene expression profiling

Gene expression profiling has emerged as a powerful tool to identify genes involved in specified biological processes. The development of microarray technology over the past ten years has made it possible to measure the expression of thousands of genes simultaneously. Although sequence based methods, such as serial analysis of gene expression (SAGE) and deep sequencing, may be more accurate, the general availability, high quality and relatively low costs make commercial microarrays still the most frequently used technique to profile changes in gene expression at large scale.

Traditional gene expression arrays contain thousands of spots (or features), containing short DNA oligonucleotides corresponding to unique mRNA sequences. An RNA sample is fluorescently labeled, and hybridized to an array. The array is then scanned and the probe signal intensities extracted and normalized to remove systematic bias, resulting in a reliable measure for the expression of the corresponding genes. The ultimate goal of most microarray experiments is the identification of sets of genes that are differentially expressed between two experimental conditions. This is a statistical challenge considering the large number of data points and the relative small number of regulated genes in an average microarray experiment. Popular statistical packages assessing differentially regulated genes include Significance Analysis of Microarrays (SAM) (Tusher *et al.*, 2001) and empirical Bayes methods (Smyth, 2004). These methods often use a variation of the t-test and calculate a *p*-value for significance. This p-value can be used to select significantly regulated genes, but as a consequence of testing thousands of genes simultaneously, it is more common to control the false discovery rate, rather than the false positive rate (for a more detailed discussion on controlling false discovery rates in genomics see (Storey and Tibshirani, 2003)). Most of these statistical tests deal with one or more independent samples, but more recently, methods have been developed that consider dynamic time-course gene expression data. The statistical approaches developed by Tai and Speed (2006) and Angelini *et al.* (2007) incorporate the dynamic nature of gene expression. These methods rank genes according to the significance based on replicate variances, but also use the correlation in gene expression among the different time-points and moderation across all the genes in the analysis.

Since the first report on its use in 1995 (Schena *et al.*, 1995), microarray technology has allowed many researchers in different fields to monitor gene expression in an unbiased manner. However, it is not easy to interpret the resulting lists of up- and

down-regulated genes in the context of the underlying biological processes. Initially, follow-up studies often focused on in-depth functional analysis of only a few differentially expressed genes. However, it is now recognized that changes in the expression of individual genes are highly coordinated and cannot be regarded as independent events. Novel approaches are moving from single-gene to network-analysis, for instance by grouping co-regulated genes into functional classes or by assigning them to molecular pathways.

The Gene Ontology project (GO, http://www.geneontology.org/) was the first attempt to annotate genes in different biologically meaningful, functional categories. Genes are grouped in hierarchical classes that fall in one of the three main categories: "biological process", "molecular function" and "cellular component". Such a genome-wide classification allows researchers to analyze microarray data in terms of co-regulated functional gene groups instead of individual genes. Many applications have been developed to statistically test overrepresented GO classes in lists of (co-) regulated genes, including DAVID (Huang da *et al.*, 2007), Babelomics (Al-Shahrour *et al.*, 2008) and TopGO (Alexa *et al.*, 2006). Another way of interpreting microarray data is pathway analysis (Werner, 2008). This approach is based on the currently existing knowledge of molecular pathways in the literature. Several web-based applications enable researchers to identify specific pathways that are over-represented in their list of regulated genes. Most of these types of analyses are based on the curated KEGG database (Kyoto Encyclopedia of Genes and Genomes; http://www.genome.jp/kegg/).

Identifying differentially regulated, functional groups of genes is a first step in constructing the transcriptional regulatory network as it identifies and groups the nodes that make up the network. However, additional information on TF-gene interactions, the edges in the network, is required to link these nodes.

Identifying the edges: connecting nodes via chromatin immunoprecipitation

A key step in deciphering transcriptional regulatory networks is identifying the genomic locations bound by transcriptional regulators under specific physiological conditions. Chromatin immunoprecipitation (ChIP) is a method to determine whether TFs bind to specific regions in the genome or whether histone modifications occur at specific regions in the genome. Using a mild, reversible cross-linking reagent such as formaldehyde, the protein-DNA interactions within the chromatin of living cells or tissues can be fixed. Next, the chromatin is extracted and sheared in smaller fragments (usually 0.1–1kb in length). Using an antibody specifically recognizing the protein of interest, protein-DNA complexes are immunoprecipitated. The co-immunoprecipitated DNA fragments are then isolated and can be analyzed by PCR using primers specific for the genomic regions one expects to be bound by the protein of interest. Alternatively, the DNA fragments can be amplified and hybridized to DNA microarrays containing probes that cover all gene promoters (or even the entire genome) in order to identify all genomic binding sites

of the protein of interest. This latter technique is referred to as ChIP-on-chip or ChIP-chip. Recently, techniques were developed to sequence protein-bound DNA fragments in a high-throughput manner (ChIP-Seq), providing even better genome-wide coverage than ChIP-chip approaches.

Using ChIP one can study true *in vivo* protein-DNA interactions, which makes it a powerful method compared with classical *in vitro* techniques such as EMSA (Electrophoretic Mobility Shift Assay) and SELEX (Systematic Evolution of Ligands by Exponential Enrichment). The main disadvantage of ChIP however is the restricted availability of highly specific and efficient "ChIP-grade" antibodies. The use of epitope-tagged proteins circumvents this problem, but overexpression of tagged TFs may induce non-physiological binding. Ultimately, the *in vivo* knock-in of tagged TFs would provide the ideal starting point for the systematic identification of TF-bound DNA regions (Zhang *et al.*, 2008; Wang, 2009). Also, the high amount of starting chromatin required for ChIP, and the duration of the total experiment, limits the use of ChIP. Recent reports describe that one can reduce the amount of starting material from $>10^7$ cells to only 103 by including carrier chromatin (O'Neill *et al.*, 2006) and the total protocol time can be reduced to only one day when multiple steps are combined (Flanagin *et al.*, 2008).

The combination of ChIP with array technology (ChIP-chip) has become a widely used technique. The ChIP and total input DNA samples are amplified; usually using a linker-mediated PCR amplification step and equal amounts of both samples are labeled with fluorescent dyes. Samples are then hybridized to DNA oligonucleotide arrays. Comparison of the two labels, the ChIP/input ratio reveals target sequences with relative enrichment of the ChIP sample over the total input sample. As for gene expression arrays, discerning true enrichment from noise in ChIP-chip data is a statistical challenge. Most ChIP-chip arrays are designed in such a way that probes are tiled along chromosomal stretches. Such tiling arrays generally cover non-repetitive promoter regions only or are limited to parts of the genome (e.g., chromosome-specific arrays). As a consequence of the random DNA shearing, multiple overlapping sequences are enriched in the ChIP sample, recognizing several adjacent tiled probes on the array. This results in a peak-shaped probe response around the actual binding site. This unique feature of ChIP-chip data, referred to as the "neighbor effect", is often used to discern true binding from background noise (Buck and Lieb, 2004). Commonly, a moving average is calculated within a fixed window of probes or a fixed genomic distance, which removes the noise in the data and increases the detection power. This moving average is then tested for significance and binding sites are then mostly defined by a minimum number of adjacent probes exceeding a certain threshold for significance. Actually, multiple approaches can now be found in literature describing different normalization methods and peak-detection algorithms for ChIP-chip analysis (Buck *et al.*, 2005; Carroll *et al.*, 2005; Gibbons *et al.*, 2005; Toedling *et al.*, 2007).

Instead of studying TF-binding at individual promoters, ChIP-chip enables

the study of genome-wide TF-binding. ChIP-chip studies accurately map genome-wide binding of TFs in single-cell model organisms such as yeast (Lee *et al.*, 2002), but are now also used to map cell type-specific TF-DNA interactions (Boyer *et al.*, 2005; Scacheri *et al.*, 2006) and histone modifications (Rada-Iglesias *et al.*, 2008; Heintzman *et al.*, 2009) in mammalian cells and tissues (O'Neill *et al.*, 2006; Reed *et al.*, 2008). In the future, ChIP followed by high-throughput (deep-) sequencing (ChIP-Seq) will give higher resolution and less noise compared with ChIP-chip and the (theoretically) unbiased total genome coverage will make it an indispensable tool to study genome-wide protein-DNA interactions (Park, 2009).

Finding new node connections *in silico*: computational prediction of transcription factor binding sites

Many TFs act by directly interacting with genomic DNA in a sequence-dependent manner. The DNA sequence bound by a certain TF is referred to as transcription factor binding site (TFBS), a *cis*-regulatory sequence, or response element. Generally, TFBS consensus sequences are defined as short sequences ranging from 6 to 32bp in length in which the contributing bases often have unequal weight (Fogel *et al.*, 2005). Therefore, identification of TF binding sites in a given genome is not trivial, which is partly solved by deriving the position weight matrix (PWM) of a TFBS. A PWM holds all positional base frequencies derived from published, empirical identified TFBSs, and enables statistical calculation of the match of every base position of a TFBS with a matched sequence (Harr *et al.*, 1983; Stormo, 2000). Databases such as JASPAR (http://jaspar.genereg.net) and TRANSFAC contain hundreds of such TFBS PWMs. This has been the basis of the development of numerous software algorithms that predict the occurrence of TFBSs in given sequences (for a comprehensive review see Wasserman and Sandelin, 2004).

Apart from its sequence, the functionality of a TFBS is determined by many other factors, such as chromatin structure and the accessibility and availability of other co-regulators. In fact, computational predictions of TFBSs result in lists of predictions of which presumably only a small fraction represents physiological relevant TFBSs. On the other hand, many true TFBSs may be missed because they hold unknown base variations, and de novo binding site predictions are not possible. Thus, although computational methods can identify the occurrence of known TFBSs in the promoter regions of genes and enables researchers to predict possible target genes for a given TF, an important issue is to add confidence and relevance to these predictions by other means. Due to the evolutionary constraint on regulatory networks it is expected that functional TFBSs are evolutionary conserved, and therefore integrating the TFBS sequence conservation data among related species might add confidence to TFBS predictions. With the availability of completely sequenced eukaryotic genomes it is possible to analyze pair-wise sequence alignments and identify conserved regulatory segments. Using such an approach, it was shown that indeed there exists a strong preservation of TFBSs among

closely related mammalian genomes, however this is not true for all TFBSs, and TFBSs tend to diverge rapidly when considering more distantly related species (Stepanova *et al.*, 2005; Xie *et al.*, 2005).

Another important consideration is the definition of a gene's regulatory or promoter region. Generally, TFBSs are enriched in a 2 to 10kb region encompassing the transcription start site (TSS) of genes. However, the position of a gene's TSS is with present knowledge not always exactly determined, and many genes have multiple TSSs. Moreover, functional binding of TFs has also been reported in intronic, exonic and 3' flanking sequences of genes (Impey *et al.*, 2004). Information from deep sequencing and ChIP-chip studies will help to better map alternative TSSs and promoter and enhancer regions in the genome.

Another way to achieve more accurate TFBS predictions is to consider groups of genes instead of individual genes. Genes that share a similar expression pattern, e.g. genes that always respond together under different physiological conditions, are likely to be regulated by the same TFs and are expected to share a common set of TFBSs. By comparing the occurrence of TFBSs in a set of target genes to a set of background genes, statistically overrepresented TFBSs can be identified. In this way, TFBSs that are functional in a certain process and control the expression of a group of genes, can be identified without the need for that TFBS to be reliably detectable in every single gene in that group (for examples see Elkon *et al.*, 2003; Segal *et al.*, 2003).

The above-discussed approaches all rely on prior knowledge of the TFBS, but they do not allow discovery of new motifs. Recently, several methods were developed that aim at discovering new motifs (discussed in ref Tompa *et al.*, 2005). Instead of searching for known motifs, these algorithms scan sequences for recurring motifs that were previously unidentified. Eventually, combining different types of information, such as regulatory motifs, gene expression, TF binding data, functional annotation, literature mining, etc., will lead to more and better transcriptional regulatory models with higher predictive value (ref Beer and Tavazoie, 2004 and chapter 5 of this thesis).

Basic properties of transcriptional regulatory networks; lessons from simple model systems

The first complete transcriptional regulatory networks were described in simple pro- and eukaryotic model systems, including *Escherichia coli* (Huerta *et al.*, 1998; Thieffry *et al.*, 1998) and *Saccharomyces cerevisiae* (Lee *et al.*, 2002). Interestingly, the transcriptional regulatory networks in these simple model organisms share a number of basic principles. Transcriptional regulatory networks are "scale-free", meaning that the majority of TFs is connected to only a few target genes, while only a small number of TFs, termed "regulatory hubs", show many more connections, regulating many target genes. This property of transcriptional regulatory networks makes them hierarchical, enabling the rapid on- and off-switching of sub-networks, which makes them robust and less prone to

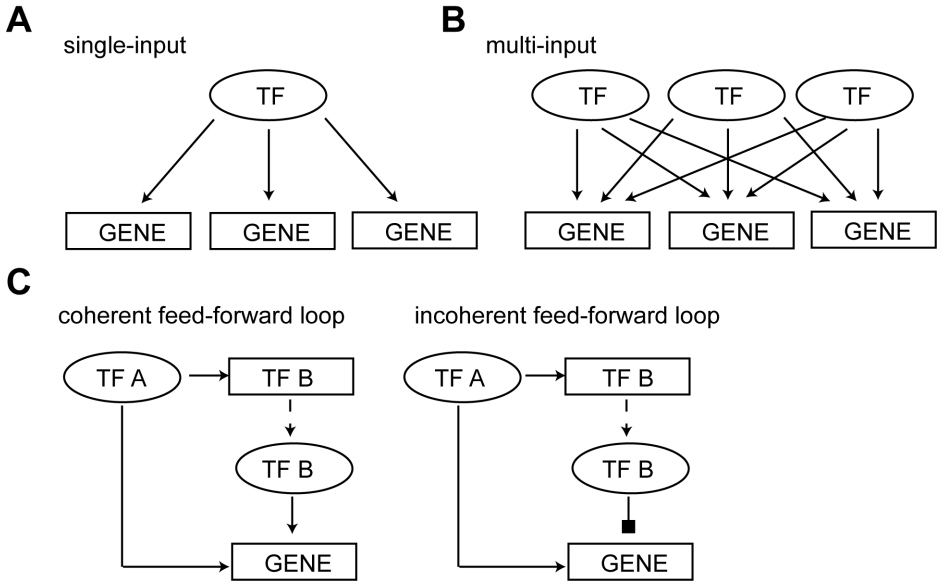

Figure 3. Network motifs frequently occurring in transcriptional regulatory networks. Single-input motif consists of one TF regulating several genes (A), and the multi-input motif, consisting of multiple TFs regulating the same set of genes (B). (C) The feed-forward loop consists of a TF, which regulates the expression of a gene directly and indirectly via another TF at the same time. The loop is termed coherent if both TFs have the same regulatory effect on the gene or incoherent if the TFs have opposite effects on the gene's expression. Note, that the feed-forward loops depicted here, are the most frequently occurring type 1 loops, in which TF A has a positive effect on both TF B and the gene.

perturbation. At a lower level, the modular nature of the network becomes apparent. TF-target interactions are organized in recurring functional units, termed "network motifs". Network motifs occur more often than by chance, and in fact recur in other types of information processing networks as well (Lee *et al.*, 2002; Milo *et al.*, 2002; Shen-Orr *et al.*, 2002). The relative simple "single-input motif" allows the coordinated expression of a group of genes in response to a single regulator (Figure 3A). In this way, one regulator can potentially activate an entire biosynthetic pathway. In contrast, the "multi-input motif" enables the regulation of groups of genes in response to a variety of inputs (Figure 3B). In yeast for instance, the activation of ribosomal protein genes can be regulated by several different TFs, to guarantee that this important group of genes can be regulated under different metabolic conditions, and does not rely on a single regulatory TF (Lee *et al.*, 2002). A more complex network motif is the "feed-forward loop" (Mangan and Alon, 2003; Alon, 2007). This motif consists of a TF that controls a second TF, while both TFs control the same target genes (Figure 3C). This loop is called "coherent" when both TFs have the same regulatory effect on the gene or "incoherent", when the two TFs have opposing effects on the target gene. The three different interactions (TF A to target, TF B to target, and TF A to TF B) all can have different signs, and thus, coherent and incoherent

feed-forward loops can be subdivided in four subtypes. It is shown however, that type-1 coherent loops (all three connections are positive) and type-1 incoherent feed-forward loops (only the connection from TF B to target is negative) appear more frequently in transcriptional networks than the other ones (Mangan and Alon, 2003). Type-1 coherent feed-forward loops are important to ensure that target genes are only activated in response to a persistent input signal (Mangan *et al.*, 2003). The requirement of two TFs to be activated generates a delay in the signal, and filters out spontaneous noise. Type-1 incoherent feed-forward loops on the other hand, generate pulses in gene expression and accelerate the activation of target genes, even though higher levels of input signal are required to induce target gene activation (Mangan *et al.*, 2006).

Most experimental evidence for the role of individual network motifs comes from experiments in simple, unicellular model organisms. However, similar network motifs are now also being discovered in more complex model organisms (Blais *et al.*, 2005; Boyer *et al.*, 2005; Odom *et al.*, 2006). An interesting finding is for instance that the oncogenic TF c-Myc transcriptionally activates the E2F1 gene and meanwhile induces the expression of two miRNAs that downregulate the protein levels of E2F1 (Leone *et al.*, 1997; O'Donnell *et al.*, 2005). This incoherent feed-forward loop controls the pulse-like expression of E2F1 upon c-Myc stimulation. Although it thus seems that transcriptional networks in more complex organisms share the same degree of structural simplicity with simple organisms, it is not said that the forces that drive evolutionary change in network motifs can be compared with those that drive evolutionary changes in genes. It is found for instance that many genes can acquire completely different modes of regulation, even in closely related organisms (Madan Babu *et al.*, 2006). Part of the interspecies variation in gene regulation is proposed to arise from fast diverging *cis*-acting regulatory sequences, which are relatively short and in which a single base mutation may already result in loss-of-function (Moses *et al.*, 2006; Jeong *et al.*, 2008). On the other hand it seems that TF genes diverge faster than other classes of genes in both pro- and eukaryotes, resulting in faster adaptation in transcriptional network properties than in the genes themselves (Madan Babu *et al.*, 2006; Jovelin, 2009). It will thus be important to better characterize more complex, eukaryotic transcriptional networks, which will undoubtedly reveal new network motifs with new gene regulatory functions.

Unraveling the transcriptional network regulating successful neuronal regeneration

In higher vertebrates an axonal injury to neurons in the central nervous system (CNS) is mostly irreversible, whereas injured neurons in the peripheral nervous system (PNS) have the ability to regenerate their axons over long distances and to restore functional connections. Research on neuronal regeneration has since long studied the environmental factors that inhibit CNS regeneration. Therefore the cellular changes at the site of injury are now quite well understood and the identification of several inhibitory factors, including Nogo and myelin-associated glycoprotein, chondroitin sulfate proteoglycans and repulsive axon-guidance factors has advanced our knowledge on the extrinsic molecular mechanism that underlie regenerative failure (Xie and Zheng, 2008). Current therapeutic strategies are aimed at neutralizing these negative extracellular signals, however, adequate treatments that promote the regeneration of injured nerve fibers and the subsequent restoration of functional synaptic contacts are as yet not available. Over the past decades, it has become increasingly clear that successful neuronal regeneration also depends on the neuron's intrinsic ability to respond to an axonal injury and regulate the expression of growth-promoting genes. Pioneering work of Skene and Willard and of Benowitz and colleagues has led to the finding that the expression of the growth cone protein GAP-43 (growth-associated protein-43) correlates with successful regeneration (Skene and Willard, 1981b, a). GAP-43 is expressed at high levels in developing neurons during periods of axon elongation, and is re-expressed in mature neurons after peripheral, but not central nerve lesion. Importantly, transgenic overexpression of GAP-43 facilitates peripheral nerve regeneration (Aigner *et al.*, 1995), but fails to induce long-range central nerve regeneration (Aigner *et al.*, 1995; Buffo *et al.*, 1997; Neumann and Woolf, 1999; Mason *et al.*, 2000). A study on double-transgenic mice overexpressing GAP-43 and CAP-23 demonstrated enhanced regeneration of sensory axons into the spinal cord (Bomze *et al.*, 2001). Together, these studies show that regeneration-associated genes (RAGs), such as GAP-43 and CAP-23 can have the ability to promote regeneration and introducing RAGs in damaged CNS neurons might enhance their regenerative capacity. In my thesis, I focus on the intrinsic ability of neurons to express a growth-promoting gene expression program that promotes axonal regeneration and I applied the above-described experimental and computational approaches to study the neuron-intrinsic transcriptional regulatory network that underlies successful axon regeneration.

The dorsal root ganglion nerve injury model

The dorsal root ganglion (DRG) is an attractive model system to decipher regeneration-associated transcriptional regulatory networks. The DRG contains sensory neurons that extend one axon via the spinal nerve into the periphery, receiving sensory inputs including heat and pain, and another axon via the dorsal root into the spinal cord, transmitting these sensory signals to the CNS (Figure 4). A crush injury to the peripheral branches

of the DRG results in vigorous and successful axon regeneration and complete functional recovery after two months in the rat. In contrast, following a comparable injury to the dorsal root fibers, axon regeneration is significantly impaired and axon extension stalls at the PNS-CNS boundary (the dorsal root entry zone). Interestingly, when a so-called preconditioning crush to the peripheral branches precedes damage to the central branches, the regenerative response of the fibers in the dorsal root is enhanced and some fibers are actually able to regrow into the spinal cord (Richardson and Issa, 1984; Chong *et al.*, 1999; Neumann and Woolf, 1999). This observation strongly supports the idea that DRG neurons have the intrinsic capacity to activate a gene program that supports axon regeneration. Upregulation of classical RAGs (GAP-43, CAP-23) and several TFs, including CREB, ATF3, c-JUN, KLF4 and SMAD1, are reported to modulate neuronal regeneration (Schreyer and Skene, 1993; Gao *et al.*, 2004; Raivich *et al.*, 2004; Seijffers *et al.*, 2007; Moore *et al.*, 2009; Zou *et al.*, 2009), and recent gene expression profiling studies in regenerating DRG neurons have yielded a more complete insight in the complex gene expression program that underlies neuronal regeneration (Costigan *et al.*, 2002; Xiao *et al.*, 2002; Stam *et al.*, 2007).

Peripheral nerve injury and the initiation of a regeneration-associated gene-expression program

Peripheral axonal injury induces a cell body response that includes a gene expression program that mediates the regenerative response of the neuron. The signals initiating and regulating the injury-induced gene expression response are largely unknown. Damage to an axon leads to an immediate influx of extracellular calcium and sodium ions that trigger a depolarization and a burst of high-frequency action potentials (Berdan *et al.*, 1993). Locally, at the lesion site, this activates calcium-dependent processes, such as proteolytic cleavage, cytoskeleton remodeling and local protein synthesis, which mediate the formation of a growth cone (Spira *et al.*, 2001; Zheng *et al.*, 2001). The rapid arrival of the electrical signals at the cell body leads to an increase in somatic calcium and cAMP levels. These second messengers subsequently activate diverse kinases, including CaM kinase II and IV, protein kinase A (PKA) and subsequent TFs. Although these early signals can thus induce a transcriptional response, they are probably not sufficient to maintain it. A second phase of retrogradely transported injury signals (Ambron and Walters, 1996) contain "positive" factors that are actively involved in injury signaling, but also includes "negative" signals, i.e. the lack of homeostatic factors that originate from the target tissue and that are suggested to repress regeneration-associated gene expression in the intact situation (Wu *et al.*, 1993). Growth-promoting signals arise from proteins that are transported from the lesion site to the cell body and are imported into the nucleus (Zhang and Ambron, 2000). Fainzilber and colleagues have identified a signal particle that is linked to the retrograde transport protein dynein via vimentin. This particle contains importin β1, a protein involved in nuclear translocation, as well as the

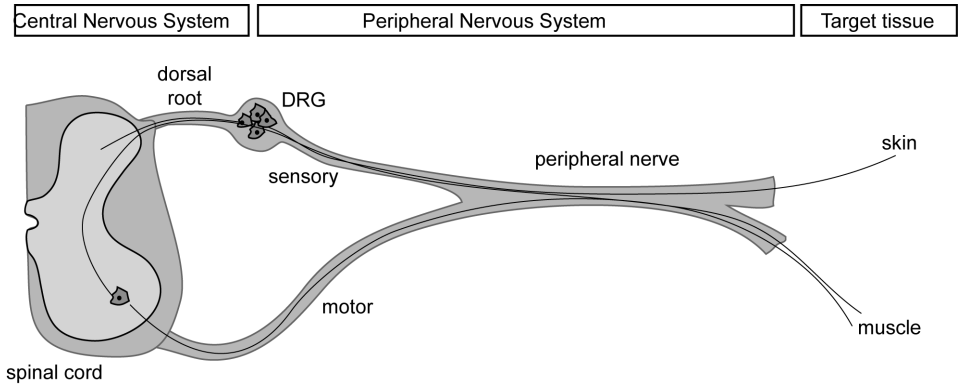

Figure 4. Schematic representation of the dorsal root ganglion (DRG).
The DRG contains sensory neurons that extend a bifurcated axon projecting both into the peripheral nervous system to target tissues such as skin and muscle, and, via the dorsal root, into the central nervous system.

activated MAP kinases Erk1 and Erk2 (Hanz *et al.*, 2003; Perlson *et al.*, 2005). Blocking nuclear import of this signaling particle after an injury significantly reduces the regenerative response. It is expected that other proteins that contain a nuclear localization signal (NLS) and bind to this complex via importin β1 may also be transported, but these have remained unidentified so far. Other studies reported the retrograde transport of c-Jun N-terminal kinase and protein kinase G (Lindwall and Kanje, 2005; Sung *et al.*, 2006).

Apart from these neuronal signaling pathways, signals secreted by surrounding cells further stimulate the regenerative response. A number of different growth factors and cytokines, including fibroblast growth factor (FGF), brain derived neurotrophic factor (BDNF), interleukin-6 (IL-6) and ciliary neurotrophic factor (CNTF) are secreted by Schwann cells or immune cells in the denervated nerve. These factors influence neuronal transcription by acting on their cognate transmembrane receptors and initiating signal transduction pathways within the injured neuron.

Transcription factors involved in neuronal regeneration

Signaling events at the site of injury result in the activation or transcriptional regulation of transcription factors, which induce a regeneration promoting gene expression program. Numerous studies by Filbin and coworkers have shown the importance of cAMP in successful neuronal regeneration. The first observation was that a peripheral nerve lesion elevates cAMP levels in the DRG within 24 hours, promoting neurite growth even when plated on myelin (Cai *et al.,* 1999; Qiu *et al.,* 2002). It was then also demonstrated that injection of cAMP analogues directly into the DRG mimic the conditioning lesion effect and cause injured axons to regenerate into the spinal cord (Neumann *et al.,* 2002; Qiu *et al.,* 2002). The ability of cAMP to overcome myelin inhibition depends on PKA

and CREB activity (Cai *et al.,* 1999; Qiu *et al.,* 2002; Gao *et al.,* 2004). An important downstream effector of the cAMP-CREB pathway is Arginase I, an enzyme that synthesizes polyamines, which can overcome myelin inhibition (Cai *et al.,* 2002; Gao *et al.,* 2004). Microarray analysis on cAMP treated DRGs also pointed to other downstream target genes, including NPY, CREM, VGF and IL-6 (Cao *et al.,* 2006). Interestingly, elevated levels of IL-6 are shown to mediate the regenerative response of DRG neurons (Cafferty *et al.,* 2004; Cao *et al.,* 2006). IL-6 acts on the IL-6/gp130 receptor and activates the Janus kinase 2 (JAK2)/STAT pathway. STAT3 is rapidly phosphorylated after sciatic nerve crush (Lee *et al.,* 2004) and preventing STAT3 phosphorylation by blocking JAK2, inhibits regeneration of dorsal root fibers induced by a conditioning-lesion (Qiu *et al.,* 2005). Conversely, activating STAT3 promotes neurite outgrowth (Miao *et al.,* 2006). In parallel, a peripheral nerve injury also activates the TGFβ/BMP signaling pathway that leads to the phosphorylation and activation of the TF SMAD1 (Zou *et al.,* 2009). Knockdown of SMAD1 decreases *in vitro* DRG neurite outgrowth and intraganglionic injection of BMP-2 or -4 activates SMAD1 and enhances the axonal growth capacity.

Many studies have shown that retinoic acid signaling is important for the development and repair of the nervous system (Mey, 2006; Maden, 2007). Retinoic acid is a vitamin A derivative that activates transcription through the nuclear retinoic acid receptors (RARs). Specifically the RARβ2 isoform is expressed in neurons that can regenerate and seems to mediate the beneficial effects of retinoic acid on neuronal outgrowth (Corcoran *et al.,* 2000; Corcoran *et al.,* 2002; So *et al.,* 2006). Furthermore, RARβ2 is not only shown to be required for peripheral nerve regeneration (So *et al.,* 2006), overexpression is already sufficient to induce nerve regeneration in spinal cord lesion models (Wong *et al.,* 2006; Yip *et al.,* 2006).

The activating transcription factor-3 (ATF3) is rapidly and strongly upregulated in the DRG after peripheral, but not central axonal injury, and overexpression of ATF3 results in increased neurite outgrowth of DRG neurons in vitro (Tsujino *et al.,* 2000; Seijffers *et al.,* 2006). Also, ATF3 transgenic mice show an increased ability to regenerate damaged peripheral nerves (Seijffers *et al.,* 2007). Although these findings demonstrate that ATF3 has a strong growth-promoting capacity, ATF3 overexpression is not sufficient to overcome the neurite outgrowth inhibition by myelin in vitro, nor did it induce axon regeneration of the dorsal root in the CNS (Seijffers *et al.,* 2007). Similarly, the related TF c-JUN is strongly induced after nerve damage (Herdegen and Leah, 1998; Kenney and Kocsis, 1998). Conditional neuronal c-JUN knockout in mice does not result in apparent developmental changes, but the regenerative capacity of the injured facial nerve is significantly impaired (Raivich *et al.,* 2004). Target genes that were implicated in the c-JUN-mediated gene response are the axon growth promoting genes *Cd44, galanin* and *alpha7beta1 integri*n.

The injury-induced TF Sox11, SRY-box containing gene 11, is a member of the group C HMG (high-mobility group) TFs. All Sox factors seem to have critical roles

in different tissues and phases in development and Sox4 and Sox11 are shown to be required for neuronal maturation by regulating the neuronal specific tubulin gene *Tuj1* (Bergsland *et al.,* 2006). Also in DRG neurons Sox11 is highly expressed during development and induced upon peripheral nerve lesion (Tanabe *et al.,* 2003; Jankowski *et al.,* 2006). As deletion of the Sox11 gene is lethal, Jankowski *et al.* used RNAi delivered to the DRG and showed that Sox11 knockdown inhibits *in vivo* neuronal regeneration (Jankowski *et al.,* 2009).

All together, these studies point to a crucial role for TFs in the regulation of growth-promoting gene expression after nerve damage and it will be of importance to learn how these TFs cooperate to orchestrate the transcriptional regulatory network that regulates successful neuronal regeneration.

References

Aigner L, Arber S, Kapfhammer JP, Laux T, Schneider C, Botteri F, Brenner HR, Caroni P (1995) Overexpression of the neural growth-associated protein GAP-43 induces nerve sprouting in the adult nervous system of transgenic mice. Cell 83:269-278.

Al-Shahrour F, Carbonell J, Minguez P, Goetz S, Conesa A, Tarraga J, Medina I, Alloza E, Montaner D, Dopazo J (2008) Babelomics: advanced functional profiling of transcriptomics, proteomics and genomics experiments. Nucleic Acids Res 36:W341-346.

Alexa A, Rahnenfuhrer J, Lengauer T (2006) Improved scoring of functional groups from gene expression data by decorrelating GO graph structure. Bioinformatics 22:1600-1607.

Alon U (2007) Network motifs: theory and experimental approaches. Nat Rev Genet 8:450-461.

Ambron RT, Walters ET (1996) Priming events and retrograde injury signals. A new perspective on the cellular and molecular biology of nerve regeneration. Mol Neurobiol 13:61-79.

Angelini C, Cutillo L, De Canditiis D, Mutarelli M, Pensky M (2007) BATS: A Bayesian user-friendly software for analyzing time series microarray data. . Technical Report CNR-IAC 331/07

Beer MA, Tavazoie S (2004) Predicting gene expression from sequence. Cell 117:185-198.

Berdan RC, Easaw JC, Wang R (1993) Alterations in membrane potential after axotomy at different distances from the soma of an identified neuron and the effect of depolarization on neurite outgrowth and calcium channel expression. J Neurophysiol 69:151-164.

Bergsland M, Werme M, Malewicz M, Perlmann T, Muhr J (2006) The establishment of neuronal properties is controlled by Sox4 and Sox11. Genes Dev 20:3475-3486.

Blais A, Tsikitis M, Acosta-Alvear D, Sharan R, Kluger Y, Dynlacht BD (2005) An initial blueprint for myogenic differentiation. Genes Dev 19:553-569.

Bomze HM, Bulsara KR, Iskandar BJ, Caroni P, Skene JH (2001) Spinal axon regeneration evoked by replacing two growth cone proteins in adult neurons. Nat Neurosci 4:38-43.

Boyer LA, Lee TI, Cole MF, Johnstone SE, Levine SS, Zucker JP, Guenther MG, Kumar RM, Murray HL, Jenner RG, Gifford DK, Melton DA, Jaenisch R, Young RA (2005) Core transcriptional regulatory circuitry in human embryonic stem cells. Cell 122:947-956.

Buck MJ, Lieb JD (2004) ChIP-chip: considerations for the design, analysis, and application of genome-wide chromatin immunoprecipitation experiments. Genomics 83:349-360.

Buck MJ, Nobel AB, Lieb JD (2005) ChIPOTle: a user-friendly tool for the analysis of ChIP-chip data. Genome Biol 6:R97.

Buffo A, Holtmaat AJ, Savio T, Verbeek JS, Oberdick J, Oestreicher AB, Gispen WH, Verhaagen J, Rossi F, Strata P (1997) Targeted overexpression of the neurite growth-associated protein B-50/GAP-43 in cerebellar Purkinje cells induces sprouting after axotomy but not axon regeneration into growth-permissive transplants. J Neurosci 17:8778-8791.

Cafferty WB, Gardiner NJ, Das P, Qiu J, McMahon SB, Thompson SW (2004) Conditioning injury-induced spinal axon regeneration fails in interleukin-6 knock-out mice. J Neurosci 24:4432-4443.

Cai D, Shen Y, De Bellard M, Tang S, Filbin MT (1999) Prior exposure to neurotrophins blocks inhibition of axonal regeneration by MAG and myelin via a cAMP-dependent mechanism. Neuron 22:89-101.

Cai D, Deng K, Mellado W, Lee J, Ratan RR, Filbin MT (2002) Arginase I and polyamines

act downstream from cyclic AMP in overcoming inhibition of axonal growth MAG and myelin in vitro. Neuron 35:711-719.

Cao Z, Gao Y, Bryson JB, Hou J, Chaudhry N, Siddiq M, Martinez J, Spencer T, Carmel J, Hart RB, Filbin MT (2006) The cytokine interleukin-6 is sufficient but not necessary to mimic the peripheral conditioning lesion effect on axonal growth. J Neurosci 26:5565-5573.

Carroll JS, Liu XS, Brodsky AS, Li W, Meyer CA, Szary AJ, Eeckhoute J, Shao W, Hestermann EV, Geistlinger TR, Fox EA, Silver PA, Brown M (2005) Chromosome-wide mapping of estrogen receptor binding reveals long-range regulation requiring the forkhead protein FoxA1. Cell 122:33-43.

Chong MS, Woolf CJ, Haque NS, Anderson PN (1999) Axonal regeneration from injured dorsal roots into the spinal cord of adult rats. J Comp Neurol 410:42-54.

Corcoran J, Shroot B, Pizzey J, Maden M (2000) The role of retinoic acid receptors in neurite outgrowth from different populations of embryonic mouse dorsal root ganglia. J Cell Sci 113 (Pt 14):2567-2574.

Corcoran J, So PL, Barber RD, Vincent KJ, Mazarakis ND, Mitrophanous KA, Kingsman SM, Maden M (2002) Retinoic acid receptor beta2 and neurite outgrowth in the adult mouse spinal cord in vitro. J Cell Sci 115:3779-3786.

Costigan M, Befort K, Karchewski L, Griffin RS, D'Urso D, Allchorne A, Sitarski J, Mannion JW, Pratt RE, Woolf CJ (2002) Replicate high-density rat genome oligonucleotide microarrays reveal hundreds of regulated genes in the dorsal root ganglion after peripheral nerve injury. BMC Neurosci 3:16.

Elkon R, Linhart C, Sharan R, Shamir R, Shiloh Y (2003) Genome-wide in silico identification of transcriptional regulators controlling the cell cycle in human cells. Genome Res 13:773-780.

Flanagin S, Nelson JD, Castner DG, Denisenko O, Bomsztyk K (2008) Microplate-based chromatin immunoprecipitation method, Matrix ChIP: a platform to study signaling of complex genomic events. Nucleic Acids Res 36:e17.

Fogel GB, Weekes DG, Varga G, Dow ER, Craven AM, Harlow HB, Su EW, Onyia JE, Su C (2005) A statistical analysis of the TRANSFAC database. Biosystems 81:137-154.

Gao Y, Deng K, Hou J, Bryson JB, Barco A, Nikulina E, Spencer T, Mellado W, Kandel ER, Filbin MT (2004) Activated CREB is sufficient to overcome inhibitors in myelin and promote spinal axon regeneration in vivo. Neuron 44:609-621.

Gibbons FD, Proft M, Struhl K, Roth FP (2005) Chipper: discovering transcription-factor targets from chromatin immunoprecipitation microarrays using variance stabilization. Genome Biol 6:R96.

Hanz S, Perlson E, Willis D, Zheng JQ, Massarwa R, Huerta JJ, Koltzenburg M, Kohler M, van-Minnen J, Twiss JL, Fainzilber M (2003) Axoplasmic importins enable retrograde injury signaling in lesioned nerve. Neuron 40:1095-1104.

Harr R, Haggstrom M, Gustafsson P (1983) Search algorithm for pattern match analysis of nucleic acid sequences. Nucleic Acids Res 11:2943-2957.

Heintzman ND et al. (2009) Histone modifications at human enhancers reflect global cell-type-specific gene expression. Nature 459:108-112.

Herdegen T, Leah JD (1998) Inducible and constitutive transcription factors in the mammalian nervous system: control of gene expression by Jun, Fos and Krox, and CREB/ATF proteins. Brain Res Brain Res Rev 28:370-490.

Huang da W, Sherman BT, Tan Q, Collins JR, Alvord WG, Roayaei J, Stephens R, Baseler MW, Lane HC, Lempicki RA (2007) The DAVID Gene Functional Classification Tool: a novel biological module-centric algorithm to functionally analyze large gene lists. Genome Biol 8:R183.

Huerta AM, Salgado H, Thieffry D, Collado-Vides J (1998) RegulonDB: a database on transcriptional regulation in Escherichia coli. Nucleic Acids Res 26:55-59.

Impey S, McCorkle SR, Cha-Molstad H, Dwyer JM, Yochum GS, Boss JM, McWeeney S, Dunn JJ, Mandel G, Goodman RH (2004) Defining the CREB regulon: a genome-wide analysis of transcription factor regulatory regions. Cell 119:1041-1054.

Jankowski MP, Cornuet PK, McIlwrath S, Koerber HR, Albers KM (2006) SRY-box containing gene 11 (Sox11) transcription factor is required for neuron survival and neurite growth. Neuroscience 143:501-514.

Jankowski MP, McIlwrath SL, Jing X, Cornuet PK, Salerno KM, Koerber HR, Albers KM (2009) Sox11 transcription factor modulates peripheral nerve regeneration in adult

mice. Brain Res 1256:43-54.

Jeong S, Rebeiz M, Andolfatto P, Werner T, True J, Carroll SB (2008) The evolution of gene regulation underlies a morphological difference between two Drosophila sister species. Cell 132:783-793.

Jovelin R (2009) Rapid sequence evolution of transcription factors controlling neuron differentiation in Caenorhabditis. Mol Biol Evol.

Kenney AM, Kocsis JD (1998) Peripheral axotomy induces long-term c-Jun amino-terminal kinase-1 activation and activator protein-1 binding activity by c-Jun and junD in adult rat dorsal root ganglia In vivo. J Neurosci 18:1318-1328.

Lee N, Neitzel KL, Devlin BK, MacLennan AJ (2004) STAT3 phosphorylation in injured axons before sensory and motor neuron nuclei: potential role for STAT3 as a retrograde signaling transcription factor. J Comp Neurol 474:535-545.

Lee TI et al. (2002) Transcriptional regulatory networks in Saccharomyces cerevisiae. Science 298:799-804.

Leone G, DeGregori J, Sears R, Jakoi L, Nevins JR (1997) Myc and Ras collaborate in inducing accumulation of active cyclin E/Cdk2 and E2F. Nature 387:422-426.

Lindwall C, Kanje M (2005) Retrograde axonal transport of JNK signaling molecules influence injury induced nuclear changes in p-c-Jun and ATF3 in adult rat sensory neurons. Mol Cell Neurosci 29:269-282.

Madan Babu M, Teichmann SA, Aravind L (2006) Evolutionary dynamics of prokaryotic transcriptional regulatory networks. J Mol Biol 358:614-633.

Maden M (2007) Retinoic acid in the development, regeneration and maintenance of the nervous system. Nat Rev Neurosci 8:755-765.

Mangan S, Alon U (2003) Structure and function of the feed-forward loop network motif. Proc Natl Acad Sci U S A 100:11980-11985.

Mangan S, Zaslaver A, Alon U (2003) The coherent feedforward loop serves as a sign-sensitive delay element in transcription networks. J Mol Biol 334:197-204.

Mangan S, Itzkovitz S, Zaslaver A, Alon U (2006) The incoherent feed-forward loop

accelerates the response-time of the gal system of Escherichia coli. J Mol Biol 356:1073-1081.

Mason MR, Campbell G, Caroni P, Anderson PN, Lieberman AR (2000) Overexpression of GAP-43 in thalamic projection neurons of transgenic mice does not enable them to regenerate axons through peripheral nerve grafts. Exp Neurol 165:143-152.

Mey J (2006) New therapeutic target for CNS injury? The role of retinoic acid signaling after nerve lesions. J Neurobiol 66:757-779.

Miao T, Wu D, Zhang Y, Bo X, Subang MC, Wang P, Richardson PM (2006) Suppressor of cytokine signaling-3 suppresses the ability of activated signal transducer and activator of transcription-3 to stimulate neurite growth in rat primary sensory neurons. J Neurosci 26:9512-9519.

Milo R, Shen-Orr S, Itzkovitz S, Kashtan N, Chklovskii D, Alon U (2002) Network motifs: simple building blocks of complex networks. Science 298:824-827.

Moore DL, Blackmore MG, Hu Y, Kaestner KH, Bixby JL, Lemmon VP, Goldberg JL (2009) KLF family members regulate intrinsic axon regeneration ability. Science 326:298-301.

Moses AM, Pollard DA, Nix DA, Iyer VN, Li XY, Biggin MD, Eisen MB (2006) Large-scale turnover of functional transcription factor binding sites in Drosophila. PLoS Comput Biol 2:e130.

Neumann S, Woolf CJ (1999) Regeneration of dorsal column fibers into and beyond the lesion site following adult spinal cord injury. Neuron 23:83-91.

Neumann S, Bradke F, Tessier-Lavigne M, Basbaum AI (2002) Regeneration of sensory axons within the injured spinal cord induced by intraganglionic cAMP elevation. Neuron 34:885-893.

O'Donnell KA, Wentzel EA, Zeller KI, Dang CV, Mendell JT (2005) c-Myc-regulated microRNAs modulate E2F1 expression. Nature 435:839-843.

O'Neill LP, VerMilyea MD, Turner BM (2006) Epigenetic characterization of the early embryo with a chromatin immunoprecipitation protocol applicable to small cell populations. Nat Genet 38:835-841.

Odom DT, Dowell RD, Jacobsen ES, Nekludova L, Rolfe PA, Danford TW, Gifford DK, Fraenkel E, Bell GI, Young RA (2006) Core transcriptional regulatory circuitry in human hepatocytes. Mol Syst Biol 2:2006 0017.

Park PJ (2009) ChIP-seq: advantages and challenges of a maturing technology. Nat Rev Genet 10:669-680.

Perlson E, Hanz S, Ben-Yaakov K, Segal-Ruder Y, Seger R, Fainzilber M (2005) Vimentin-dependent spatial translocation of an activated MAP kinase in injured nerve. Neuron 45:715-726.

Qiu J, Cafferty WB, McMahon SB, Thompson SW (2005) Conditioning injury-induced spinal axon regeneration requires signal transducer and activator of transcription 3 activation. J Neurosci 25:1645-1653.

Qiu J, Cai D, Dai H, McAtee M, Hoffman PN, Bregman BS, Filbin MT (2002) Spinal axon regeneration induced by elevation of cyclic AMP. Neuron 34:895-903.

Rada-Iglesias A, Ameur A, Kapranov P, Enroth S, Komorowski J, Gingeras TR, Wadelius C (2008) Whole-genome maps of USF1 and USF2 binding and histone H3 acetylation reveal new aspects of promoter structure and candidate genes for common human disorders. Genome Res 18:380-392.

Raivich G, Bohatschek M, Da Costa C, Iwata O, Galiano M, Hristova M, Nateri AS, Makwana M, Riera-Sans L, Wolfer DP, Lipp HP, Aguzzi A, Wagner EF, Behrens A (2004) The AP-1 transcription factor c-Jun is required for efficient axonal regeneration. Neuron 43:57-67.

Reed BD, Charos AE, Szekely AM, Weissman SM, Snyder M (2008) Genome-wide occupancy of SREBP1 and its partners NFY and SP1 reveals novel functional roles and combinatorial regulation of distinct classes of genes. PLoS Genet 4:e1000133.

Richardson PM, Issa VM (1984) Peripheral injury enhances central regeneration of primary sensory neurones. Nature 309:791-793.

Scacheri PC, Davis S, Odom DT, Crawford GE, Perkins S, Halawi MJ, Agarwal SK, Marx SJ, Spiegel AM, Meltzer PS, Collins FS (2006) Genome-wide analysis of menin binding provides insights into MEN1 tumorigenesis. PLoS Genet 2:e51.

Schena M, Shalon D, Davis RW, Brown PO (1995) Quantitative monitoring of gene ex-

pression patterns with a complementary DNA microarray. Science 270:467-470.

Schreyer DJ, Skene JH (1993) Injury-associated induction of GAP-43 expression displays axon branch specificity in rat dorsal root ganglion neurons. J Neurobiol 24:959-970.

Segal E, Shapira M, Regev A, Pe'er D, Botstein D, Koller D, Friedman N (2003) Module networks: identifying regulatory modules and their condition-specific regulators from gene expression data. Nat Genet 34:166-176.

Seijffers R, Allchorne AJ, Woolf CJ (2006) The transcription factor ATF-3 promotes neurite outgrowth. Mol Cell Neurosci 32:143-154.

Seijffers R, Mills CD, Woolf CJ (2007) ATF3 increases the intrinsic growth state of DRG neurons to enhance peripheral nerve regeneration. J Neurosci 27:7911-7920.

Shen-Orr SS, Milo R, Mangan S, Alon U (2002) Network motifs in the transcriptional regulation network of Escherichia coli. Nat Genet 31:64-68.

Skene JH, Willard M (1981a) Changes in axonally transported proteins during axon regeneration in toad retinal ganglion cells. J Cell Biol 89:86-95.

Skene JH, Willard M (1981b) Characteristics of growth-associated polypeptides in regenerating toad retinal ganglion cell axons. J Neurosci 1:419-426.

Smyth GK (2004) Linear models and empirical bayes methods for assessing differential expression in microarray experiments. Stat Appl Genet Mol Biol 3:Article3.

So PL, Yip PK, Bunting S, Wong LF, Mazarakis ND, Hall S, McMahon S, Maden M, Corcoran JP (2006) Interactions between retinoic acid, nerve growth factor and sonic hedgehog signalling pathways in neurite outgrowth. Dev Biol 298:167-175.

Spira ME, Oren R, Dormann A, Ilouz N, Lev S (2001) Calcium, protease activation, and cytoskeleton remodeling underlie growth cone formation and neuronal regeneration. Cell Mol Neurobiol 21:591-604.

Stam FJ, MacGillavry HD, Armstrong NJ, de Gunst MC, Zhang Y, van Kesteren RE, Smit AB, Verhaagen J (2007) Identification of candidate transcriptional modulators involved in successful regeneration after nerve injury. Eur J Neurosci 25:3629-3637.

Stepanova M, Tiazhelova T, Skoblov M, Baranova A (2005) A comparative analysis of

relative occurrence of transcription factor binding sites in vertebrate genomes and gene promoter areas. Bioinformatics 21:1789-1796.

Storey JD, Tibshirani R (2003) Statistical significance for genomewide studies. Proc Natl Acad Sci U S A 100:9440-9445.

Stormo GD (2000) DNA binding sites: representation and discovery. Bioinformatics 16:16-23.

Sung YJ, Chiu DT, Ambron RT (2006) Activation and retrograde transport of protein kinase G in rat nociceptive neurons after nerve injury and inflammation. Neuroscience 141:697-709.

Tai YC, Speed TP (2006) A multivariate empirical Bayes statistic for replicated microarray time course data. Annals of Statistics 34:2387-2412.

Tanabe K, Bonilla I, Winkles JA, Strittmatter SM (2003) Fibroblast growth factor-inducible-14 is induced in axotomized neurons and promotes neurite outgrowth. J Neurosci 23:9675-9686.

Thieffry D, Huerta AM, Perez-Rueda E, Collado-Vides J (1998) From specific gene regulation to genomic networks: a global analysis of transcriptional regulation in Escherichia coli. Bioessays 20:433-440.

Toedling J, Skylar O, Krueger T, Fischer JJ, Sperling S, Huber W (2007) Ringo--an R/Bioconductor package for analyzing ChIP-chip readouts. BMC Bioinformatics 8:221.

Tompa M et al. (2005) Assessing computational tools for the discovery of transcription factor binding sites. Nat Biotechnol 23:137-144.

Tsujino H, Kondo E, Fukuoka T, Dai Y, Tokunaga A, Miki K, Yonenobu K, Ochi T, Noguchi K (2000) Activating transcription factor 3 (ATF3) induction by axotomy in sensory and motoneurons: A novel neuronal marker of nerve injury. Mol Cell Neurosci 15:170-182.

Tusher VG, Tibshirani R, Chu G (2001) Significance analysis of microarrays applied to the ionizing radiation response. Proc Natl Acad Sci U S A 98:5116-5121.

Wang Z (2009) Epitope tagging of endogenous proteins for genome-wide chromatin immunoprecipitation analysis. Methods Mol Biol 567:87-98.

Wasserman WW, Sandelin A (2004) Applied bioinformatics for the identification of regulatory elements. Nat Rev Genet 5:276-287.

Werner T (2008) Bioinformatics applications for pathway analysis of microarray data. Curr Opin Biotechnol 19:50-54.

Wong LF, Yip PK, Battaglia A, Grist J, Corcoran J, Maden M, Azzouz M, Kingsman SM, Kingsman AJ, Mazarakis ND, McMahon SB (2006) Retinoic acid receptor beta2 promotes functional regeneration of sensory axons in the spinal cord. Nat Neurosci 9:243-250.

Wu W, Mathew TC, Miller FD (1993) Evidence that the loss of homeostatic signals induces regeneration-associated alterations in neuronal gene expression. Dev Biol 158:456-466.

Xiao HS, Huang QH, Zhang FX, Bao L, Lu YJ, Guo C, Yang L, Huang WJ, Fu G, Xu SH, Cheng XP, Yan Q, Zhu ZD, Zhang X, Chen Z, Han ZG, Zhang X (2002) Identification of gene expression profile of dorsal root ganglion in the rat peripheral axotomy model of neuropathic pain. Proc Natl Acad Sci U S A 99:8360-8365.

Xie F, Zheng B (2008) White matter inhibitors in CNS axon regeneration failure. Exp Neurol 209:302-312.

Xie X, Lu J, Kulbokas EJ, Golub TR, Mootha V, Lindblad-Toh K, Lander ES, Kellis M (2005) Systematic discovery of regulatory motifs in human promoters and 3' UTRs by comparison of several mammals. Nature 434:338-345.

Yip PK, Wong LF, Pattinson D, Battaglia A, Grist J, Bradbury EJ, Maden M, McMahon SB, Mazarakis ND (2006) Lentiviral vector expressing retinoic acid receptor beta2 promotes recovery of function after corticospinal tract injury in the adult rat spinal cord. Hum Mol Genet 15:3107-3118.

Zhang X, Guo C, Chen Y, Shulha HP, Schnetz MP, LaFramboise T, Bartels CF, Markowitz S, Weng Z, Scacheri PC, Wang Z (2008) Epitope tagging of endogenous proteins for genome-wide ChIP-chip studies. Nat Methods 5:163-165.

Zhang XP, Ambron RT (2000) Positive injury signals induce growth and prolong survival in Aplysia neurons. J Neurobiol 45:84-94.

Zheng JQ, Kelly TK, Chang B, Ryazantsev S, Rajasekaran AK, Martin KC, Twiss JL

(2001) A functional role for intra-axonal protein synthesis during axonal regeneration from adult sensory neurons. J Neurosci 21:9291-9303.

Zou H, Ho C, Wong K, Tessier-Lavigne M (2009) Axotomy-induced Smad1 activation promotes axonal growth in adult sensory neurons. J Neurosci 29:7116-7123.

Chapter 2

NFIL3 and cAMP Response Element-Binding Protein form a transcriptional feed-forward loop that controls neuronal regeneration-associated gene expression

Harold D. MacGillavry[1,3], Floor J. Stam[1,3], Marion M. Sassen[1], Linde Kegel[1], William T.J. Hendriks[1], Joost Verhaagen[2], August B. Smit[1] and Ronald E. van Kesteren[1]

[1]Department of Molecular and Cellular Neurobiology, Center for Neurogenomics and Cognitive Research, VU University Amsterdam, De Boelelaan 1085, 1081 HV Amsterdam, The Netherlands
[2]Department of Neuroregeneration, Netherlands Institute for Neuroscience, Meibergdreef 47, 1105 BH Amsterdam, The Netherlands
[3]Authors contributed equally to this work

Journal of Neuroscience. 2009 Dec.9;29(49):15542-50

Abstract

Successful regeneration of damaged neurons depends on the coordinated expression of neuron-intrinsic genes. At present however, there is no comprehensive view of the transcriptional regulatory mechanisms underlying neuronal regeneration. We used high-content cellular screening to investigate the functional contribution of 62 transcription factors to regenerative neuron outgrowth. Ten transcription factors are identified that either increase or decrease neurite outgrowth. One of these, NFIL3, is specifically upregulated during successful regeneration in vivo. Paradoxically however, knockdown of NFIL3 and overexpression of dominant-negative NFIL3 both increase neurite outgrowth. Our data show that NFIL3, together with CREB, forms an incoherent feed-forward transcriptional regulatory loop in which NFIL3 acts as a negative regulator of CREB-induced regeneration-associated genes

Introduction

Neurons in the central nervous system (CNS) do normally not regenerate after injury, whereas in the peripheral nervous system (PNS) damaged axons spontaneously re-grow and re-innervate their targets. Current strategies to promote regeneration of injured neurons are often aimed at manipulating the molecular and cellular environment of damaged neurons (Yiu and He, 2006; Cafferty *et al.*, 2008). Importantly, successful axonal regeneration also depends on the intrinsic ability of neurons to translate growth-promoting signals into an appropriate gene expression response (Raivich and Makwana, 2007). Dorsal root ganglion (DRG) neurons are an attractive model to study neuron-intrinsic mechanisms of regeneration. DRG neurons extend one peripheral axon into the spinal nerve which regenerates spontaneously after damage, and one central axon into the dorsal root which shows little regenerative capacity (for review, see Teng and Tang, 2006). Successful regeneration following peripheral nerve crush of DRG neurons is transcription-dependent (Smith and Skene, 1997) and requires retrograde transport of injury-induced signals from the lesion site to the nuclei of the injured neurons (Chong *et al.*, 1999; Neumann and Woolf, 1999; Hanz *et al.*, 2003). Injured DRG neurons show increased expression of many regeneration-associated genes, including *Gap43*, *Cap23*, *Arg1* and *Sppr1a*, and overexpression of these genes stimulates axonal outgrowth in injured neurons (Frey *et al.*, 2000; Bomze *et al.*, 2001; Bonilla *et al.*, 2002; Cai *et al.*, 2002). Injury-induced expression of regeneration-associated genes requires the coordinated activity of regeneration-associated transcription factors (TFs). To date, several injury-responsive TFs have been identified that promote neuron outgrowth, including CREB (Gao *et al.*, 2004), STAT3 (Qiu *et al.*, 2005), ATF3 (Seijffers *et al.*, 2006; Seijffers *et al.*, 2007), c-JUN (Broude *et al.*, 1997; Raivich *et al.*, 2004), SOX11 (Jankowski *et al.*, 2006) and several KLF family members (Moore *et al.*, 2009). At present however there is no comprehensive view of the transcriptional regulatory mechanisms underlying neuronal regeneration.

Recent advances in gene regulation analysis have made it possible to accurately

map gene regulatory networks underlying complex physiological processes. In particular, simple and robust cellular models combined with large scale application of gene expression profiling, RNA interference, TF binding site prediction and TF-promoter binding analysis, allow accurate reconstruction of gene regulatory networks and prediction of the key components within these networks (Lee *et al.*, 2002; Blais and Dynlacht, 2005; Tegner and Bjorkegren, 2007). Here, we applied these methods to uncover novel aspects of the gene regulatory network underlying successful neuronal regeneration. Specifically, we performed an RNAi-based screen on a large set of TFs that were previously shown to be early and differentially regulated in DRG neurons following either peripheral or central nerve crush (Stam *et al.*, 2007). Ten transcription factors were identified that robustly and significantly affect neurite outgrowth. One of these, NFIL3, is specifically upregulated during successful regeneration *in vivo*. Paradoxically however, knockdown of NFIL3 and overexpression of dominant-negative NFIL3 both increase neurite outgrowth. Our data show that NFIL3, together with CREB, forms an incoherent feed-forward transcriptional regulatory loop in which NFIL3 acts as a negative regulator of the CREB-induced expression of regeneration-associated genes.

Results

High-content screening identifies novel transcriptional regulators of DRG neuron outgrowth

F11 cells were used to test 62 TFs for their ability to regulate neurite outgrowth. These 62 TFs are differentially regulated in DRG neurons following sciatic nerve injury compared with dorsal root injury (Stam *et al.*, 2007), and include bona fide TFs as well as many putative transcriptional regulators based on gene ontology or subcellular localization (see Supplementary Table 1 for selection criteria). F11 cells are neuroblastoma cells derived from rat embryonic DRG neurons (Platika *et al.*, 1985). They express many DRG neuron markers (Francel *et al.*, 1987; Boland and Dingledine, 1990) and display cAMP-induced neurite outgrowth (Ghil *et al.*, 2000). We used F11 cells for screening because high transfection efficiencies (>90%) can reproducibly be obtained and neurite outgrowth can be quantified in an automated and reproducible manner (Figure 1A-C), which we have validated by manual tracing (data not shown). Systematic knockdown of all 62 TFs followed by high-throughput automated analysis of neurite lengths identified TFs that affect neurite outgrowth. Examples of reduced neurite outgrowth in ATF3 knockdown cells and enhanced neurite outgrowth in NFIL3 knockdown cells are shown in Figure 1D-F. Knockdown of 19 TFs significantly affected the neurite total length per neuron (Figure 1G), whereas 10 out of these 19 TFs also significantly affected the proportion of outgrowth-positive cells per well after knockdown (Figure 1H). All significant effects were observed in at least two independent experiments; representative data for all TFs are summarized in Supplementary Figure 1. For the 10 candidate TFs that scored

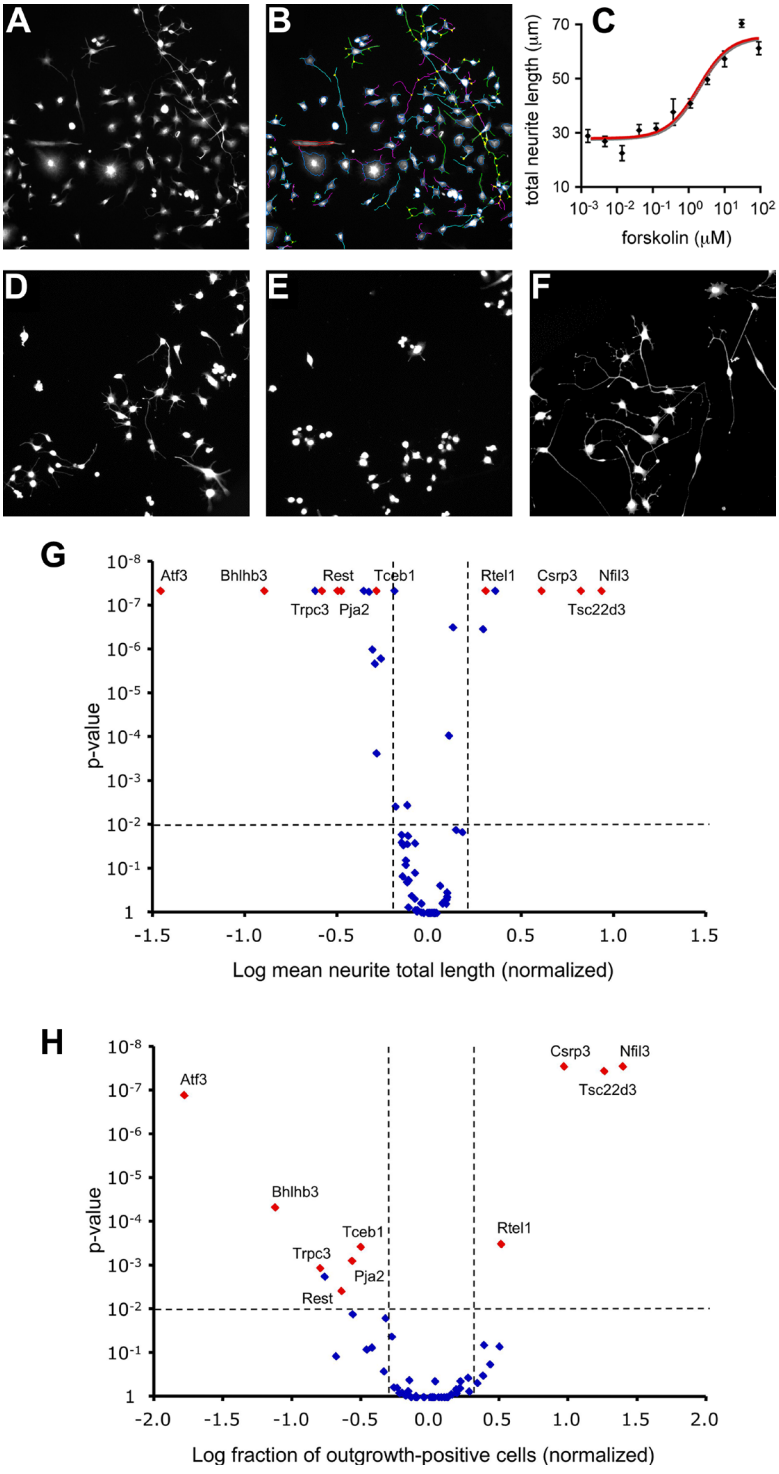
A
B
C
total neurite length (μm)
70
50
30
10
10-3 10-2 10-1 100 101 102
forskolin (μM)
D
E
F
G
p-value
10-8
10-7
10-6
10-5
10-4
10-3
10-2
10-1
1
Atf3
Bhlhb3
Rest
Tceb1
Rtel1
Csrp3
Nfil3
Trpc3
Pja2
Tsc22d3
-1.5 -1.0 -0.5 0.0 0.5 1.0 1.5
Log mean neurite total length (normalized)
H
p-value
Atf3
Csrp3
Nfil3
Tsc22d3
Bhlhb3
Tceb1
Rtel1
Trpc3
Pja2
Rest
-2.0 -1.5 -1.0 -0.5 0.0 0.5 1.0 1.5 2.0
Log fraction of outgrowth-positive cells (normalized)

positive in both analyses, the four individual siRNAs constituting the siRNA pool were tested separately to further validate the screening results (Supplementary Figure 2). In eight cases, the pool-induced effect was observed for at least two individual siRNAs. For two TFs (BHLHB3 and RTEL1) the pool-induced effect was observed for only one of the individual siRNAs.

NFIL3 expression correlates with DRG neurite outgrowth *in vitro* and *in vivo*

Functional screening identified the bZIP TF NFIL3 as the strongest repressor of neurite outgrowth (Figure 1). This appeared paradoxical since NFIL3 expression is specifically induced in DRG neurons following sciatic nerve injury and not after dorsal root injury (Stam *et al.*, 2007). Therefore we decided to further characterize NFIL3 expression in injured DRG neurons *in vivo*, and in forskolin-stimulated F11 cells and primary adult DRG neurons *in vitro*. Quantitative PCR analysis revealed a robust and early induction of *Nfil3* mRNA in DRGs *in vivo* following sciatic nerve crush, but not after dorsal root crush (Figure 2A), corroborating our earlier microarray data (Stam *et al.*, 2007). Western blot analysis confirmed the upregulation of NFIL3 protein after sciatic nerve crush (Figure 2B). To determine the cellular source of *Nfil3* mRNA we performed in situ hybridization. *Nfil3* mRNA is almost absent in DRG neurons of control animals, but is abundantly expressed in most neurons at 24 hours after sciatic nerve crush (Figure 2C). Elevation of intracellular cAMP levels in F11 cells and in primary adult DRG neurons resulted in a similar rapid induction of *Nfil3* mRNA as observed in injured DRGs *in vivo* (Figure 2D, G). In DRG neurons, the forskolin-induced mRNA upregulation was almost completely abolished when neurons were pre-treated with the protein kinase A (PKA) inhibitor H89 (Figure 2G). Because cAMP, PKA and CREB all promote successful regeneration of injured DRG neurons *in vivo* (Qiu *et al.*, 2002; Gao *et al.*, 2004), we also compared the temporal patterns of CREB activation and NFIL3 protein expression in DRGs after sciatic nerve crush *in vivo*, in forskolin-stimulated F11 cells, and in primary adult DRG

Figure 1. High-content screening identifies TFs involved in regenerative neurite outgrowth. (A) Cellomics KineticScan HCS Reader-obtained images of F11 cells stained with anti-neurofilament showing forskolin-induced neurite outgrowth. (B) The same image as in (A) showing how the Cellomics Neuronal Profiling algorithm accurately traces neurites and calculates neurite lengths based on anti-neurofilament staining. (C) Cellomics quantification of forskolin-induced neurite outgrowth from F11 cells showing a dose-dependent increase in neurite total length. Data points represent means ± SEM; n = 6 wells for each concentration of forskolin. (D-F) Examples of forskolin-stimulated F11 cells transfected with control siRNA (D) siATF3 (E) and siNFIL3 (F), showing reduced neurite outgrowth after knockdown of ATF3 and enhanced neurite outgrowth after knockdown of NFIL3. (G-H) Volcano plots summarizing the screening results for all 62 TFs. Data points represent neurite total length per cell (G) and fraction of outgrowth positive cells per well (H) after TF knockdown. Ten TFs showing effects that are statistically significant ($p < 0.01$; horizontal dotted lines) and biologically relevant (effect size > 1 SD of the combined negative controls; vertical dotted lines) in both assays are indicated in red.

neurons in culture. In each case we observed a rapid activation of CREB, while NFIL3 protein levels only started to increase several hours later (Figure 2B, E, H). Finally, we find that NFIL3 protein is primarily expressed in the nucleus of F11 cells and primary adult DRG neurons in culture (Figure 2F, I). Together, these results show that NFIL3 is downstream of the cAMP-PKA-CREB pathway, and that *Nfil3* mRNA expression, protein synthesis and localization are consistent with a transcriptional regulatory role in injured DRG neurons.

NFIL3 is a suppressor of neurite outgrowth in DRG neurons

In F11 cells, siRNA-mediated knockdown of NFIL3 resulted in a significant increase in total neurite length (Figure 1). In order to demonstrate a similar role for NFIL3 in DRG neurons we used RNA interference and dominant-negative expression. First, we confirmed that NFIL3 siRNAs are able to knockdown NFIL3 protein levels. Both the pool as well as two out of the four individual siRNAs significantly reduced NFIL3 protein levels in HEK293 cells over-expressing NFIL3 (Figure 3A). Next, adult primary DRG neurons were transfected using nucleofection, which resulted in >50% siRNA transfection efficiency. qPCR analysis confirmed efficient knockdown of *Nfil3* mRNA levels in DRG neurons (Figure 3B). After transfection, neurons were cultured for 40 hours and neurite lengths were measured. Consistent with our results obtained in F11 cells, we found a significant increase in DRG neurite length when NFIL3 expression was knocked down using the pool of siRNAs (Figure 3C, D). This effect could be replicated with three out of the four individual siRNAs (Figure 3E). Notably, the increase in neurite length induced by each individual siRNA in DRG neurons correlated well with their efficacy to knockdown NFIL3 protein levels in HEK293 cells (Figure 3A). In these experiments we find that all DRG neurons extend neurites, independent of NFIL3 knockdown.

To exclude the possibility that the siRNA-induced increase in neurite outgrowth is due to off-target effects, we also over-expressed a dominant-negative NFIL3 (DN-NFIL3) protein in primary adult DRG neurons. DN-NFIL3 lacks the basic DNA-binding domain and the nuclear localization sequence, which are replaced by an acidic region and an N-terminal Flag tag (Figure 4A). A similar dominant-negative CREB protein has previously been used to specifically inhibit CREB function and reduce DRG neuron outgrowth (Ahn *et al.*, 1998; Gao *et al.*, 2004). Co-immunoprecipitation experiments show that DN-NFIL3 specifically interacts with NFIL3 and not with CREB (Figure 4B). As expected, DN-NFIL3 resides in the cytoplasm and fails to translocate to the nucleus after overexpression in primary adult DRG neurons (Figure 4C). Overexpression of DN-NFIL3 in primary adult DRG neurons resulted in a similar increase in neurite length as observed in siRNA-transfected neurons (Figure 4D). This finding shows that in addition to knock down of NFIL3 expression, functional inactivation of NFIL3 also induces neurite outgrowth.

Overexpression of NFIL3 had no effect on DRG neurite outgrowth compared

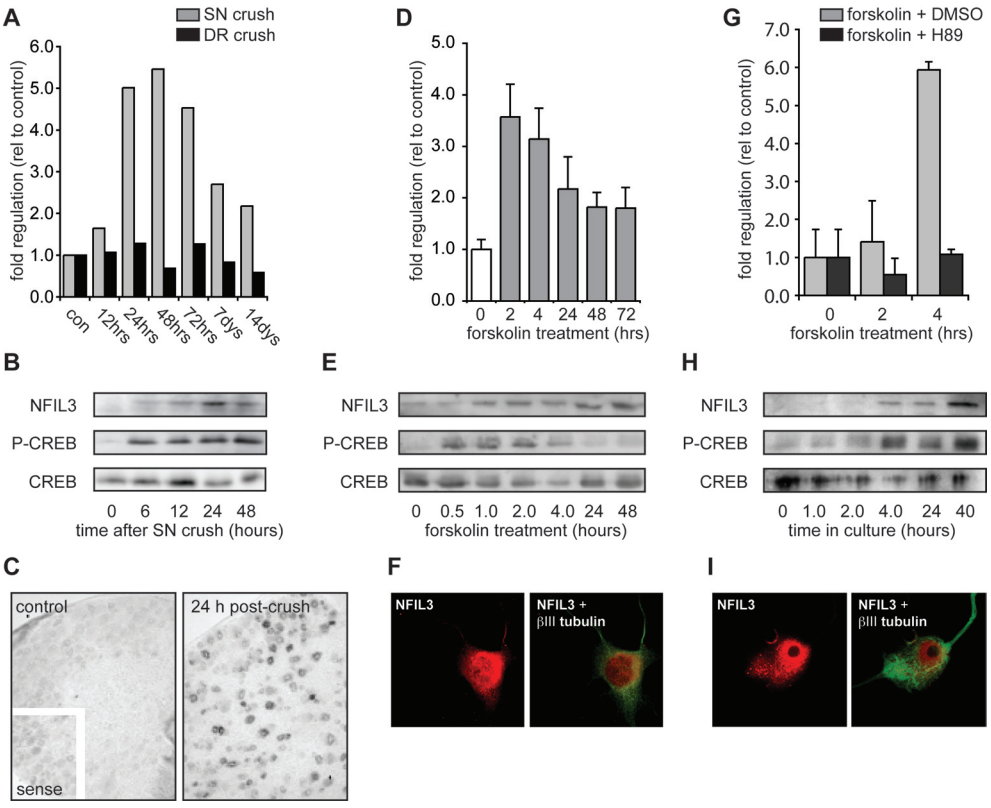

Figure 2. NFIL3 expression correlates with neurite outgrowth *in vivo* and *in vitro.* (A) qPCR analysis demonstrates a robust and specific up-regulation of *Nfil3* mRNA after sciatic nerve crush (SN), and not after dorsal root crush (DR), corroborating previously reported microarray data. (B) Western blot analysis shows upregulation of NFIL3 protein in DRGs *in vivo* 12-24 hours after SN crush. NFIL3 induction is preceded by CREB activation as indicated by phospho-CREB (P-CREB) levels. Total CREB levels are measured for comparison. (C) In situ hybridisation confirms that expression of *Nfil3* is induced in DRG neurons by peripheral axonal lesion. (D) *Nfil3* mRNA expression is induced in forskolin-stimulated F11 cells as measured by qPCR. Data points represent means ± SEM; n = 5 for each time-point. (E) Western blot analysis shows upregulation of NFIL3 protein after 4 hours in forskolin stimulated F11 cells. NFIL3 induction is preceded by CREB activation as indicated by phospho-CREB levels. (F) Confocal images showing nuclear localization of NFIL3 in F11 cells. (G) *Nfil3* mRNA expression is induced in cultured primary adult DRG neurons as measured by qPCR. Addition of the PKA inhibitor H89 blocks Nfil3 mRNA induction. Data points represent means ± SEM; n = 3 for each time-point. (H) Western blot analysis shows upregulation of NFIL3 protein in primary adult DRG neurons after 4 hours in culture. NFIL3 induction is preceded by CREB activation as indicated by phospho-CREB levels. (I) Confocal images showing nuclear localization of NFIL3 in cultured DRG neurons.

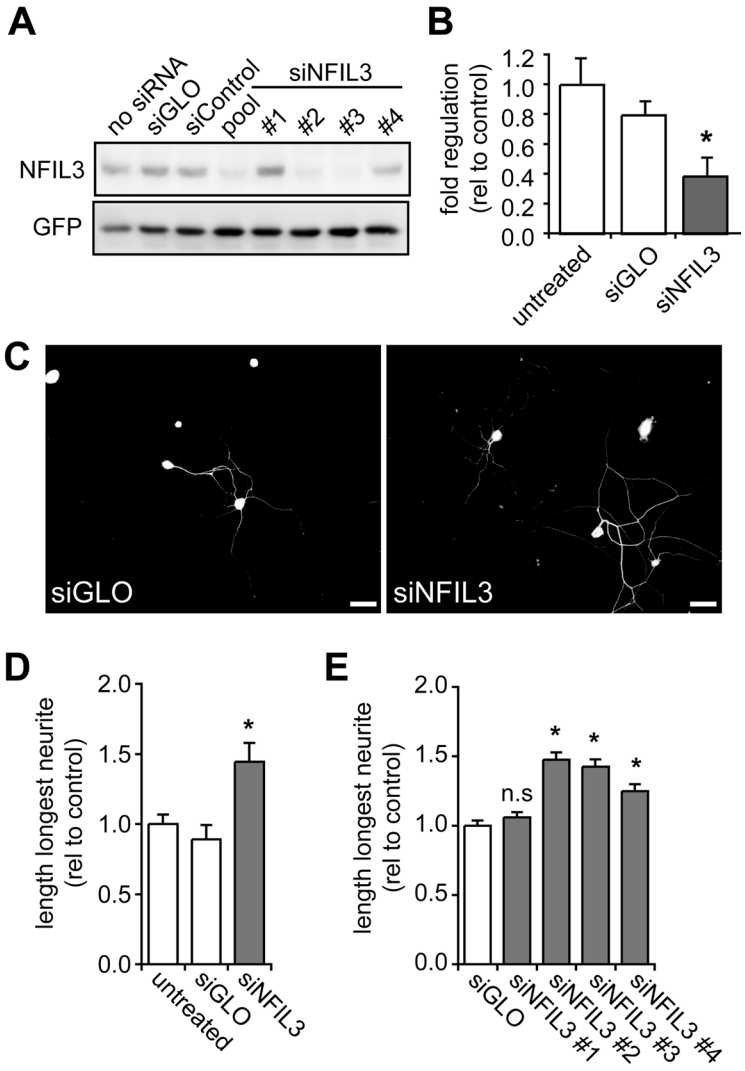

Figure 3. NFIL3 knockdown increases neurite outgrowth from primary adult DRG neurons. (A) siRNA-mediated knockdown of NFIL3 protein levels was analyzed in HEK293 cells. Western blotting confirmed that siNFIL3 causes knockdown of NFIL3 protein in HEK293 cells over-expressing rat NFIL3. The siNFIL3 pool and two individual siRNAs (#2 and #3) significantly reduced NFIL3 protein levels; control siRNAs (siGLO and siCONTROL) did not affect NFIL3 protein levels. (B) qPCR measurements confirm a 50-60% knockdown of *Nfil3* mRNA levels in siNFIL3-transfected DRG neurons. (C-E) Primary adult DRG neurons transfected with the siNFIL3 pool show a 51% increase in neurite outgrowth. Three out the four individual NFIL3 siRNAs (#2, #3 and #4) also induce a significant increase in neurite outgrowth. The length of the longest neurite was measured for 100-150 cells per condition. Note that the individual siRNAs resulting in the strongest increase in neurite outgrowth (E) also give the highest reduction in protein expression in HEK293 cells (A). Bars represent means ± SD; * $p < 0.01$. Scale bar = 100 µm.

with GFP-transfected controls (Figure 4D). Also, in F11 cells we observed no effect of NFIL3 overexpression on forskolin-induced neurite outgrowth (data not shown). These findings seem to suggest that forskolin stimulation (F11 cells) or dissociation and plating (DRG neurons) result in maximally effective levels of NFIL3, and that further increasing NFIL3 levels has no additive effect. Previous studies showed that overexpression of NFIL3 promotes the survival of embryonic chicken spinal cord motor neurons (Junghans *et al.*, 2004). Overexpression of either wild type NFIL3 or dominant-negative NFIL3 had no effect on the percentage of viable DRG neurons (Figures 4E and 4F). Together, these observations demonstrate that NFIL3 represses cAMP- and lesion-induced neurite outgrowth in DRG neurons without affecting neuronal survival.

NFIL3 and CREB compete for the same binding sites and control gene transcription together

NFIL3 binds to the E4BP4 response element (EBPRE; TTA[CT]GTAA). To study NFIL3-mediated transcription we used a luciferase reporter construct containing three repeats of the consensus E4BP4 response element (Ozkurt and Tetradis, 2003). Because the EBPRE consensus sequence is very similar to the cAMP response element (CRE; TGACGT[AC]A) to which CREB binds, we also used a luciferase reporter construct containing the CREB-responsive part of the rat somatostatin gene promoter (Montminy *et al.*, 1986) to monitor CRE-mediated transcription.

Forskolin treatment of F11 cells transfected with either the EBPRE-luciferase construct or the CRE-luciferase construct resulted in an induction of luciferase activity showing peak levels at 24h after stimulation (Figure 5A). In order to discriminate between the effects of NFIL3 and CREB in this experiment, we combined expression of the luciferase constructs with overexpression of NFIL3 or CREB in HEK293 and in F11 cells. Interestingly, NFIL3 overexpression repressed the activity of both the EBPRE- and the CRE-reporter, whereas both reporters were strongly induced by CREB (Figure 5B). Importantly, when we co-expressed CREB with increasing amounts of NFIL3, we observed a decrease in CREB-induced EBPRE-reporter activation (Figure 5C), indicating that NFIL3 represses CREB-mediated transcription in a dose-dependent manner. Consistent with these data we found that in F11 cells the forskolin-stimulated EBPRE-reporter activity is further enhanced by NFIL3 knockdown, and repressed by CREB knockdown (Figure 5D). These results show that cAMP-induced DRG neuron outgrowth correlates with dynamic EBPRE/CRE-mediated gene transcription, which is controlled by NFIL3 and CREB. Specifically, NFIL3 and CREB bind to the same promoter elements, but have opposite effects on gene transcription.

To test whether NFIL3 can also inhibit EBPRE-mediated gene transcription in neurons, we transfected primary adult DRG neurons with the EBPRE-reporter plasmid and simultaneously knocked down NFIL3 using either siRNAs or DN-NFIL3 overexpression. Both knockdown of NFIL3 and overexpression of DN-NFIL3 significantly in-

creased EBPRE-reporter activity (Figure 5E). Together with the above observations in cell lines, these findings unequivocally confirm that NFIL3 acts as a repressor of EBPRE/CRE-mediated gene transcription in DRG neurons.

NFIL3 binds to regeneration-associated genes *in vivo* and represses their transcription

We next tested whether NFIL3 is also able to bind to and repress expression of known regeneration-associated target genes. Of the genes that were previously shown to be regulated during regeneration (Stam *et al.*, 2007), 67 contain predicted CRE or EBPRE sites, including *Arg1*, *Gap43* and *Nfil3* itself. To establish direct binding of NFIL3 to these sites, we first overexpressed NFIL3 in F11 cells and performed chromatin immunoprecipitation using two antibodies against NFIL3. Co-precipitated DNA was amplified using primers specific for the sequences surrounding each predicted binding site. Both antibodies co-precipitated the promoters of *Arg1*, *Gap43*, and *Nfil3*, but not the promoter of the beta-actin gene (*Actb*), which does not contain EBPRE or CRE sites (Figure 6A). We next tested whether both CREB and NFIL3 could play a role in the regulation of *Arg1*, *Gap43* and *Nfil3* gene expression in regenerating DRG neurons *in vivo*. Rats were subjected to a sciatic nerve crush and lesioned DRGs were collected 48 hours later. Chromatin immunoprecipitation was performed using either anti-phospho-CREB or anti-NFIL3. Both phospho-CREB and NFIL3 were found to be present at the promoters of *Arg1*, *Gap43*, and *Nfil3*, but not at the *Actb* promoter (Figure 6B). Quantification of phospho-CREB and NFIL3 binding at earlier time points after sciatic nerve crush showed that binding at the *Arg1* and *Gap43* promoters was not detected in unlesioned, control DRGs, but becomes detectable after 6 – 24 hours after sciatic nerve crush (Figure 6C). Thus, *Arg1*, *Gap43*, and *Nfil3* are CREB and NFIL3 target genes in regenerating DRG neurons *in vivo*.

To determine the effect of NFIL3 binding to the promoters of *Arg1*, *Gap43*, and

Figure 4. Dominant-negative NFIL3 expression increases neurite outgrowth from primary adult DRG neurons.

(A) Schematic representation of full-length and dominant-negative NFIL3 (DN-NFIL3) protein. DN-NFIL3 lacks the DNA binding domain, which is replaced by an acidic amphipathic amino acid sequence resulting in a higher affinity for the endogenous full-length protein (see also Ahn *et al.*, 1998). (B) Western blot analysis shows specific co-immunoprecipitation of Flag-tagged DN-NFIL3 with Myc-tagged NFIL3 when co-expressed in HEK293 cells. All cells were transfected with Flag-DN-NFIL3 and co-transfected with Myc-NFIL3 or Myc-CREB as indicated. Note that CREB does not co-immunoprecipitate with DN-NFIL3. (C) Immunofluorescence staining shows cytoplasmic localization of Flag-DN-NFIL3 expressed in primary adult DRG neurons. (D) Overexpression of DN-NFIL3 causes a 42% increase neurite outgrowth from adult DRG neurons in culture. Overexpression of full-length NFIL3 has no effect on neurite outgrowth. Bars represent means ± SEM; * $p < 0.01$. (E) EthD-1 uptake assays of transfected primary adult DRG neurons indicates that most cells are viable after transfection. As a control ethanol treatment induces EthD-1 uptake in most cells (inset). (F) Quantification of EthD-1-negative neurons shows no difference in cell viability between GFP-, DN-NFIL3- and NFIL3-expressing neurons.

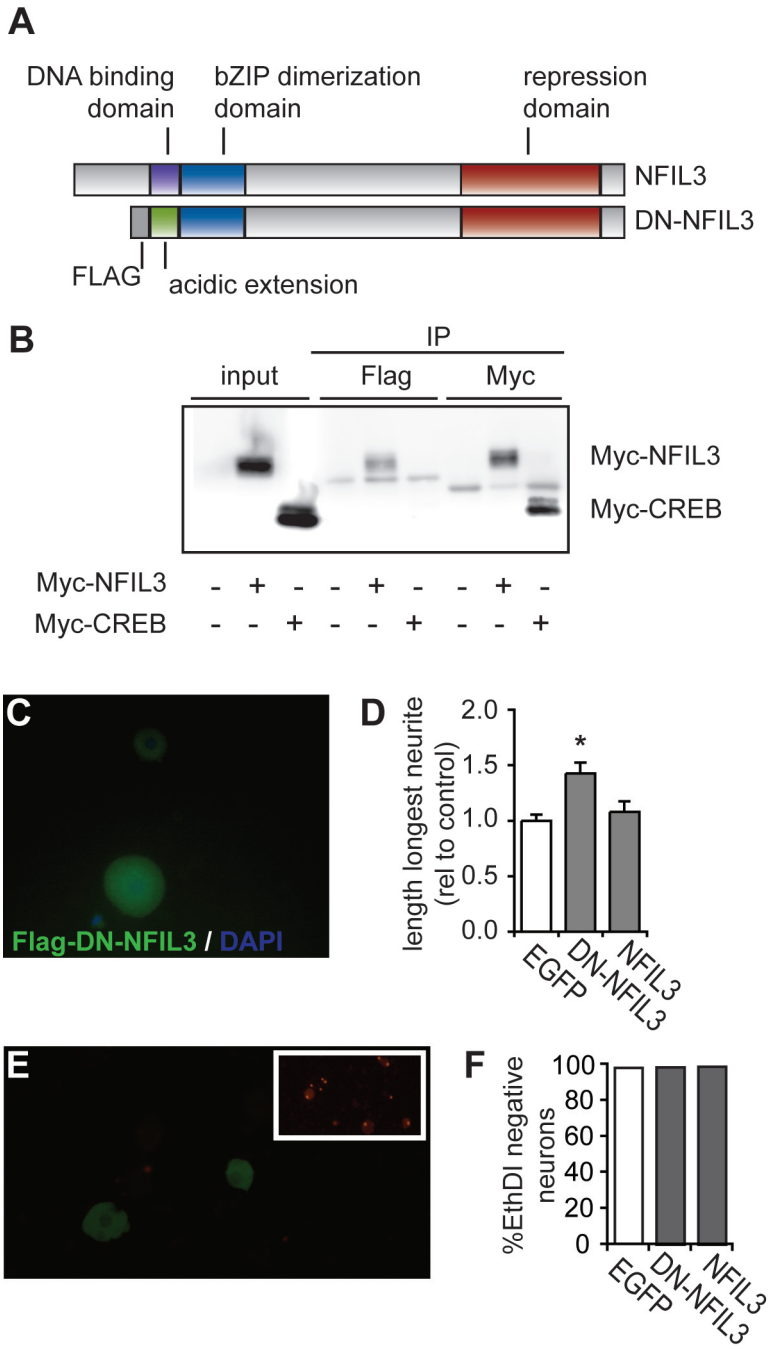
A
DNA binding domain
bZIP dimerization domain
repression domain
NFIL3
DN-NFIL3
FLAG
acidic extension
B
IP
input
Flag
Myc
Myc-NFIL3
Myc-CREB
Myc-NFIL3 - + - - + - - + -
Myc-CREB - - + - - + - - +
C
Flag-DN-NFIL3 / DAPI
D
length longest neurite (rel to control)
2.0
1.5
1.0
0.5
0.0
*
EGFP
DN-NFIL3
NFIL3
E
F
%EthDI negative neurons
100
80
60
40
20
0
EGFP
DN-NFIL3
NFIL3

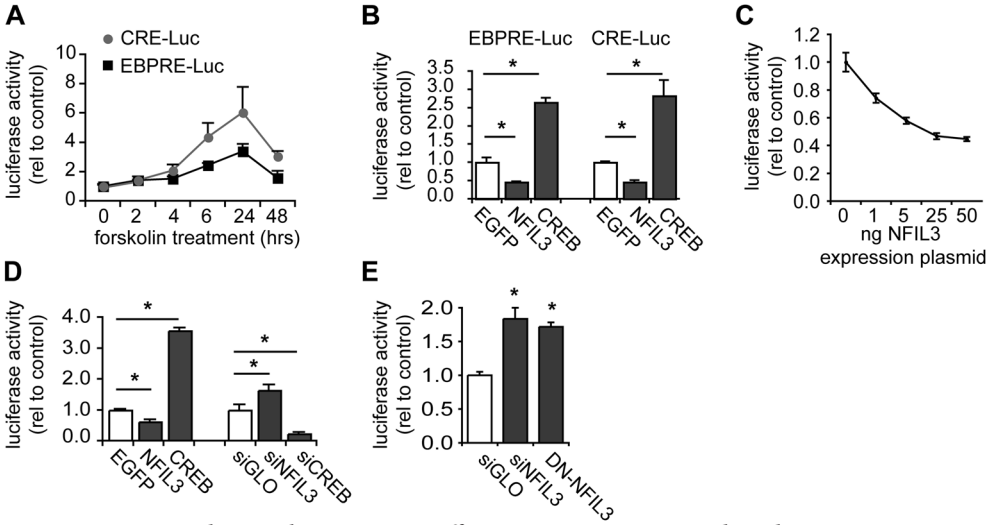

Figure 5. NFIL3 and CREB have opposite effects on CRE/EBPRE-mediated gene transcription. (A) Forskolin induces EBPRE- and CRE-mediated transcriptional activity in F11 cells. F11 cells were transfected with either the EBPRE or the CRE reporter construct and stimulated with forskolin for indicated times. Normalized luciferase activities are plotted (means ± SD; n = 3 for each condition). (B) Luciferase assays in HEK293 cells showing the effects of overexpression of CREB and NFIL3 on forskolin-stimulated transcriptional activity. CREB activates both CRE and EBPRE sites, whereas NFIL3 represses both sites. Bars represent means ± SD; n = 3 for each condition; * $p < 0.01$. (C) Co-expression of CREB with increasing amounts of NFIL3 shows a dose-dependent repression by NFIL3 of CREB-mediated EBPRE-luciferase activity. (D) Luciferase assays in forskolin-stimulated F11 cells showing that EBPRE activity is repressed by overexpression of NFIL3 and enhanced by overexpression of CREB. Moreover, knockdown of endogenous NFIL3 and CREB expression by siRNAs produced opposite effects on luciferase activity, confirming that CREB activates EBPRE sites, whereas NFIL3 represses EBPRE sites. (E) In primary adult DRG neurons, both knockdown of NFIL3 and overexpression DN-NFIL3 enhance EBPRE-luciferase activity.

Nfil3, we cloned the predicted binding site regions of all three genes in luciferase reporter plasmids (Figure 6C). These reporter plasmids were introduced in HEK293 cells, which lack endogenous NFIL3 expression. Expression of the reporters alone resulted in an increase in luciferase activity compared with empty luciferase constructs, but co-expression of NFIL3 almost completely reduced luciferase activity to basal levels (Figure 6C). Importantly, a peripheral myelin P0 promoter-luciferase construct which lacks EBPRE sites (Brown and Lemke, 1997) was not repressed by NFIL3. These data show that in addition to the direct binding of NFIL3 to EBPRE sites in these genes, NFIL3 represses gene transcription mediated by these sites, indicating that NFIL3 is a repressor of regeneration-associated gene expression. The observed transcriptional repression of the *Nfil3* gene by NFIL3 furthermore suggests the presence of a direct negative feedback loop.

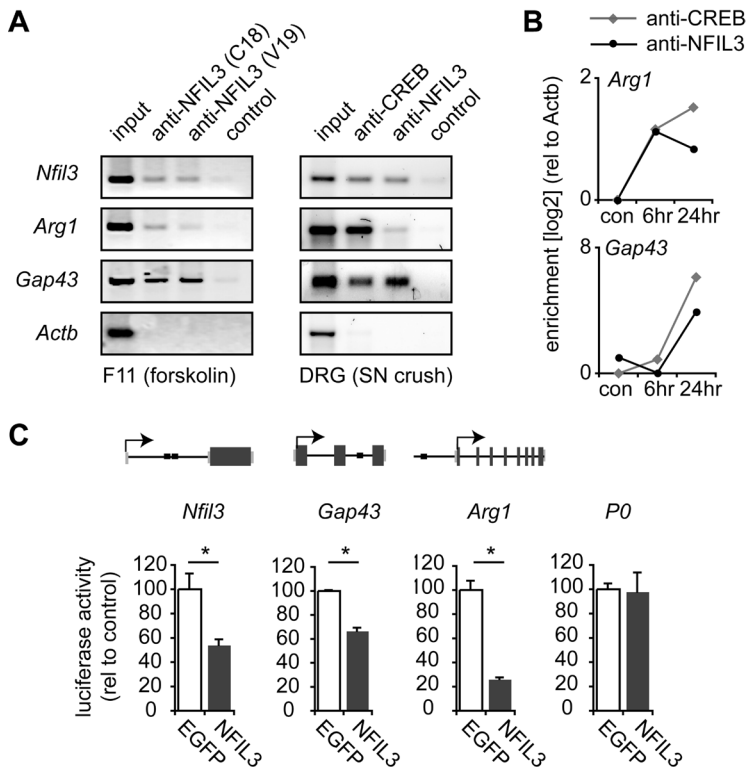

Figure 6. NFIL3 binds to and represses transcription of regeneration-associated genes.
(A) Chromatin immunoprecipitation assay demonstrating NFIL3 binding to promoter regions of *Nfil3*, *Arg1* and *Gap43* in F11 cells overexpressing NFIL3. Two different NFIL3 antibodies were used that both precipitated all three promoters. No immunoprecipitation was observed in the absence of antibodies or for a negative control gene (*Actb*). (B) Chromatin immunoprecipitation assay demonstrating both phospho-CREB and NFIL3 binding to promoter regions of *Nfil3*, *Arg1* and *Gap43* in DRG neurons two days after sciatic nerve crush. All three promoters bind both phospho-CREB and NFIL3. No immunoprecipitation was observed in the absence of antibodies or for a negative control gene (*Actb*). (B) Quantitative ChIP- showing phospho-CREB and NFIL3 occupancy at the *Arg1* and *Gap43* promoters 6 – 24 hours after sciatic nerve crush, and not in control, unlesioned DRGs. (C) Schematic diagrams of the *Nfil3*, *Gap43* and *Arg1* genes indicating predicted EBPRE sites (black boxes). Indicated are coding exon regions (dark grey boxes), untranslated exon regions (light grey boxes), introns (black lines) and transcription start sites (arrows). Genomic fragments of the *Nfil3*, *Gap43* and *Arg1* genes containing predicted EBPRE sites were cloned into the pGL2-B-luciferase plasmid. Luciferase assays show that these constructs are transcriptionally active in HEK293 cells (white bars), and that transcriptional activity is repressed when NFIL3 is co-transfected (grey bars). Activity of the *P0* promotor is not repressed by NFIL3. Bars represent means ± SEM; n = 3 for each condition; * $p < 0.01$.

Discussion

Axonal damage to neurons in the PNS activates a gene response which enables the injured neuron to successfully regenerate and re-innervate targets (Skene, 1989; Smith and Skene, 1997; Gao *et al.*, 2004; Raivich and Makwana, 2007). The coordination of this gene expression program probably requires tight transcriptional regulation, but the underlying transcriptional regulatory mechanisms remain largely unknown. Here, we identify NFIL3 as a novel transcriptional repressor of CREB-mediated gene transcription, and we demonstrate that NFIL3 and CREB form a transcription network motif, which is involved in the regulation of neuronal regeneration-associated genes.

Based on previously published *in vivo* gene expression data (Stam *et al.*, 2007) we investigated the role of 62 TFs in neurite outgrowth from DRG-like F11 cells. This resulted in the identification of ten TFs that significantly affect neurite outgrowth following siRNA-mediated knockdown. Nine of these have not previously been implicated in neuronal regeneration. The number of positive hits (10 out of 62) may seem relatively low given that all 62 TFs were selected based on *in vivo* gene expression data. This might be due to (i) the fact that regulation of some TFs is the result rather than the cause of regeneration, (ii) limitations of F11 cells as a model for *in vivo* neuronal regeneration, (iii) redundancy or synergism in TF functions that prevented their detection because we did not knockdown TFs in combination, and (iv) the stringent selection criteria that were applied in order to eliminate false-positives. Nevertheless, the finding of nine novel putative transcriptional regulators of neuronal outgrowth is exciting and may shed new light on transcriptional regulatory mechanisms underlying neuronal regeneration.

Paradoxically, we did not always observe a positive correlation between TF gene regulation *in vivo* and the siRNA-induced effect on neurite outgrowth *in vitro*. For instance, knockdown of both NFIL3 and CSRP3 enhanced neurite outgrowth, even though these factors are upregulated during successful regeneration. Little if anything is known about the possible roles of these TFs in neuronal outgrowth, but it is intriguing that regenerating neurons upregulate TFs that have inhibitory roles in the process of neurite outgrowth. To further address this issue in detail, we studied the transcriptional regulatory functions of NFIL3 in cell lines, in adult primary DRG neurons, and *in vivo* after sciatic nerve crush. Interestingly, NFIL3 belongs to the same class of TFs as CREB, which is known to stimulate DRG neuron regeneration (Qiu *et al.*, 2002; Gao *et al.*, 2004). Our data show that NFIL3 expression follows phospho-CREB induction in DRG neurons. The *Nfil3* gene contains two functional EBPRE sites, which according to our data can also bind CREB. Although recent genome-wide promoter binding studies failed to identify the *Nfil3* gene as a direct CREB target in PC12 and HEK293 cells (Impey *et al.*, 2004; Zhang *et al.*, 2005), we suggest that in DRG neurons *Nfil3* gene expression is regulated by the cAMP-CREB pathway. In line with this suggestion, we found that PKA inhibition suppressed *Nfil3* mRNA levels in primary adult DRG neurons and that CREB binds the

Nfil3 promoter *in vivo* after a SN crush. Another important finding in our study is that NFIL3 competes with CREB for EBPRE and CRE motifs in the promoters of regeneration-associated genes. These sites appear to be functionally equivalent: CREB enhances gene expression via both sites, whereas NFIL3 represses gene expression via both sites. These results are consistent with a model in which, as part of the cAMP-regulated gene program, NFIL3 is upregulated to exert control over the CREB-mediated transcriptional response (Figure 7).

A gene regulatory network motif in which one TF in parallel activates a set of target genes, and a negative regulator that subsequently represses the same target genes, is referred to as a type I incoherent feed-forward loop and is frequently detected in genetic model organisms (Mangan and Alon, 2003; Alon, 2007). Computational modelling and experimental studies in bacteria both showed that type 1 incoherent feed-forward loops efficiently control the dynamics of target gene expression by accelerating target gene response time and generating non-monotonic pulses of target gene expression (Mangan and Alon, 2003; Mangan *et al.*, 2006; Kaplan *et al.*, 2008). Thus, the paradoxical upregulation of NFIL3 during successful neuronal regeneration, even though it suppresses neurite outgrowth, can be explained by the fact that NFIL3 and CREB co-evolved to form a functionally important gene regulatory network motif. Apparently, appropriate temporal regulation of growth-promoting genes by the cAMP-CREB pathway requires the induction of NFIL3 as a feed-forward repressor.

Individual components of gene regulatory network motifs often acquire different functions in different species and cellular systems (Babu *et al.*, 2007; Tuch *et al.*, 2008). Indeed, NFIL3 shows functional diversity in different organisms and cell types. This was first described in *C. elegans*, where the NFIL3 orthologue CES-2 (cell death selector-2) has differential effects on target genes and cell morphogenesis or apoptosis in different

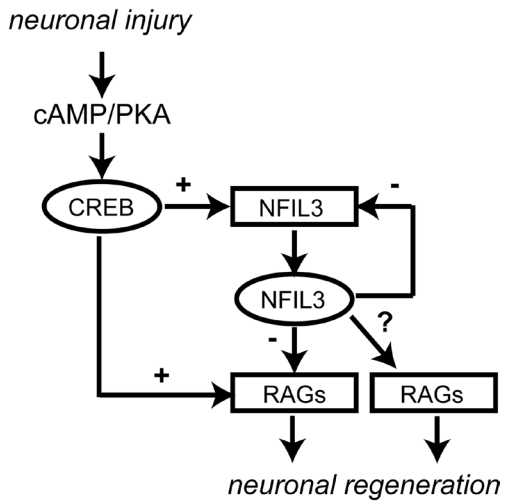

Figure 7. Model for the role of NFIL3 in regulating regeneration-associated gene expression.
Our data indicate that CREB and NFIL3 form a incoherent transcriptional feed-forward loop. Elevation of cAMP levels triggered by peripheral neuronal injury activates PKA and CREB. CREB then activates regeneration-associated genes (RAGs) containing CRE/EBPRE sites, including Nfil3. NFIL3 acts as a negative regulator on CRE/EBPRE-mediated transcription. At this moment we cannot exclude the possibility that NFIL3 in parallel regulates the expression of other regeneration-associated genes, independent of CREB.

cell types (Metzstein *et al.*, 1996; Wang and Chamberlin, 2002; Wang *et al.*, 2006). In the mammalian circadian clock, NFIL3 acts as a transcriptional repressor, and regulates the complex diurnal oscillating expression patterns of clock genes (Doi *et al.*, 2001; Mitsui *et al.*, 2001). In lymphoid tissues NFIL3 has a strong anti-apoptotic effect (Ikushima *et al.*, 1997; Kuribara *et al.*, 1999), and in developing chick spinal cord motor neurons NFIL3 overexpression promotes survival and axonal growth (Junghans *et al.*, 2004). These latter findings seem contradictory to ours; however, we clearly show with two independent methods (RNA interference and dominant-negative expression) that loss of NFIL3 function stimulates outgrowth of adult DRG neurons, and that neither overexpression nor inhibition of NFIL3 affects DRG neuron survival. Taken together, we conclude that the precise role of NFIL3 in gene regulatory networks appears to depend on the cell type and the developmental stage. Also, we cannot exclude that the function of NFIL3 differs in different species.

In conclusion, we show that NFIL3 is a suppressor of regenerative DRG neuron outgrowth. Together with CREB, NFIL3 forms an incoherent transcriptional feed-forward loop controlling the expression of regeneration-associated genes. These findings provide for the first time insight into the architecture of transcriptional regulatory networks that underlie neuronal regeneration, and highlight the importance of transcriptional repressors in determining a neuron's regenerative response. Other regeneration-associated TFs may be subject to similar negative regulatory control mechanisms. For instance, suppressor of cytokine signaling-3 (SOCS3) is upregulated by injured DRG neurons, and negatively regulates STAT3 function and neurite outgrowth (Miao *et al.*, 2006). Clearly, further insight into transcription regulatory network interactions is indispensable for our understanding of how neuronal regeneration is regulated at the level of gene expression.

Materials and methods

Cell culture and transfections

F11 and HEK293 cells were maintained as described (Stam *et al.*, 2007). F11 cells were transfected with Dharmacon siGENOME siRNA SMARTpools using the DharmaFECT 3 transfection reagent according to the manufacturer's instructions (Dharmacon, Lafayette, CO). For transfection with DNA plasmids Lipofectamine 2000 Reagent (Invitrogen, San Diego, CA) was used. Dissection and dissociation of primary adult DRG neurons was carried out as described (Stam *et al.*, 2007). Dissociated neurons were transfected using the Nucleofector 96-well system (Amaxa Biosystems, Cologne, Germany) according to the manufacturer's protocol. After nucleofection, neurons were immediately plated on poly-L-lysine and laminin coated 8-well chambers (Lab-Tek). After 40 hours in culture neurons were fixed and immunostained. The longest neurite of each of 100-200 neurons was measured. For survival assays, DRG cultures were incubated 30 minutes prior to fixation in medium containing 2 μM ethidium homodimer-1 (EthD-1; Invitrogen). GFP

expressing neurons were inspected and the number of EthDI negative neurons was assessed as a measure for the percentage of viable neurons.

High-content screening

F11 cells were cultured in 96-well plates and transfected with Dharmacon siGENOME siRNA SMARTpools, including three negative controls (siCONTROL non-targeting pool; siGLO RISC-free siRNA; transfection without siRNA) as well as one positive control (siATF3). Outgrowth was induced 4 hours after transfection by replacing the medium with DMEM containing 0.5% FCS and 10 μM forskolin. After 2 days cells were fixed and stained. Neurite outgrowth was quantified using a Cellomics KineticScan HCS Reader and the Neuronal Profiling Bioapplication (Cellomics Inc., Pittsburgh, PA, USA). Per well 500-1,000 cells were analyzed and neurite total length per cell (cell-based analysis) and the percentage of cells per well having a neurite average length of >25 μm (population-based analysis) were calculated.

Statistics and target selection

Statistical significance was determined per plate by One-Way ANOVA and Kruskal Wallis test for cell-based features and by One-Way ANOVA only for well-based features. A Dunnett's post-hoc test was used for ANOVA analyses. Post-hoc multiple comparison's tests for Kruskal Wallis analyses were performed as described by Siegel and Castellan (1988). siRNA effects were compared to one of the controls (usually siGLO) and deemed significant when $p < 0.01$. In addition to the statistical significance criterion, hits were only selected when the size effect of the siRNA was larger than 1 standard deviation of all combined negative controls throughout the screen. All positive hits were replicated 2-3 times using the siRNA pools, and a selection of 13 positive hits were also replicated using the four individual siRNAs that comprise each siRNA pool.

Expression constructs

Full-length rat NFIL3 cDNA was PCR amplified from rat whole-brain cDNA and inserted into the pcDNA3.1 expression vector (Invitrogen). The pCMV-Myc-CREB plasmid was kindly provided by Dr. A. Riccio (Johns Hopkins University School of Medicine, Baltimore, MD). For generation of the NFIL3 dominant-negative inhibitor, the C-terminal portion of NFIL3 including the leucine zipper was inserted into pcDNA3.1, and was modified to contain an N-terminal Flag epitope followed by a Φ10 sequence and an acidic extension as described (Ahn *et al.*, 1998).

Animals and surgical procedures

Adult male Wistar rats were subjected to either sciatic nerve or dorsal root crush for indicated time-points. L4-6 DRGs were isolated and stored at -80° C until use for qPCR, western blot or in situ hybridization. All procedures were performed as previously de-

scribed (Stam *et al.*, 2007).

RNA isolation and quantitative real-time PCR

Total RNA was isolated using Trizol (Invitrogen) and reverse transcribed with moloney murine leukemia virus reverse transcriptase (MMLV-RT; Invitrogen). Quantitative RT-PCR was performed on the ABI 7900HT detection system (Applied Biosystems, Foster City, CA, USA) with the 2x SYBR green ready reaction mix (Applied Biosystems). GAPDH and NSE transcripts were measured for normalization.

Western blot analysis

Cells were directly lysed in 1x Laemmli sample buffer and run on a 10% SDS-PAGE gel. Proteins were blotted onto a PVDF membrane (Bio-Rad Laboratories, Hercules, CA), blocked with 5% low-fat milk, 1% Tween-20 in PBS. Membranes were incubated with phospho-CREB (Ser133), anti-CREB (both from Cell Signaling Technology, Danvers, MA) or anti-NFIL3 antibody (V19; Santa Cruz Biotechnology, Santa Cruz, CA), washed three times with PBS-T (PBS with 1% Tween-20) and incubated with alkaline phosphatase-conjugated secondary antibodies (DAKO, Glostrup, Denmark). Immunoreactivity was analyzed using the ECF detection system (Amersham Biosciences, Piscataway, NJ).

Luciferase assays

The pTK-EBPRE vector was a kind gift of Dr. S. Tetradis (UCLA School of Dentistry, Los Angeles, CA). The SST-Luciferase vector was a kind gift of Dr. S. Herzig (University of Kiel, Germany). The *Nfil3*-, *Gap43*- and *Arg1*-luciferase constructs were created by inserting a ~1kb fragment encompassing the predicted EBPREs into the pGL2-BASIC-luciferase plasmid (Invitrogen). F11 or HEK293 cells were transfected with indicated constructs/siRNAs and medium was replaced with DMEM containing 0.5% FCS and antibiotics with or without 10 μM forskolin the next day. Primary DRG neurons were transfected with indicated constructs and siRNAs using nucleofection as described. After 2 days, cells were lysed with Steady-Glo luciferase lysis buffer (Promega, Madison, WI) and luciferase activity was analyzed with a luminometer (Wallac Victor 1420 Luminometer; Perkin Elmer, Waltham, MA). The luminescent signal was corrected for transfection efficiency using lacZ measurement. Experiments were carried out in triplicate and each experiment was repeated 2-3 times.

Chromatin immunoprecipitation (ChIP)

ChIP experiments were performed on F11 cells transiently expressing NFIL3 and on rat L4-6 DRGs that had received a sciatic nerve crush. Cells/tissues were isolated and chromatin was cross-linked with 1% formaldehyde for 10 minutes and subsequently quenched with 125 mM glycine for 5 minutes. DRGs were then homogenized in homogenization

buffer (0.35 M sucrose, 5 mM HEPES/NaOH pH7.4) using a dounce homogenizer. Cells were pelleted and washed with cold PBS, nuclei were lysed with SDS lysis buffer (1% SDS, 10 mM EDTA in 20 mM Tris-HCl). F11 cells were washed and lysed without homogenization. Cross-linked chromatin was sheared with 4 pulses of 15 sec each, yielding products of 200-1,000 bp long. Immunoprecipitation was performed with NFIL3 (C18 and V19, Santa Cruz Biotechnology) or phospho-CREB (Ser133) (Cell Signaling Technology, Danvers, MA) antibodies overnight with rotation at 4°C. Immuno-complexes were captured with protein A/G beads (Santa Cruz Biotechnology) pre-incubated with sonicated salmon sperm DNA, washed, and eluted with elution buffer (1% SDS, 100 mM $NaHCO_3$). The eluates were proteinase K treated (215 µg/ml) and incubated overnight at 65°C. DNA was purified by phenol/chloroform extraction and subsequent ethanol precipitation. IP and input fractions were analyzed by PCR with primers flanking the predicted EBPRE/CRE sites of *Arg1* (5'-CAAAGCTGTTCGGTTCTTGA-3 and 5'-GCTTTGGTCTCCTGAATCGT-3'), *Nfil3* (5'-GTTTGATGGTGAGGCCAGAG-3' and 5'-CTACAACGGCGACCAAAAC-3'), *Gap43* (5'-TGCTCAGAATGCTTGACTGC-3' and 5'-CCACAAGAAGGAAAATGCAAA-3') and *Actb* as a negative control region (5'-AGAGCAAGAGAGGCATCCTG-3' and 5'-GGGTCATCTTTTCACGGTTGG-3'). DNA was amplified using HotStart Taq polymerase (Eppendorf), using the following cycling conditions; 10min at 95^0C, then 35 - 40 cycles of 30s 95^0C, 30s 58^0C and 30s 65^0C. Resulting PCR products were run on 3% agarose gels. Real-time qPCR analysis was performed as described above. Enrichment was calculated as $(Ct_{target,mock} - Ct_{target,IP}) - (Ct_{Actb,mock} - Ct_{Actb,IP})$.

References

Ahn S, Olive M, Aggarwal S, Krylov D, Ginty DD, Vinson C (1998) A dominant-negative inhibitor of CREB reveals that it is a general mediator of stimulus-dependent transcription of c-fos. Mol Cell Biol 18:967-977.

Alon U (2007) Network motifs: theory and experimental approaches. Nat Rev Genet 8:450-461.

Babu MM, Balaji S, Aravind L (2007) General trends in the evolution of prokaryotic transcriptional regulatory networks. Genome Dyn 3:66-80.

Blais A, Dynlacht BD (2005) Constructing transcriptional regulatory networks. Genes Dev 19:1499-1511.

Boland LM, Dingledine R (1990) Expression of sensory neuron antigens by a dorsal root ganglion cell line, F-11. Brain Res Dev Brain Res 51:259-266.

Bomze HM, Bulsara KR, Iskandar BJ, Caroni P, Skene JH (2001) Spinal axon regeneration evoked by replacing two growth cone proteins in adult neurons. Nat Neurosci 4:38-43.

Bonilla IE, Tanabe K, Strittmatter SM (2002) Small proline-rich repeat protein 1A is expressed by axotomized neurons and promotes axonal outgrowth. J Neurosci 22:1303-1315.

Broude E, McAtee M, Kelley MS, Bregman BS (1997) c-Jun expression in adult rat dorsal root ganglion neurons: differential response after central or peripheral axotomy. Exp Neurol 148:367-377.

Brown AM, Lemke G (1997) Multiple regulatory elements control transcription of the peripheral myelin protein zero gene. J Biol Chem 272:28939-28947.

Cafferty WB, McGee AW, Strittmatter SM (2008) Axonal growth therapeutics: regeneration or sprouting or plasticity? Trends Neurosci 31:215-220.

Cai D, Deng K, Mellado W, Lee J, Ratan RR, Filbin MT (2002) Arginase I and polyamines act downstream from cyclic AMP in overcoming inhibition of axonal growth MAG and myelin *in vitro*. Neuron 35:711-719.

Chong MS, Woolf CJ, Haque NS, Anderson PN (1999) Axonal regeneration from injured dorsal roots into the spinal cord of adult rats. J Comp Neurol 410:42-54.

Doi M, Nakajima Y, Okano T, Fukada Y (2001) Light-induced phase-delay of the chicken pineal circadian clock is associated with the induction of cE4bp4, a potential transcriptional repressor of cPer2 gene. Proc Natl Acad Sci U S A 98:8089-8094.

Francel PC, Harris K, Smith M, Fishman MC, Dawson G, Miller RJ (1987) Neurochemical characteristics of a novel dorsal root ganglion X neuroblastoma hybrid cell line, F-11. J Neurochem 48:1624-1631.

Frey D, Laux T, Xu L, Schneider C, Caroni P (2000) Shared and unique roles of CAP23 and GAP43 in actin regulation, neurite outgrowth, and anatomical plasticity. J Cell Biol 149:1443-1454.

Gao Y, Deng K, Hou J, Bryson JB, Barco A, Nikulina E, Spencer T, Mellado W, Kandel ER, Filbin MT (2004) Activated CREB is sufficient to overcome inhibitors in myelin and promote spinal axon regeneration *in vivo*. Neuron 44:609-621.

Ghil SH, Kim BJ, Lee YD, Suh-Kim H (2000) Neurite outgrowth induced by cyclic AMP can be modulated by the alpha subunit of Go. J Neurochem 74:151-158.

Hanz S, Perlson E, Willis D, Zheng JQ, Massarwa R, Huerta JJ, Koltzenburg M, Kohler M, van-Minnen J, Twiss JL, Fainzilber M (2003) Axoplasmic importins enable retrograde injury signaling in lesioned nerve. Neuron 40:1095-1104.

Ikushima S, Inukai T, Inaba T, Nimer SD, Cleveland JL, Look AT (1997) Pivotal role for the NFIL3/E4BP4 transcription factor in interleukin 3-mediated survival of pro-B lymphocytes. Proc Natl Acad Sci U S A 94:2609-2614.

Impey S, McCorkle SR, Cha-Molstad H, Dwyer JM, Yochum GS, Boss JM, McWeeney S, Dunn JJ, Mandel G, Goodman RH (2004) Defining the CREB regulon: a genome-wide analysis of transcription factor regulatory regions. Cell 119:1041-1054.

Jankowski MP, Cornuet PK, McIlwrath S, Koerber HR, Albers KM (2006) SRY-box containing gene 11 (Sox11) transcription factor is required for neuron survival and neurite growth. Neuroscience 143:501-514.

Junghans D, Chauvet S, Buhler E, Dudley K, Sykes T, Henderson CE (2004) The CES-2-related transcription factor E4BP4 is an intrinsic regulator of motoneuron growth and survival. Development 131:4425-4434.

Kaplan S, Bren A, Dekel E, Alon U (2008) The incoherent feed-forward loop can generate non-monotonic input functions for genes. Mol Syst Biol 4:203.

Kuribara R, Kinoshita T, Miyajima A, Shinjyo T, Yoshihara T, Inukai T, Ozawa K, Look AT, Inaba T (1999) Two distinct interleukin-3-mediated signal pathways, Ras-NFIL3 (E4BP4) and Bcl-xL, regulate the survival of murine pro-B lymphocytes. Mol Cell Biol 19:2754-2762.

Lee TI *et al.* (2002) Transcriptional regulatory networks in Saccharomyces cerevisiae. Science 298:799-804.

Mangan S, Alon U (2003) Structure and function of the feed-forward loop network motif. Proc Natl Acad Sci U S A 100:11980-11985.

Mangan S, Itzkovitz S, Zaslaver A, Alon U (2006) The incoherent feed-forward loop accelerates the response-time of the gal system of Escherichia coli. J Mol Biol 356:1073-

1081.

Metzstein MM, Hengartner MO, Tsung N, Ellis RE, Horvitz HR (1996) Transcriptional regulator of programmed cell death encoded by Caenorhabditis elegans gene ces-2. Nature 382:545-547.

Miao T, Wu D, Zhang Y, Bo X, Subang MC, Wang P, Richardson PM (2006) Suppressor of cytokine signaling-3 suppresses the ability of activated signal transducer and activator of transcription-3 to stimulate neurite growth in rat primary sensory neurons. J Neurosci 26:9512-9519.

Mitsui S, Yamaguchi S, Matsuo T, Ishida Y, Okamura H (2001) Antagonistic role of E4BP4 and PAR proteins in the circadian oscillatory mechanism. Genes Dev 15:995-1006.
Montminy MR, Sevarino KA, Wagner JA, Mandel G, Goodman RH (1986) Identification of a cyclic-AMP-responsive element within the rat somatostatin gene. Proc Natl Acad Sci U S A 83:6682-6686.

Moore DL, Blackmore MG, Hu Y, Kaestner KH, Bixby JL, Lemmon VP, Goldberg JL (2009) KLF family members regulate intrinsic axon regeneration ability. Science 326:298-301.

Neumann S, Woolf CJ (1999) Regeneration of dorsal column fibers into and beyond the lesion site following adult spinal cord injury. Neuron 23:83-91.

Ozkurt IC, Tetradis S (2003) Parathyroid hormone-induced E4BP4/NFIL3 down-regulates transcription in osteoblasts. J Biol Chem 278:26803-26809.

Platika D, Boulos MH, Baizer L, Fishman MC (1985) Neuronal traits of clonal cell lines derived by fusion of dorsal root ganglia neurons with neuroblastoma cells. Proc Natl Acad Sci U S A 82:3499-3503.

Qiu J, Cafferty WB, McMahon SB, Thompson SW (2005) Conditioning injury-induced spinal axon regeneration requires signal transducer and activator of transcription 3 activation. J Neurosci 25:1645-1653.

Qiu J, Cai D, Dai H, McAtee M, Hoffman PN, Bregman BS, Filbin MT (2002) Spinal axon regeneration induced by elevation of cyclic AMP. Neuron 34:895-903.

Raivich G, Makwana M (2007) The making of successful axonal regeneration: genes, molecules and signal transduction pathways. Brain Res Rev 53:287-311.

Raivich G, Bohatschek M, Da Costa C, Iwata O, Galiano M, Hristova M, Nateri AS, Makwana M, Riera-Sans L, Wolfer DP, Lipp HP, Aguzzi A, Wagner EF, Behrens A (2004) The AP-1 transcription factor c-Jun is required for efficient axonal regeneration. Neuron 43:57-67.

Seijffers R, Allchorne AJ, Woolf CJ (2006) The transcription factor ATF-3 promotes neurite outgrowth. Mol Cell Neurosci 32:143-154.

Seijffers R, Mills CD, Woolf CJ (2007) ATF3 increases the intrinsic growth state of DRG neurons to enhance peripheral nerve regeneration. J Neurosci 27:7911-7920.

Siegel S, Castellan NJ (1988) Nonparametric statistics for the behavioural sciences (2nd edition). New York: McGraw-Hill.

Skene JH (1989) Axonal growth-associated proteins. Annu Rev Neurosci 12:127-156.
Smith DS, Skene JH (1997) A transcription-dependent switch controls competence of adult neurons for distinct modes of axon growth. J Neurosci 17:646-658.

Stam FJ, MacGillavry HD, Armstrong NJ, de Gunst MC, Zhang Y, van Kesteren RE, Smit AB, Verhaagen J (2007) Identification of candidate transcriptional modulators involved in successful regeneration after nerve injury. Eur J Neurosci 25:3629-3637.

Tegner J, Bjorkegren J (2007) Perturbations to uncover gene networks. Trends Genet 23:34-41.

Teng FY, Tang BL (2006) Axonal regeneration in adult CNS neurons--signaling molecules and pathways. J Neurochem 96:1501-1508.

Tuch BB, Li H, Johnson AD (2008) Evolution of eukaryotic transcription circuits. Science 319:1797-1799.

Wang X, Chamberlin HM (2002) Multiple regulatory changes contribute to the evolution of the Caenorhabditis lin-48 ovo gene. Genes Dev 16:2345-2349.

Wang X, Jia H, Chamberlin HM (2006) The bZip proteins CES-2 and ATF-2 alter the timing of transcription for a cell-specific target gene in C. elegans. Dev Biol 289:456-465.
Yiu G, He Z (2006) Glial inhibition of CNS axon regeneration. Nat Rev Neurosci 7:617-627.

Zhang X, Odom DT, Koo SH, Conkright MD, Canettieri G, Best J, Chen H, Jenner R, Herbolsheimer E, Jacobsen E, Kadam S, Ecker JR, Emerson B, Hogenesch JB, Unterman T, Young RA, Montminy M (2005) Genome-wide analysis of cAMP-response element binding protein occupancy, phosphorylation, and target gene activation in human tissues. Proc Natl Acad Sci U S A 102:4459-4464.

Supplementary Table and Figures

UniGene Cluster	Gene Name	Gene Symbol	TF / TM	TF-Associated Domains
Rn.11495	Amino-terminal enhancer of split	Aes	TF	wd repeat groucho/tle family transcription factor
Rn.3789	Ankyrin repeat domain 1 (cardiac muscle)	Ankrd1	TM	ank repeat domain
Rn.9664	Activating transcription factor 3	Atf3	TF	bZIP transcription factor
Rn.10784	Basic helix-loop-helix domain containing, class B3	Bhlhb3	TF	bHLH transcription factor
Rn.23255	Cyclin H	Ccnh	(TM)	
Rn.11345	Cysteine and glycine-rich protein 3	Csrp3	TM	
Rn.8402	Damage-specific DNA binding protein 1	Ddb1	TF	cpsf160 family transcription factor
Rn.11183	DNA-damage inducible transcript 3	Ddit3	TM	
Rn.161716	DEAD (Asp-Glu-Ala-Asp) box polypeptide 39	Ddx39	(TM)	DEAD box RNA helicase
Rn.107359	DEAH (Asp-Glu-Ala-His) box polypeptide 9 (predicted)	Dhx9_predicted	(TM)	DEAD box RNA helicase
Rn.88756	V-ets erythroblastosis virus E26 oncogene homolog 1 (avian)	Ets1	TF	ets family transcription factor
Rn.18397	Ets variant gene 5 (ets-related molecule) (predicted)	Etv5_predicted	(TF)	ets family transcription factor
Rn.201494	GLI-Kruppel family member GLI1	Gli1	TF	zinc finger transcription factor
Rn.22813	Germ cell-less homolog 1 (Drosophila)	Gmcl1	(TM)	similar to putative DNA binding protein RY-1
Rn.22422	Hairy and enhancer of split 5 (Drosophila)	Hes5	TF	bHLH transcription factor
Rn.10852	Hypoxia inducible factor 1, alpha subunit	Hif1a	(TF)	bHLH domain
Rn.3272	Inhibitor of DNA binding 2	Id2	TM	bHLH domain
Rn.2760	Inhibitor of DNA binding 3	Id3	TM	bHLH domain
Rn.23984	Immunoglobulin mu binding protein 2	Ighmbp2	TM	
Rn.36202	ISL1 transcription factor, LIM/homeodomain 1	Isl1	TF	zinc finger transcription factor
Rn.10026	Insulin related protein 2 (islet 2)	Isl2	TF	LIM/homeobox transcription factor
Rn.93714	Jun oncogene	Jun	TF	bZIP transcription factor
Rn.7719	Kruppel-like factor 4 (gut)	Klf4	TF	Krueppel family transcription factor
Rn.102325	Kruppel-like factor 7 (ubiquitous) (predicted)	Klf7_predicted	(TF)	Krueppel family transcription factor
Rn.48696	Lipolysis stimulated lipoprotein receptor	Lsr	TF	bHLH transcription factor
Rn.2592	Mitogen activated protein kinase 3	Mapk3	TM	
Rn.6775	Multiple endocrine neoplasia 1	Men1	(TM)	
Rn.20005	Metal response element binding transcription factor 1 (predicted)	Mtf1_predicted	(TF)	zinc finger transcription factor
Rn.54147	Nuclear factor, interleukin 3 regulated	Nfil3	TF	bZIP transcription factor
Rn.88129	Nuclear receptor subfamily 4, group A, member 2	Nr4a2	TF	nuclear receptor
Rn.7274	PDZ and LIM domain 7	Pdlim7		LIM domain
Rn.17591	Paired-like homeodomain transcription factor 2	Pitx2	TF	paired homeobox transcription factor
Rn.18446	Praja 2, RING-H2 motif containing	Pja2		RING-H2 domain
Rn.3290	Polymerase (DNA directed), epsilon 3 (p17 subunit)	Pole3	TF	polymerase
Rn.82733	POU domain, class 3, transcription factor 2	Pou3f2	TF	POU domain transcription factor
Rn.198983	POU domain, class 4, transcription factor 1	Pou4f1	TF	POU domain transcription factor
Rn.10189	Paired related homeobox protein-like 1	Prrxl1	TF	paired homeobox transcription factor
Rn.55115	Retinoblastoma 1	Rb1	TM	retinoblastoma family protein
Rn.10879	RE1-silencing transcription factor	Rest	TF	
Rn.34221	Reversion induced LIM gene	Ril		LIM domain
Rn.98315	Regulator of telomere elongation helicase 1	Rtel1	(TM)	DNA helicase
Rn.198907	SAP30 binding protein (predicted)	Sap30bp_predicted	TM	
Rn.11258	Short stature homeobox 2	Shox2	TF	paired homeobox transcription factor
Rn.10635	MAD homolog 1 (Drosophila)	Smad1	TF	dwarfin/smad family transcription factor
Rn.128772	SWI/SNF related, matrix associated, actin dependent regulator of chromatin, subfamily a, member 5 (predicted)	Smarca5_predicted	(TM)	snf2/rad54 helicase family protein
Rn.10883	SRY-box containing gene 10	Sox10	TF	hmg box transcription factor
Rn.198857	Sterol regulatory element binding factor 1	Srebf1	TF	bHLH transcription factor
Rn.10247	Signal transducer and activator of transcription 3	Stat3	TF	stat family transcription factor
Rn.78891	Transcription elongation factor A (SII), 2	Tcea2	TF	transcription elongation factor
Rn.48516	Transcription elongation factor B (SIII), polypeptide 1	Tceb1	TF	transcription elongation factor
Rn.18770	Transcription elongation regulator 1 (CA150) (predicted)	Tcerg1_predicted	(TF)	transcription elongation factor
Rn.10600	Transcription factor 8	Tcf8	TF	zinc finger and homeobox transcription factor
Rn.10290	Transcription factor E2a	Tcfe2a	TF	bHLH transcription factor
Rn.24106	Transducin-like enhancer of split 3, E(spl) homolog (Drosophila)	Tle3	TM	wd repeat groucho/tle family transcription factor
Rn.45385	Transient receptor potential cation channel, subfamily C, member 3	Trpc3		ank repeat domain
Rn.21970	TSC22 domain family 3	Tsc22d3	TF	tsc-22/dip/bun family transcription factor
Rn.9637	Zinc finger protein 384	Zfp384	(TF)	Krueppel family transcription factor
Rn.105961	Zinc finger protein 422 (predicted)	Zfp422_predicted	(TF)	zinc finger domain
Rn.1772	Zinc finger protein 91	Zfp91	(TF)	zinc finger domain
Rn.11634	Zinc finger RNA binding protein	Zfr	(TR)	zinc finger RNA binding protein
Rn.98676	Zinc finger protein 213 (predicted)	Znf213_predicted	(TF)	Krueppel family transcription factor
Rn.163002	Zinc finger protein 291	Znf291	(TF)	zinc finger domain

Supplementary Table 1. Selection of 62 transcription factors tested in the neurite outgrowth screen.

Transcription factors were selected as described in Stam *et al.* (2007), and are indicated by UniGene cluster ID, gene name and gene symbol. TF and TM indicate whether genes represent transcription factors per se (i.e. factors that bind to DNA and regulated transcription directly) or transcriptional modulators (i.e. factors that regulate transcription indirectly). When indicated between bracktes, TF or TM annotation is based on sequence similarity with established factors. The presence of transcription factor-associated protein domains is indicated in the last column.

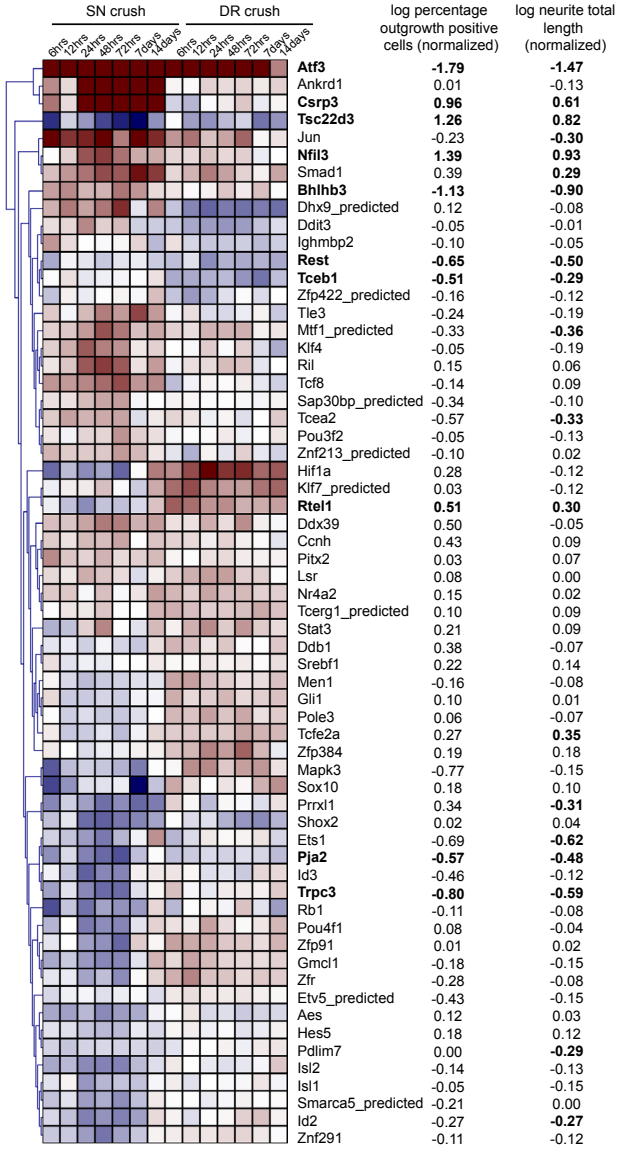

Supplementary Figure 1. Summary of neurite outgrowth screening results for 62 TFs.
The heatmap shows differential expression of 62 TF genes in DRG neurons following either SN crush or DR crush (Stam et al., 2007). Genes were hierarchically clustered based on expression. Colour encoding represents log fold change; red indicates up- and blue indicates down-regulated relative to control. The numbers on the right hand side represent log fold changes in either total neurite length or the percentage of outgrowth positive cells after knockdown. Bold numbers indicate statistically significant changes (see text for details).

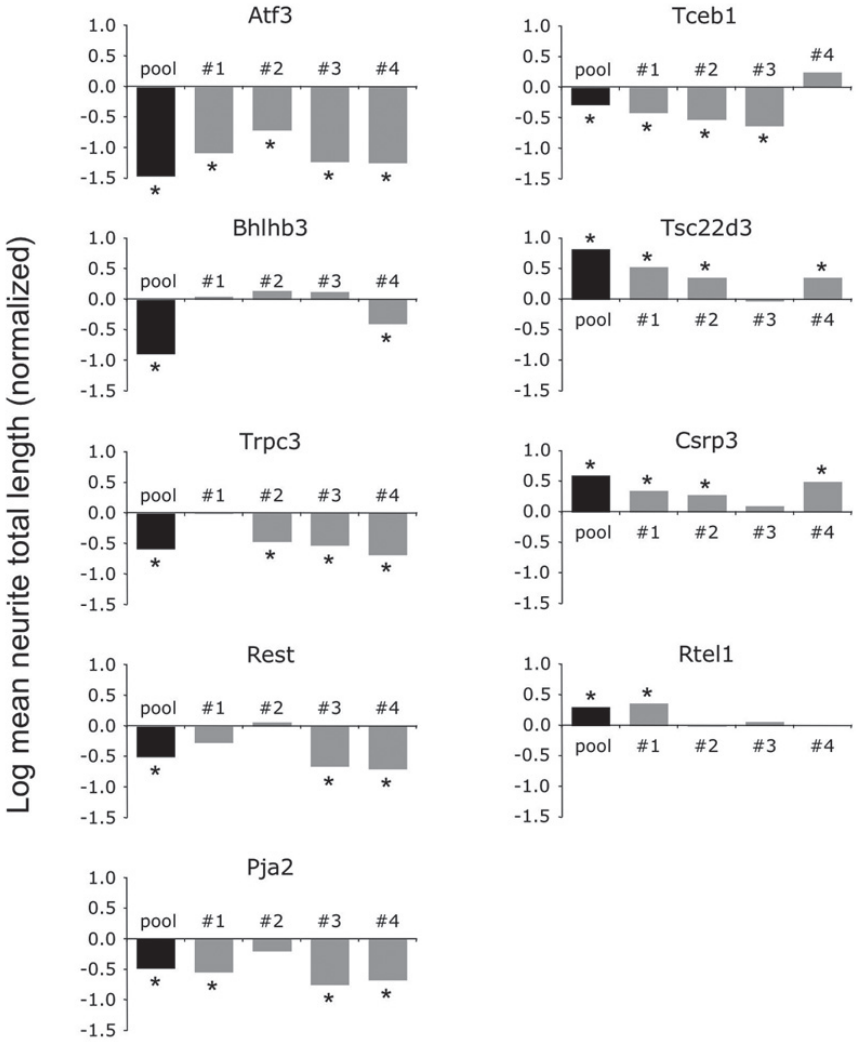

Supplementary Figure 2. Confirmation of Dharmacon SMART siRNA pool-induced effects on neurite outgrowth by individual siRNAs.

Effects of SMART siRNA pools that were significant in initial screens were validated by testing the effect of individual siRNAs on neurite outgrowth. Bars represent the normalized mean neurite total length. * $p < 0.05$. Validation of the NFIL3 siRNA pool is described in the main text and in Figures 3 and 4.

Chapter 3

Preliminary evidence that *in vivo* expression of a dominant-negative mutant of the transcription factor NFIL3 promotes regeneration of DRG neurons after a sciatic nerve crush lesion

Harold D. MacGillavry[1], Ruben Eggers[2], Erich M. Ehlert[2], Angelina Huseinovic[3], Bas Blits[3], August B. Smit[1], Joost Verhaagen[2], Ronald E. van Kesteren[1]

[1]Department of Molecular and Cellular Neurobiology, Center for Neurogenomics and Cognitive Research, Neuroscience Campus Amsterdam, VU University, De Boelelaan 1085, 1081 HV Amsterdam, The Netherlands
[2]Department of Neuroregeneration, Netherlands Institute for Neuroscience, Meibergdreef 47, 1105 BH Amsterdam, The Netherlands
[3]Amsterdam Molecular Therapeutics, Meibergdreef 61, 1105 BA Amsterdam

Abstract

Successful peripheral nerve regeneration depends on specific changes in neuronal gene expression that are required for the extension of nerve fibers and the restoration of function. The neuron-intrinsic regulation of this gene expression program by transcription factors is poorly understood. We have recently shown that the transcription factor NFIL3 is a repressor of regeneration-associated gene expression and that neurite outgrowth of cultured primary adult DRG neurons can be promoted by reducing the activity of NFIL3. To investigate the role of NFIL3 in axon regeneration *in vivo*, we used adeno-associated viral vectors to express a dominant-negative mutant form of NFIL3 (DN-NFIL3) in the sensory neurons of lumbar DRGs of adult rats, and examined the effect of DN-NFIL3 on the regeneration of peripheral nerve fibers in the sciatic nerve after a nerve crush. Preliminary results indicate that DN-NFIL3 increases the number of regenerating nerve fibers one week after a sciatic nerve crush. These observations provide the first *in vivo* evidence that functional interference with a transcriptional repressor of the regeneration-associated gene expression program promotes axonal regeneration.

Introduction

In the peripheral nervous system (PNS), axonal injury induces a neuron-intrinsic gene expression program that is a prerequisite for the successful and vigorous regrowth of injured axons and the re-innervation of target tissues. Coordinated changes in neuronal gene expression depend on retrograde signaling from the lesion site to the nucleus and eventually results in the (re)-expression of growth-promoting proteins (Smith and Skene, 1997; Hanz *et al.*, 2003). Several regeneration-associated proteins, including GAP-43, CAP-23 and SPRR1A, promote axonal growth following overexpression *in vivo* (Aigner *et al.*, 1995; Bomze *et al.*, 2001; Bonilla *et al.*, 2002).

Gene expression profiling studies showed that hundreds of genes are differentially regulated during successful regeneration (Costigan *et al.*, 2002; Xiao *et al.*, 2002; Schmitt *et al.*, 2003; Stam *et al.*, 2007 and Chapter 5 of this thesis). The coordinated expression of regeneration-associated genes is regulated by injury-associated transcription factors (TFs). Several injury-induced/associated TFs have been identified and characterized, including CREB, STAT3, ATF3, c-JUN, SOX11 and SMAD1 (Broude *et al.*, 1997; Herdegen and Leah, 1998; Gao *et al.*, 2004; Raivich *et al.*, 2004; Qiu *et al.*, 2005; Seijffers *et al.*, 2007; Jankowski *et al.*, 2009; Zou *et al.*, 2009).

We recently identified the bZIP TF NFIL3 (nuclear factor interleukin-3 regulated) as a transcriptional regulator of neuronal outgrowth (Stam *et al.*, 2007; MacGillavry *et al.*, 2009). NFIL3 is upregulated after peripheral nerve injury, while it represses neurite outgrowth *in vitro*. We could explain this seemingly paradoxical finding by showing that NFIL3, together with CREB, forms an incoherent feed-forward transcriptional regula-

tory loop in which NFIL3 acts as a negative regulator of the CREB-induced expression of regeneration-associated genes. This transcriptional network motif thus presumably contributes to the temporal regulation of growth-promoting gene expression after an injury. On basis of these results we hypothesized that repressing the function of NFIL3 would promote peripheral nerve regeneration *in vivo*.

Here we tested this hypothesis by expressing a dominant-negative mutant form of NFIL3 (DN-NFIL3) in the sensory neurons of the L4 and L5 DRG prior to a sciatic nerve crush. DN-NFIL3 was developed using a strategy that was successfully used by others to create dominant-negative basic leucine zipper (bZIP) TFs, including CREB (Ahn *et al.*, 1998). The NFIL3 DNA binding domain was replaced by an acidic extension, resulting in a dominant-negative protein that forms a stable dimer with endogenous wildtype NFIL3. This acidic extension, which mimics the acidic DNA target site, forms a stable interaction with the basic DNA binding domain of the wildtype NFIL3 protein, and prevents the dimer from binding to DNA (Krylov *et al.*, 1997). We previously showed that DN-NFIL3 specifically interacts with NFIL3 and increases reporter gene activity and primary DRG neurite outgrowth (MacGillavry *et al.*, 2009).

DN-NFIL3 was expressed in lumbar adult rat DRGs using an adeno-associated viral (AAV) vector. Vectors based on AAV are increasingly regarded as one of the most attractive gene therapy vectors, due to their low immunogenicity, their apparent lack of cellular toxicity, and their capacity to direct high level, stable transgene expression in a variety of tissues, including the nervous system (McCown, 2005). The most frequently used AAV vectors are based on AAV serotype 2 (AAV2), but a number of AAV vectors have been generated based on novel serotypes that have different cellular transduction profiles. AAV serotype 5 (AAV5) is the most effective AAV vector to transduce sensory neurons in the adult rat DRG (Mason *et al.*, 2010) and was therefore used in the present study to test the effects of inhibiting NFIL3 function on peripheral nerve regeneration.

Results

Rationale and characterization of a dominant-negative NFIL3 mutant

To target DN-NFIL3 to the DRG *in vivo* we cloned DN-NFIL3 (Figure 1A, B) into an AAV targeting vector downstream of a CMV promoter and upstream of an IRES-GFP (IGFP) cassette (AAV-DN-NFIL3-IGFP; Figure 1C). F11 neuroblastoma cells were transfected with this plasmid to test if this AAV-targeting vector drives the expression of both DN-NFIL3 and IGFP. Unlike full-length NFIL3, DN-NFIL3 lacks a nuclear localization domain. Indeed, Flag-tagged DN-NFIL3 was exclusively localized in the cytoplasm of GFP positive cells (Figure 1D). This demonstrates that the AAV targeting vector directs the expression of DN-NFIL3 and shows that transduced cells can be easily identified by GFP expression.

Dominant-negative NFIL3 expression increases the number of regenerating fibers after sciatic nerve crush

To test the effect of DN-NFIL3 on the regenerative capacity of DRG neurons, L4 and L5 DRGs were transduced with AAV5-DN-NFIL3-IGFP or with AAV5-empty-IGFP as a negative control (Figure 2A). L4 and L5 lumbar ganglia together contain more than 98% of all sensory axons in the sciatic nerve (Swett *et al.*, 1991). Two weeks after injection, animals were subjected to a sciatic nerve crush and fiber growth beyond the lesion site was assessed seven days later. The percentage of GFP expressing, Tuj1 positive DRG neurons was quantified. The transduction efficiencies in the AAV5-empty-IGFP infected group (33.9 ± 7.7%; mean ± SEM; n = 7) and AAV5-DN-NFIL3-IGFP infected group (43.3 ± 6.9%; mean ± SEM; n = 8) were comparable (Figure 2B, C). The total number of DRG neurons did not differ between groups (data not shown) and all GFP expressing cells were Tuj1 positive. These findings show that AAV5-DN-NFIL3-IGFP selectively transduces DRG neurons, and does not transduce satellite or Schwann cells.

We subsequently quantified the effect of DN-NFIL3 on peripheral nerve regeneration by counting the number of regenerating nerve fibers at one week after sciatic nerve crush, at 0.5 cm and 1.0 cm distal from the lesion site (Figure 2A). Regenerating fibers were visualized in transverse sections by immuno-histochemical staining using an anti-neurofilament antibody (Figure 3A). Images of the sections were captured and individual nerve fascicles were segmented using Image-Pro software. Fibers were counted manually in segments that were randomly chosen by the computer and representing a sample size of approximately 20% of the total nerve surface area. Next, the total nerve surface area was measured and the total number of regenerating axons was calculated. As shown in Figure 3B, a small but non-significant reduction in the number of regenerating fibers was observed in the DN-NFIL3 group (5,298 ± 324.9; mean ± SEM) compared with the control group (6,384 ± 392.5; mean ± SEM) at 0.5 cm distal from the lesion site. At 1.0 cm distal from the lesion site, however, the number of regenerated nerve fibers was significantly higher in the DN-NFIL3 condition (3,625 ± 167; mean ± SEM) than in the control group (2,888 ± 212; mean ± SEM; $p = 0.022$, Student's *t*-test).

Dominant-negative NFIL3 increases neuronal injury-induced GAP-43 expression

NFIL3 binds to and represses the expression of the *Gap43* gene (MacGillavry *et al.*, 2009). Reducing NFIL3 activity is thus expected to increase GAP-43 levels in DRG neurons. To test if DN-NFIL3 affects *Gap43* expression, we analyzed GAP-43 protein levels in individual DRG neurons transduced with AAV5-empty-IGFP or AAV5-DN-NFIL3-IGFP at seven days after sciatic nerve crush. Cross-sections of DRGs were stained for GAP-43 and the staining intensity in GFP expressing neurons was quantified.

GAP-43 immuno-staining was clearly detectable in neuronal cell bodies and in nerve fibers (Figure 4A), and the total number of infected, GFP-positive neurons that expressed GAP-43 was not different between groups (Figure 4B). We next compared the

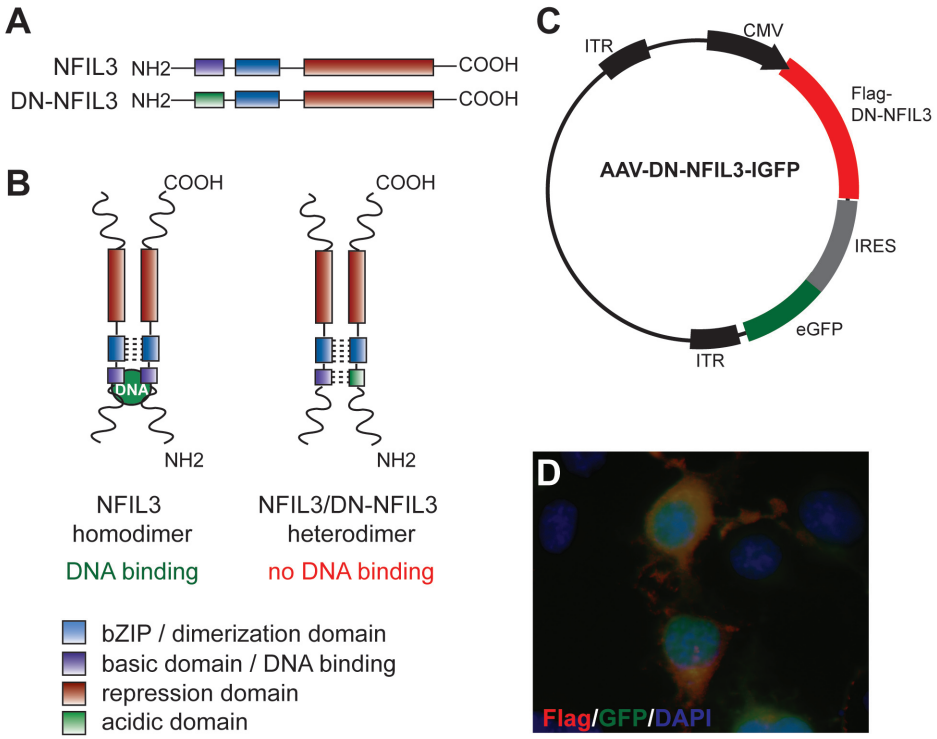

Figure 1. Design of a dominant-negative inhibitor of NFIL3.
(A) Schematic representation of wildtype NFIL3 and dominant-negative NFIL3 (DN-NFIL3). Wild type NFIL3 consists of C-terminal basic DNA-binding domain and a leucine zipper (bZIP) domain required for dimerization. Unlike other bZIP TFs, NFIL3 lacks a transactivation domain, but has an N-terminal repression domain instead. In DN-NFIL3 the C-terminal basic DNA-binding domain was replaced with an acidic domain. (B) The acidic domain binds to the wildtype NFIL3 basic DNA binding domain, resulting in a stable NFIL3/DN-NFIL3 heterodimer which cannot bind DNA and thus interferes with the of endogenous wildtype NFIL3 function. (C) Schematic representation of the AAV vector used to generate AAV5 particles. The bicistronic expression cassette, driven by a cytomegalovirus (CMV) promoter, consists of the dominant-negative NFIL3, followed by an internal ribosome entry site (IRES) sequence fused to eGFP. The expression cassette is flanked by two inverted terminal repeats (ITRs) to enable efficient packaging of the viral particles. (D) Immuno-fluorescent image showing cytosolic localization of Flag-DN-NFIL3 in F11 neuroblastoma cells. Note that only GFP-positive (green) cells show Flag immunoreactivity (red). All cells are stained with the nuclear marker DAPI (blue).

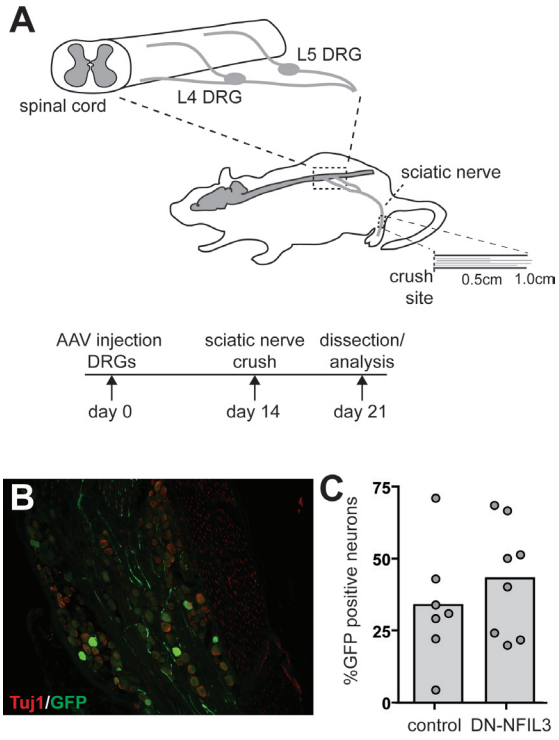

Figure 2. Schematic overview of the experimental design.
(A) Dorsal root ganglia (DRG) at lumbar level 4 and 5 (L4 and 5) were exposed and injected with AAV5-DN-NFIL3-IGFP or with AAV5-empty-IGFP (negative control). Two weeks later, the sciatic nerve was crushed. One week after lesion, animals were sacrificed and the number of regenerating fibers was analyzed at 0.5 cm and at 1.0 cm distal from the crush site. (B) Cross-section through infected DRG, stained for GFP (green) to identify transduced neurons, and for Tuj1 (red) to mark all neurons. (C) The percentages of DRG neurons transduced with either AAV5-DN-NFIL3-IGFP or AAV5-empty-IGFP were comparable. Dots represent individual animals; bars represent means per group.

levels of GAP-43 in GFP-positive versus GFP-negative neurons in each group. In the control (AAV-empty-IGFP) group, no differences in GAP-43 levels were observed between infected (GFP-positive) and uninfected neurons (GFP-negative) (Figure 4C, left graph). In DRG neurons that expressed DN-NFIL3 on the other hand, we observed higher GAP-43 levels in DN-NFIL3 expressing GFP-positive neurons (360.0 ± 27; mean ± SEM) than in non-transduced GFP-negative neurons (322.1 ± 23; mean ± SEM; Figure 4C, right graph). This effect showed a trend towards significance (p = 0.088; paired t-test). Thus, lesion-induced levels of GAP-43 in sensory neurons in L4 and L5 lumbar DRGs appear to be enhanced by DN-NFIL3 expression at 7 days after sciatic nerve lesion.

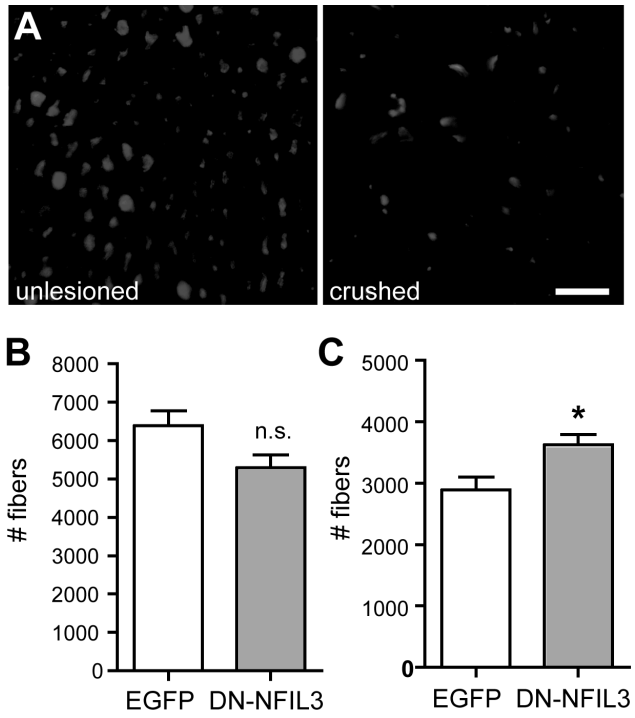

Figure 3. Expression of dominant-negative NFIL3 increases the number of regenerating sciatic nerve fibres after nerve crush.
(A) Cross-sections through the sciatic nerves of a control, unlesioned animal (left) and of a lesioned animal one week after a sciatic nerve crush (right) stained with anti-neurofilament. The number of regenerating nerve fibers in control animals and DN-NFIL3-transduced animals was quantified at 0.5 cm (B) and 1.0 cm (C) distal from the crush site. Bars represent mean ± SEM, * indicates $p < 0.05$, n.s. not significant.

Discussion

The present observations provide the first *in vivo* evidence that functional interference with NFIL3, a transcriptional repressor of the regeneration-associated gene program, can promote axonal regeneration. AAV5-mediated expression of DN-NFIL3 in sensory neurons of L4 and L5 DRGs leads to a modest, but significant increase in the number of regenerating fibers one week after sciatic nerve crush at 1.0 cm, but not 0.5 cm, distal from the lesion site. The effects of DN-NFIL3 on axon regeneration are accompanied by a slightly increased expression of the regeneration-associated protein GAP-43.

The effects of DN-NFIL3 measured in this study may have been underestimated for at least two reasons. First, DN-NFIL3 was expressed in only ~40% of the total L4/L5 neuron population, and second, we quantified all neurofilament-positive axons in the sciatic nerve, including motor axons. Quantification of GFP-positive axons would have provided a better comparison between the two treatment groups, however, we could not

detect GFP fluorescence in the axons of transduced neurons. The use of farnesylated GFP, which is targeted to the plasma membrane of axons and growth cones, might in follow-up experiments enable selective identification of axons that are extended by the transduced sensory neurons only. We also attempted to separately identify the sensory and motor axon population in crushed sciatic nerves using an antibody against choline acetyltransferase (ChAT) as a specific marker for motor axons. Although, we could consistently identify ChAT-positive fibers in cross-sections of the intact sciatic nerve, ChAT immunoreactivity was almost undetectable in sciatic nerves at one week after nerve crush (data not shown). This might be due to a down-regulation of ChAT expression in injured motor neurons at 7 days post-lesion (Rende *et al.*, 1995) or to a predominant regeneration of sensory fibers at this time point (Suzuki *et al.*, 1998). Follow-up experiments will be of critical importance to confirm our initial observations that DN-NFIL3 enhances axonal regeneration of injured DRG sensory neurons. Co-expression of farnesylated GFP to specifically mark axons of transduced neurons and/or retrograde tracing techniques to specifically label regenerating neurons (Tannemaat *et al.*, 2008) are options that will both be explored. Furthermore, an expansion of post-lesion time course of axon regeneration combined with longitudinal studies of the effect of DN-NFIL3 on the functional recovery of hind paw function need to be performed.

From our data it is not directly clear whether DN-NFIL3 affects the number of regenerating axons or the speed at which they regrow. We observed a slightly smaller number of fibers close to the injury site at 0.5 cm from the crush, while there is an increased number of fibers at 1.0 cm from the crush compared with controls. This might indicate that DN-NFIL3 either increased the number of neurons that form a regenerating axon during the initial phase of regeneration, or that it enhanced the velocity of the axons that grow out during the early post-lesion time period. As discussed above, techniques that better mark transduced neurons and their regenerating axons will be essential to disentangle these two processes and to better understand the mechanism by which NFIL3 affects axon regeneration.

Our results are consistent with the hypothesis that NFIL3 acts as a feed-forward repressor of the cAMP-CREB pathway and represses peripheral nerve regeneration. It is tempting to speculate that NFIL3 also acts as a repressor of axon regeneration in the central nervous system (CNS). To our knowledge it has not been shown that NFIL3 expression is changed after a central nerve lesion, and our own data indicate that a dorsal root crush does not induce NFIL3 expression in DRG neurons (Stam *et al.*, 2007; MacGillavry *et al.*, 2009). Overexpression of DN-NFIL3 might therefore not stimulate axonal regeneration of injured central neurons. However, it will be of interest to investigate whether regeneration of dorsal root axons that is induced by a conditioning lesion (Richardson and Issa, 1984; Neumann and Woolf, 1999), by injection of cAMP analogues (Qiu *et al.*, 2002), or by constitutive-active CREB expression (Gao *et al.*, 2004) can be further enhanced by simultaneously expressing DN-NFIL3. We expect that regeneration-

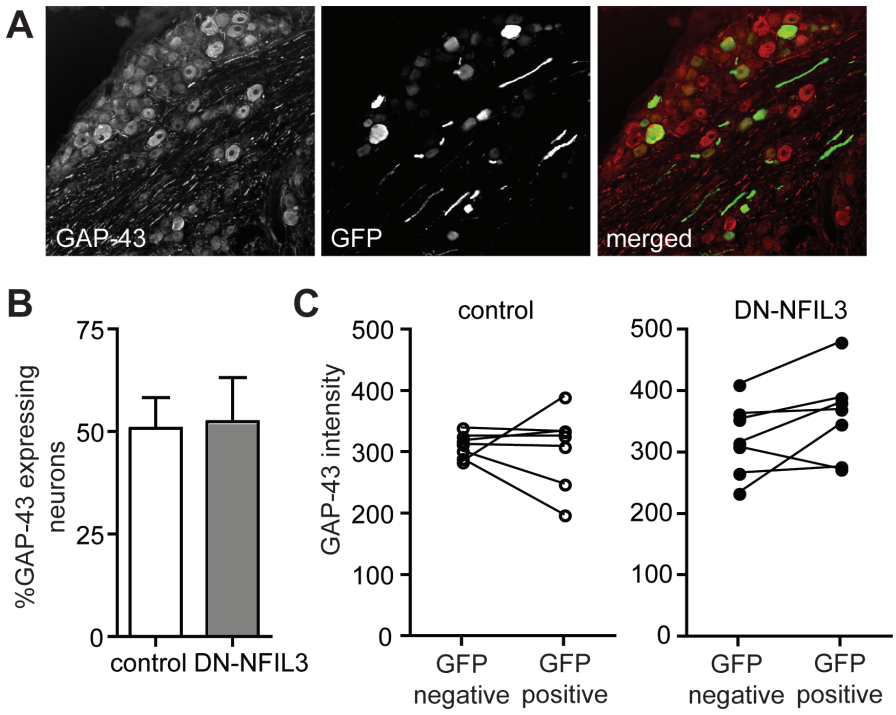

Figure 4. Expression of dominant-negative NFIL3 increases GAP-43 expression in regenerating DRG neurons.
(A) Cross-section through a DRG stained for GAP-43 (left, red in the merged image) and GFP (middle, green in the merged image). (B) The number of neurons expressing both GAP-43 and GFP is the same in control and DN-NFIL3-transduced neurons. Bars represent mean ± SEM. (C) The GAP-43 intensity in the control group is the same in GFP-negative and GFP-positive neurons (left), whereas in the DN-NFIL3 group, GFP-positive neurons show overall higher GAP-43 levels than GFP-negative neurons (right).

promoting interventions that are based on stimulating the cAMP/PKA/CREB pathway result in the concomitant upregulation of NFIL3. Combined functional interference with NFIL3 might thus further enhance the regeneration of dorsal root axons or may prolong the time window of the post-lesion regenerative response of these axons.

Our observations confirm the notion that regenerating neurons express intrinsic repressors of the growth-promoting gene expression program. Previous studies showed that SOCS3 (signal transducer of cytokine signaling-3), which is also upregulated in regenerating DRG neurons, represses neurite outgrowth (Miao *et al.*, 2006). Moreover, the regeneration-promoting effects of cAMP on injured retinal ganglion cells are probably mediated by a downregulation of SOCS3 (Park *et al.*, 2009), and genetic deletion of SOCS3 promotes optic nerve regeneration (Smith *et al.*, 2009). Likewise, PTEN, TSC1 and KLF4 are intrinsic negative regulators of CNS regeneration (Park *et al.*, 2008; Moore *et al.*, 2009). Targeting intrinsic repressors of neuronal regeneration is an emerging and

exciting novel potential strategy to promote regeneration in the damaged nervous system.

Materials and methods

Plasmids and virus production

The generation of DN-NFIL3 was described earlier (MacGillavry *et al.*, 2009). DN-NFIL3 was subcloned into the AAV-IRES-EGFP construct kindly provided by dr. Dietmar Fischer (University of Ulm, Germany). As a control, an empty AAV-IRES-EGFP construct (AAV-empty-IRES-EGFP) was used. AAV serotype 5 (AAV5; plasmid generously provided by dr. Jurgen Kleinschmidt, University of Heidelberg, Germany) particles were produced and isolated as described previously (Hermens *et al.*, 1999; Blits *et al.*, 2009; Mason *et al.*, 2010). Virus particles were banded using an iodixanol cushion as described in Blits *et al.* (2009). Viral vector stocks were stored at -80^{0}C in Dulbecco's phosphate buffered saline with $MgCl_2$ and $CaCl_2$ (DPBS +/+; Invitrogen) supplemented with 5% sucrose. Virus titers were determined by quantitative PCR and were $1.1x10^{12}$ (AAV5-DN-NFIL3-IGFP) and $3.4x10^{12}$ (AAV5-empty-IGFP) genomic copies (GC)/ml.

Animals and virus injections

All experiments were approved by the KNAW animal experimentation committee for animal well fare. Female adult Wistar rats (~200 g; Harlan, Horst, The Netherlands) were used. An overview of the experimental design is given in Figure 2. For a detailed description of the virus injections, see Mason *et al.* (2010). DRGs L4 and 5 were exposed and 1.0 µl of virus solution (containing $1.1x10^9$ GCs of AAV5-DN-NFIL3-IGFP and $3.4x10^9$ GCs of AAV5-empty-IGFP) per DRG was injected using a glass capillary, pulled to a fine point and attached to a Hamilton syringe, at a speed of 0.2 µl/min. To visualize the injection of the virus solution into the ganglia, 0.1% Fast Green (Sigma) was added to the virus solution. Two weeks after injection, animals were subjected to a sciatic nerve crush as described (Stam *et al.*, 2007) and a 10-0 nylon suture was placed through the epineurium to mark the lesion site. Seven days after sciatic nerve crush, animals were transcardially perfused with saline, followed by 4% paraformaldehyde (PFA) in saline. Injected DRGs and crushed sciatic nerves were dissected, post-fixed overnight and transferred to a 25% sucrose solution overnight at 4^{0}C. Tissue was then embedded in Tissue-Tek OCT compound (Sakura, Zoeterwoude, The Netherlands), snap frozen in liquid nitrogen-cooled isopentane and stored at -80^{0}C.

Quantification of transduction efficiencies

For the quantification of the transduction efficiencies of sensory neurons in the L4 and L5 DRG, 8-10 sections (20 µm) per DRG were post-fixed in 4% PFA, blocked in blocking buffer (PBS containing 1% BSA, 5% FCS and 0.3% Triton X-100) and stained with

anti-βIII-tubulin (1:500; clone Tuj1; Covance, Berkeley, CA, USA) and anti-GFP (1:4000; Abcam, Cambridge, UK), followed by donkey anti-mouse Alexa594 (1:400), biotinylated goat anti-rabbit (1:300) and streptavidin-Alexa488 (1:400). All sections were captured at fixed exposure settings using an Axioplan 2 fluorescence microscope (Zeiss, Sliedrecht, The Netherlands) using a 10x objective. Images were analyzed using a custom algorithm in Image-Pro Plus software (MediaCybernetics, Silverspring, USA) as described in Mason *et al.* (2010). This algorithm automatically identifies all DRG nuclei on basis of the Tuj1 staining in the red channel, which specifically stains neuronal cytoplasm and leaves the nucleus unstained and visible as a dark, semi-round object. GFP intensity was then measured only in the identified nuclear area. Background intensity levels were measured in un-injected DRGs processed in the same way. Neurons expressing GFP at higher levels than the mean background level were classified as transduced cells.

Quantification of regenerating axons

To quantify nerve fiber growth beyond the lesion site, 20 μm transversal sciatic nerve sections were stained with mouse-anti-neurofilament (2H3; 1:1000; Hybridoma Bank, University of Iowa, USA). Images of sections at 0.5 cm and at 1.0 cm distal from the lesion site were captured at fixed exposure settings using an Axioplan 2 fluorescence microscope with a 10x objective. The areas of the different nerve fascicles were calculated with Image-Pro Plus software. The area was then automatically segmented, and segments were randomly chosen to sample approximately 20% of the total nerve area. In each selected segment, all NF positive axons were counted manually using a light cursor. The total number of regenerating axons was then calculated by multiplying the number of counted axons with the total fascicle area divided by the measured area. The observer was blind for the condition during image acquisition and analysis. A two-sided Student's *t*-test was performed to test for significance with a p-value < 0.05 considered statistically significant.

Quantification of GAP-43 expression in the DRG

For the quantification of GAP-43 expression levels in transduced DRG neurons, 8-10 sections (20 μm) per DRG were stained with mouse anti-GAP-43 (1:500; Sigma) and with rabbit anti-GFP as described above. All sections were captured at fixed exposure settings using an Axioplan 2 fluorescence microscope with a 10x objective. Images were analyzed as described above, except that DRG nuclei were identified on basis of the cytoplasmic GAP-43 staining in the red channel. The GFP intensity was then measured only in the identified nuclear area and the GAP-43 intensity in an automatically generated cytoplasmic ring around the nucleus. Neurons expressing both GFP and GAP-43 at levels higher than the mean background level were classified as transduced, GAP-43 expressing cells. For the statistical analysis of GAP-43 intensity in the two groups a paired *t*-test was

used.

References

Ahn S, Olive M, Aggarwal S, Krylov D, Ginty DD, Vinson C (1998) A dominant-negative inhibitor of CREB reveals that it is a general mediator of stimulus-dependent transcription of c-fos. Mol Cell Biol 18:967-977.

Aigner L, Arber S, Kapfhammer JP, Laux T, Schneider C, Botteri F, Brenner HR, Caroni P (1995) Overexpression of the neural growth-associated protein GAP-43 induces nerve sprouting in the adult nervous system of transgenic mice. Cell 83:269-278.

Blits B, Derks S, Twisk J, Ehlert E, Prins J, Verhaagen J (2009) Adeno-associated viral vector (AAV)-mediated gene transfer in the red nucleus of the adult rat brain: Comparative analysis of the transduction properties of seven AAV serotypes and lentiviral vectors. J Neurosci Methods.

Bomze HM, Bulsara KR, Iskandar BJ, Caroni P, Skene JH (2001) Spinal axon regeneration evoked by replacing two growth cone proteins in adult neurons. Nat Neurosci 4:38-43.

Bonilla IE, Tanabe K, Strittmatter SM (2002) Small proline-rich repeat protein 1A is expressed by axotomized neurons and promotes axonal outgrowth. J Neurosci 22:1303-1315.

Broude E, McAtee M, Kelley MS, Bregman BS (1997) c-Jun expression in adult rat dorsal root ganglion neurons: differential response after central or peripheral axotomy. Exp Neurol 148:367-377.

Costigan M, Befort K, Karchewski L, Griffin RS, D'Urso D, Allchorne A, Sitarski J, Mannion JW, Pratt RE, Woolf CJ (2002) Replicate high-density rat genome oligonucleotide microarrays reveal hundreds of regulated genes in the dorsal root ganglion after peripheral nerve injury. BMC Neurosci 3:16.

Gao Y, Deng K, Hou J, Bryson JB, Barco A, Nikulina E, Spencer T, Mellado W, Kandel ER, Filbin MT (2004) Activated CREB is sufficient to overcome inhibitors in myelin and promote spinal axon regeneration *in vivo*. Neuron 44:609-621.

Hanz S, Perlson E, Willis D, Zheng JQ, Massarwa R, Huerta JJ, Koltzenburg M, Kohler M, van-Minnen J, Twiss JL, Fainzilber M (2003) Axoplasmic importins enable retrograde injury signaling in lesioned nerve. Neuron 40:1095-1104.

Herdegen T, Leah JD (1998) Inducible and constitutive transcription factors in the mammalian nervous system: control of gene expression by Jun, Fos and Krox, and CREB/ATF proteins. Brain Res Brain Res Rev 28:370-490.

Hermens WT, ter Brake O, Dijkhuizen PA, Sonnemans MA, Grimm D, Kleinschmidt JA, Verhaagen J (1999) Purification of recombinant adeno-associated virus by iodixanol gradient ultracentrifugation allows rapid and reproducible preparation of vector stocks for gene transfer in the nervous system. Hum Gene Ther 10:1885-1891.

Jankowski MP, McIlwrath SL, Jing X, Cornuet PK, Salerno KM, Koerber HR, Albers KM (2009) Sox11 transcription factor modulates peripheral nerve regeneration in adult mice. Brain Res 1256:43-54.

Krylov D, Kasai K, Echlin DR, Taparowsky EJ, Arnheiter H, Vinson C (1997) A general method to design dominant negatives to B-HLHZip proteins that abolish DNA binding. Proc Natl Acad Sci U S A 94:12274-12279.

MacGillavry HD, Stam FJ, Sassen MM, Kegel L, Hendriks WT, Verhaagen J, Smit AB, van Kesteren RE (2009) NFIL3 and cAMP response element-binding protein form a transcriptional feedforward loop that controls neuronal regeneration-associated gene expression. J Neurosci 29:15542-15550.

Mason MRJ, Eggers RE, Ehlert EME, Pool CW, Hermening S, Huseinovic A, Timmermans E, Blits B, Verhaagen J (2010) Comparison of AAV serotypes for gene delivery to dorsal root ganglion neurons. Mol Ther 18:670-673.

McCown TJ (2005) Adeno-associated virus (AAV) vectors in the CNS. Curr Gene Ther 5:333-338.

Miao T, Wu D, Zhang Y, Bo X, Subang MC, Wang P, Richardson PM (2006) Suppressor of cytokine signaling-3 suppresses the ability of activated signal transducer and activator of transcription-3 to stimulate neurite growth in rat primary sensory neurons. J Neurosci 26:9512-9519.

Moore DL, Blackmore MG, Hu Y, Kaestner KH, Bixby JL, Lemmon VP, Goldberg JL (2009) KLF family members regulate intrinsic axon regeneration ability. Science 326:298-301.

Neumann S, Woolf CJ (1999) Regeneration of dorsal column fibers into and beyond the

lesion site following adult spinal cord injury. Neuron 23:83-91.

Park KK, Hu Y, Muhling J, Pollett MA, Dallimore EJ, Turnley AM, Cui Q, Harvey AR (2009) Cytokine-induced SOCS expression is inhibited by cAMP analogue: impact on regeneration in injured retina. Mol Cell Neurosci 41:313-324.

Park KK, Liu K, Hu Y, Smith PD, Wang C, Cai B, Xu B, Connolly L, Kramvis I, Sahin M, He Z (2008) Promoting axon regeneration in the adult CNS by modulation of the PTEN/mTOR pathway. Science 322:963-966.

Qiu J, Cafferty WB, McMahon SB, Thompson SW (2005) Conditioning injury-induced spinal axon regeneration requires signal transducer and activator of transcription 3 activation. J Neurosci 25:1645-1653.

Qiu J, Cai D, Dai H, McAtee M, Hoffman PN, Bregman BS, Filbin MT (2002) Spinal axon regeneration induced by elevation of cyclic AMP. Neuron 34:895-903.

Raivich G, Bohatschek M, Da Costa C, Iwata O, Galiano M, Hristova M, Nateri AS, Makwana M, Riera-Sans L, Wolfer DP, Lipp HP, Aguzzi A, Wagner EF, Behrens A (2004) The AP-1 transcription factor c-Jun is required for efficient axonal regeneration. Neuron 43:57-67.

Rende M, Giambanco I, Buratta M, Tonali P (1995) Axotomy induces a different modulation of both low-affinity nerve growth factor receptor and choline acetyltransferase between adult rat spinal and brainstem motoneurons. J Comp Neurol 363:249-263.

Richardson PM, Issa VM (1984) Peripheral injury enhances central regeneration of primary sensory neurones. Nature 309:791-793.

Schmitt AB, Breuer S, Liman J, Buss A, Schlangen C, Pech K, Hol EM, Brook GA, Noth J, Schwaiger FW (2003) Identification of regeneration-associated genes after central and peripheral nerve injury in the adult rat. BMC Neurosci 4:8.

Seijffers R, Mills CD, Woolf CJ (2007) ATF3 increases the intrinsic growth state of DRG neurons to enhance peripheral nerve regeneration. J Neurosci 27:7911-7920.

Smith DS, Skene JH (1997) A transcription-dependent switch controls competence of adult neurons for distinct modes of axon growth. J Neurosci 17:646-658.

Smith PD, Sun F, Park KK, Cai B, Wang C, Kuwako K, Martinez-Carrasco I, Connolly L,

He Z (2009) SOCS3 deletion promotes optic nerve regeneration *in vivo*. Neuron 64:617-623.

Stam FJ, MacGillavry HD, Armstrong NJ, de Gunst MC, Zhang Y, van Kesteren RE, Smit AB, Verhaagen J (2007) Identification of candidate transcriptional modulators involved in successful regeneration after nerve injury. Eur J Neurosci 25:3629-3637.

Suzuki G, Ochi M, Shu N, Uchio Y, Matsuura Y (1998) Sensory neurons regenerate more dominantly than motoneurons during the initial stage of the regenerating process after peripheral axotomy. Neuroreport 9:3487-3492.

Swett JE, Torigoe Y, Elie VR, Bourassa CM, Miller PG (1991) Sensory neurons of the rat sciatic nerve. Exp Neurol 114:82-103.

Tannemaat MR, Eggers R, Hendriks WT, de Ruiter GC, van Heerikhuize JJ, Pool CW, Malessy MJ, Boer GJ, Verhaagen J (2008) Differential effects of lentiviral vector-mediated overexpression of nerve growth factor and glial cell line-derived neurotrophic factor on regenerating sensory and motor axons in the transected peripheral nerve. Eur J Neurosci 28:1467-1479.

Xiao HS, Huang QH, Zhang FX, Bao L, Lu YJ, Guo C, Yang L, Huang WJ, Fu G, Xu SH, Cheng XP, Yan Q, Zhu ZD, Zhang X, Chen Z, Han ZG, Zhang X (2002) Identification of gene expression profile of dorsal root ganglion in the rat peripheral axotomy model of neuropathic pain. Proc Natl Acad Sci U S A 99:8360-8365.

Zou H, Ho C, Wong K, Tessier-Lavigne M (2009) Axotomy-induced Smad1 activation promotes axonal growth in adult sensory neurons. J Neurosci 29:7116-7123.

Chapter 4

Genome-wide identification of target genes reveals NFIL3 as a general feed-forward repressor in neuronal outgrowth

Harold D. MacGillavry[1], Jochem Cornelis[1], Joost Verhaagen[2], August B. Smit[1] and Ronald E. van Kesteren[1]

[1]Department of Molecular and Cellular Neurobiology, Center for Neurogenomics and Cognitive Research, Neuroscience Campus Amsterdam, VU University, De Boelelaan 1085, 1081 HV Amsterdam, The Netherlands
[2]Department of Neuroregeneration, Netherlands Institute for Neuroscience, Meiberg-dreef 47, 1105 BH Amsterdam, The Netherlands

manuscript in preparation

Abstract

NFIL3 is a multifunctional transcription factor implicated in a wide range of physiological processes, including cellular survival, circadian gene expression and natural killer cell development. We recently demonstrated that NFIL3 acts as a repressor of CREB-induced gene expression underlying the regeneration of axotomized DRG sensory neurons. In this study we performed chromatin immunoprecipitation assays combined with microarray technology (ChIP-chip) to reveal direct NFIL3 and CREB target genes in an in vitro cell model for regenerating DRG neurons. We identified 505 promoter regions bound by NFIL3 and 924 promoter regions bound by CREB. Histone H3 acetylation profiling showed that a large fraction (>60%) of NFIL3 target genes were transcriptionally silent, whereas CREB target genes in general were transcriptionally active. Only a small subset of NFIL3 target genes also bound CREB. In addition, we found that a substantial number of NFIL3 target genes share a C/EBP DNA binding site. Both C/EBPα and C/EBPβ were identified as CREB targets in our ChIP-chip analysis, and knockdown of C/EBPα and C/EBPβ significantly reduced neurite outgrowth in vitro. Together, our findings show that NFIL3 may be a general feed-forward repressor of basic leucine zipper transcription factors that control neurite outgrowth.

Introduction

The transcription factor (TF) NFIL3 (nuclear factor IL-3 regulated, also known as E4 binding protein 4 or E4BP4) was first found to bind and repress viral promoter sequences (Chen *et al.,* 1995), and shortly thereafter identified as a positive regulator of the human IL-3 gene (Zhang *et al.,* 1995). Later studies describe diverse roles for NFIL3 in IL-3-dependent survival of B-cells (Ikushima *et al.,* 1997), transcriptional control of the circadian clock (Mitsui *et al.,* 2001), survival of spinal cord motor neurons (Junghans *et al.,* 2004), and development of natural killer cells (Gascoyne *et al.,* 2009; Kamizono *et al.,* 2009). NFIL3 thus seems to have evolved many different specialized functions in a broad range of physiological processes.

NFIL3 is a member of the basic leucine zipper (bZIP) TF family. bZIP TFs share a basic domain, which interacts with the major groove of the DNA, and a leucine zipper domain, which is required for dimerization. On basis of DNA binding site preference, bZIP TFs fall in one of several classes, e.g., CREB/ATF, AP-1, C/EBP and PAR. NFIL3 is a member of the PAR bZIP TFs, which further includes HLF, DBP and TEF. The latter three TFs share a proline and acidic amino-acid rich (PAR) domain, which is located amino-terminally of the basic DNA-binding region and acts as a transactivation domain. NFIL3 lacks this PAR transactivation domain and instead contains a C-terminal repression domain (Cowell and Hurst, 1994, 1996). The NFIL3 repression domain has many charged residues, mutations of which result in complete loss of transcriptional repressor activity of an NFIL3-GAL4 fusion protein (Cowell and Hurst, 1994). The NFIL3 repression domain interacts with the repressor protein Dr1 (Cowell and Hurst, 1996), which in turn binds

the TATA-box binding protein TBP and thereby precludes formation of the pre-initiation complex (Inostroza *et al.,* 1992). These data are consistent with a model in which NFIL3 represses target gene expression by interfering with the basal transcriptional machinery via Dr1. In contrast, NFIL3 also acts as a positive regulator of IL-3 gene expression in human T-cells (Zhang *et al.,* 1995), indicating that selective co-factor availability can play a role in determining the context-specific actions of NFIL3. It has also been suggested that NFIL3 can heterodimerize with other bZIP TFs to form context-specific transcriptional complexes (Acharya *et al.,* 2006; Vinson *et al.,* 2006). Finally, in the circadian clock NFIL3 directly competes with activating PAR TFs for DNA binding (Mitsui *et al.,* 2001). Thus, the context-specific actions of NFIL3 can result from differential co-factor availability, selective heterodimerization and direct competition with activating TFs.

We recently described that NFIL3 represses neuronal regeneration-associated genes by competing with CREB for target gene binding (MacGillavry *et al.,* 2009). Peripheral axonal injury of sensory neurons in the dorsal root ganglion (DRG) results in activation of CREB and transcription of CREB-induced regeneration-associated genes. Paradoxically, NFIL3 expression was found to be upregulated by CREB, and shown to inhibit DRG neurite regeneration. We next showed that both CREB and NFIL3 bind to similar DNA binding sites in regeneration-associated genes and that upon stimulation of the cAMP/PKA pathway, CREB is activated and initiates a transcriptional response, which is subsequently repressed by NFIL3. We propose that this so-called transcriptional incoherent feed-forward loop fine-tunes transcription of regeneration-associated genes. To further substantiate these findings, we now performed genome-wide ChIP-chip identification of NFIL3 and CREB targets in the context of neuronal outgrowth. Our findings confirm the role for NFIL3 as a transcriptional repressor in outgrowing neurons, and suggest that NFIL3 may be a general repressor of bZIP TF-activated gene expression.

Results

Genome-wide analysis identifies NFIL3-bound gene promoters in neuronal cells

We used ChIP-chip analysis to identify direct target genes of NFIL3 in the DRG-like F11 cell line. F11 cells share many characteristics with DRG neurons (Platika *et al.,* 1985; Francel *et al.,* 1987; Boland and Dingledine, 1990), and we previously showed that the CREB/NFIL3 transcriptional feed-forward loop that we described in regenerating DRG neurons is also regulating neurite outgrowth in F11 cells (MacGillavry *et al.,* 2009). We performed ChIP-chip analysis on F11 cells transfected with a Flag-tagged NFIL3 overexpression construct (Flag ChIP-chip) and used untransfected cells as a negative control (background ChIP-chip). Chromatin was isolated two hours after forskolin stimulation and immunoprecipitated with an anti-Flag antibody. The immunoprecipitated DNA was amplified using linker-mediated PCR, labelled and hybridized to custom Agilent promoter arrays (see Materials and Methods for detailed information on array coverage).

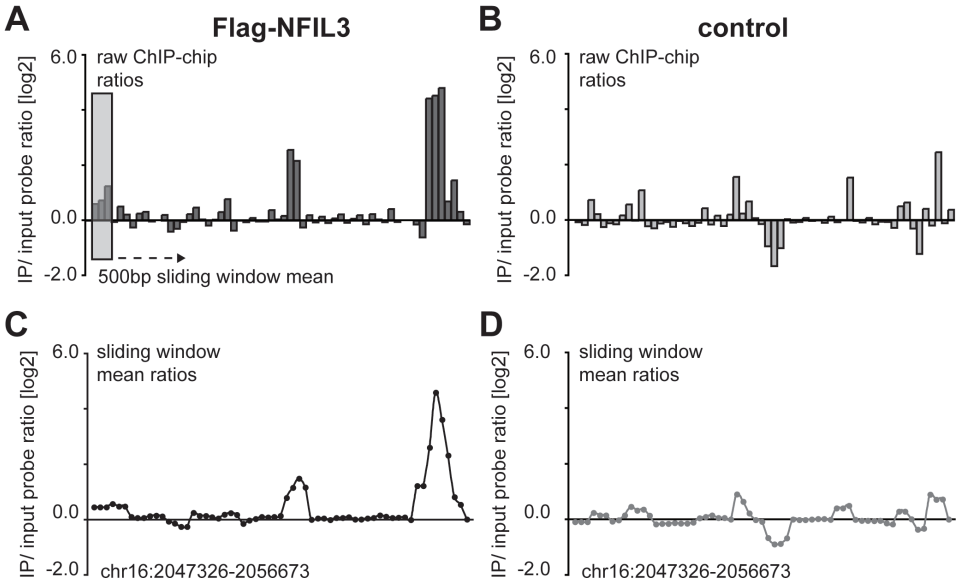

Figure 1. Overview of ChIP-chip data analysis.
(A-B) Raw IP/input log2 probe ratios for the Flag-NFIL3 ChIP-chip (A) and the control ChIP-chip (B). (C-D) Raw log2 probe ratios were averaged using a sliding window of 500 bp. This resulted in sliding window mean probe ratios that were directly compared between the Flag-NFIL3 and control ChIP-chips and tested for significance. NFIL3-bound regions were defined as genomic regions containing at least three adjacent significant ($p < 0.01$) sliding window ratios.

Raw probe intensities were background subtracted and loess normalized. To further reduce the noise in the signal, and to test for significance of binding, we used a 500 bp sliding window mean ratio centred on all probe locations (Figure 1). Within each window we calculated a *p*-value by directly comparing the Flag ChIP-chip and background ChIP-chip signals (usually three or four per window). Binding peaks were defined as regions where three or more adjacent sliding window mean ratios showed significant higher binding in the Flag ChIP-chip than in the background ChIP-chip ($p < 0.01$). Using this method, 526 significant peaks were identified, corresponding to 505 unique promoter regions (Figure 2A).

To validate the ChIP-chip results we randomly picked 18 regions and measured enrichment using quantitative PCR (qPCR), comparing the enrichment of promoter regions in the NFIL3-transfected ChIP sample versus the background ChIP sample. We thus confirmed NFIL3 binding at 17 of the 18 promoter regions (94%; Figure 2B). Enrichments found by ChIP-chip correlated well with qPCR measurements (Pearson r = 0.66, $p < 0.01$; Figure 2C). Importantly, negative ChIP-chip regions (i.e., the *Dapk3* and *Pick1* promoters) did not show enrichment as measured by qPCR. To further validate these results, we also performed ChIP experiments on forskolin stimulated F11 cells with an antibody against endogenous NFIL3. As shown in Figure 2D we find significant en-

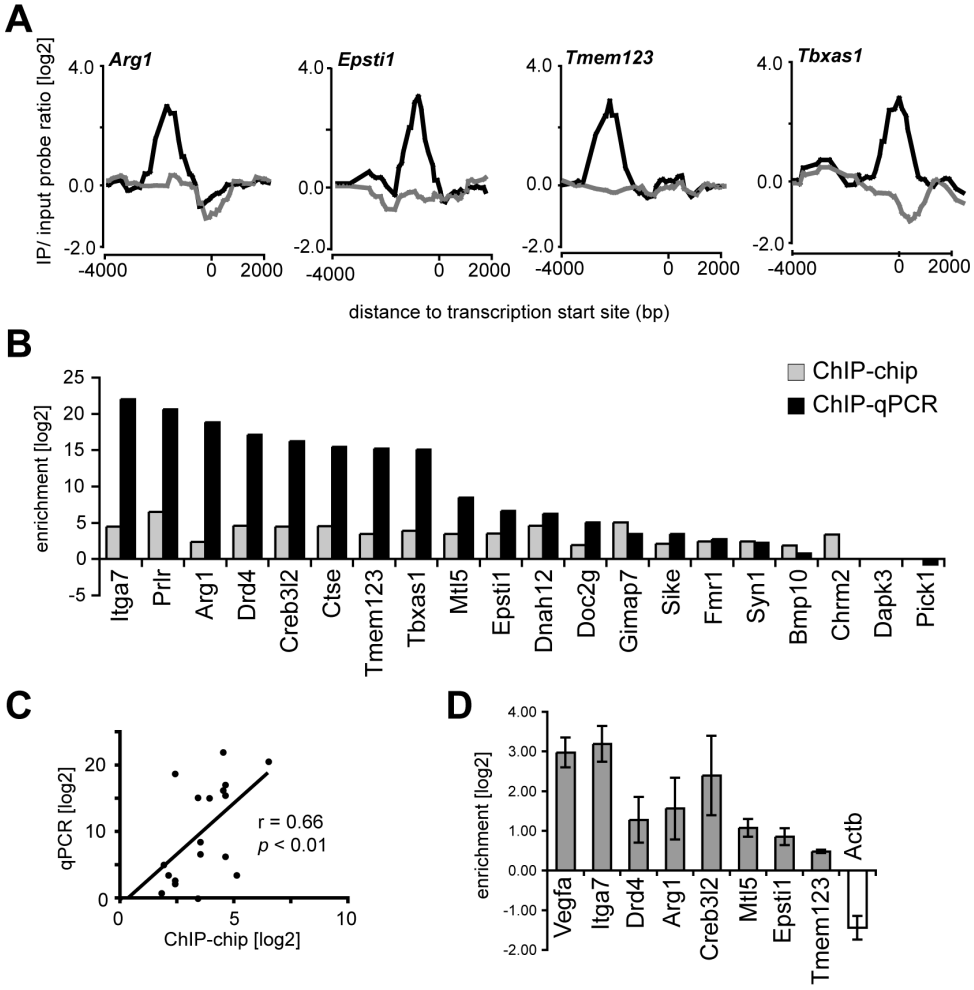

Figure 2. Identification of neuronal NFIL3 target genes.
(A) Examples of Flag-NFIL3 ChIP-chip enrichment at the promoters of *Arg1, Epsti1, Tmem123* and *Tbxas1*. Graphs indicate sliding window Cy5/Cy3 probe ratios extracted from Flag-NFIL3 (black) and background (grey) ChIP-chip probe signals. (B) qPCR measurements of ChIP enrichment (dark-grey bars) validates 17 out of 18 NFIL3-bound promoter regions identified by ChIP-chip (light-grey bars). Two negative control promoter regions (*Dapk3* and *Pick1*) show no enrichment as measured by qPCR. (C) Enrichment measured with qPCR (y-axis) is overall higher, but correlates well with the ChIP-chip maximal peak values (x-axis); Pearson r = 0.66, $p < 0.01$. (D) Independent ChIP-qPCR validation of endogenous NFIL3 binding in forskolin-stimulated F11 cells at 8 randomly chosen promoter regions (grey bars) and not a negative control region (Actb; white bar). Bars represent means ± SEM.

C

JASPAR MA0025	ChIP-chip	random sequences
PRESENT	86	79
ABSENT	114	121

MDSCan motif	ChIP-chip	random sequences
PRESENT	179	129
ABSENT	21	71

Figure 3. *De novo* motif analysis identifies a novel NFIL3 DNA binding site.
(A) The NFIL3 consensus DNA position weight matrix logo as annotated in the JASPAR database. (B) The top-scoring motif identified by MDScan in 17 validated NFIL3-bound promoter regions. (C) Contingency tables showing the frequencies of the JASPAR and the MDScan NFIL3 binding sites in NFIL3-bound genes identified by ChIP-chip and in randomly selected genomic sequences. Only the MDScan motif shows significant enrichment in the NFIL3-bound sequences compared with the background sequences (Fisher's exact test, $p = 2.9 \times 10^{-9}$).

richment of endogenous NFIL3 at 8 randomly chosen regions that were also identified in the ChIP-chip analysis, and not at the negative control Actb promoter. Together these results confirm that most NFIL3-bound DNA regions identified by ChIP-chip reflect true NFIL3 target genes.

De novo motif analysis identifies a novel NFIL3 DNA binding site

The NFIL3 consensus binding site annotated in the JASPAR database (MA0025; Figure 3A) is based on artificial in vitro binding assays (Cowell *et al.,* 1992). Therefore we used MDScan (Liu *et al.,* 2002) to search in our 17 validated NFIL3 bound sequences for a DNA motif that could mediate the *in vivo* NFIL3-DNA interaction. The resulting consensus sequence is depicted as a sequence logo that indicates the observed nucleotide frequency for each position in the alignment (Figure 3B). This sequence shows some similarity with the known NFIL3 consensus motif, however, the core sequence ([T/C]

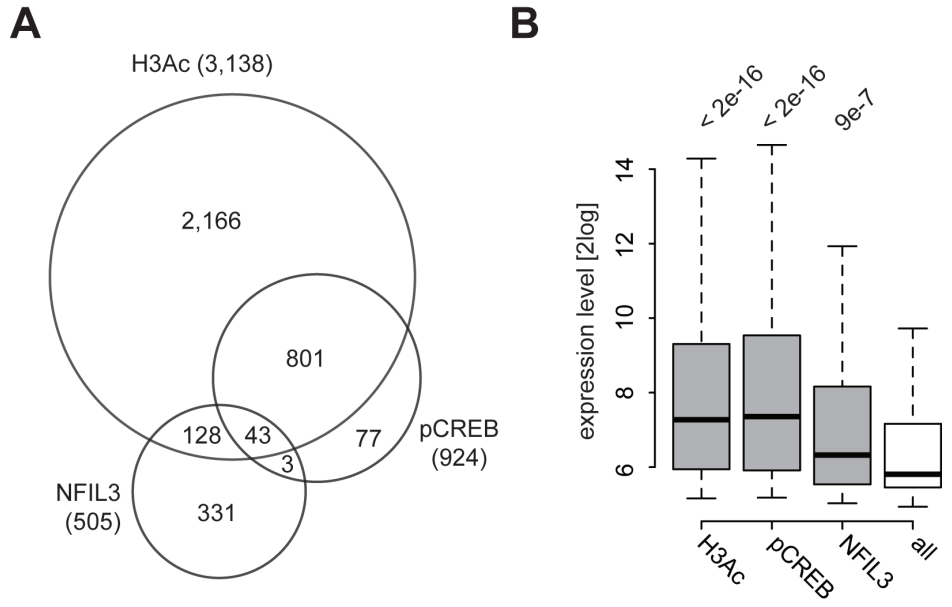

Figure 4. NFIL3 predominantly occupies promoters of transcriptionally silent genes.
(A) Venn-diagram showing the overlap in H3Ac-containing regions (3,138 in total), pCREB-bound regions (924 in total) and NFIL3-bound regions (505 in total). (B) Box-plots showing the distribution of the expression levels of genes enriched for H3Ac, pCREB and NFIL3 (grey boxes) compared with the distribution of the expression levels of all genes on the microarray (white box). Numbers above the box-plots indicate the *p*-values of two-sample Wilcoxon rank sum tests comparing mean expression values of ChIP-chip-enriched genes with the mean expression value of all genes.

G) differs from the *de novo* identified motif core sequence (G[C/T]). If we scan the 200 most significant ChIP-chip peak regions, we find this new motif present in 90% of the identified regions, whereas the JASPAR motif is present in only 40% of (Figure 3C). Using a Fisher's exact, the new motif is significantly overrepresented in the ChIP-chip data set ($p = 2.9 \times 10^{-9}$) compared with a random background set of genomic DNA sequences, whereas the JASPAR motif is not ($p = 0.54$). These results indicate that this newly discovered motif better represents NFIL3 binding sites than the previously reported in vitro binding site, and that it can better predict *in vivo* NFIL3 binding.

NFIL3 predominantly occupies promoters of transcriptionally silent genes

We next performed ChIP-chip analysis using antibodies recognizing endogenous Ser-133 phosphorylated CREB (pCREB) and histone H3 acetylated at K9 and K14 (H3Ac), a well-established histone mark for open chromatin structure associated with active transcription (Bernstein *et al.,* 2005). We identified 924 regions bound by pCREB and 3,138 regions showing H3 K9/14 acetylation (Figure 4A). Of the 505 promoter regions bound by NFIL3, <40% (171 regions) also show H3 acetylation. This indicates that NFIL3 oc-

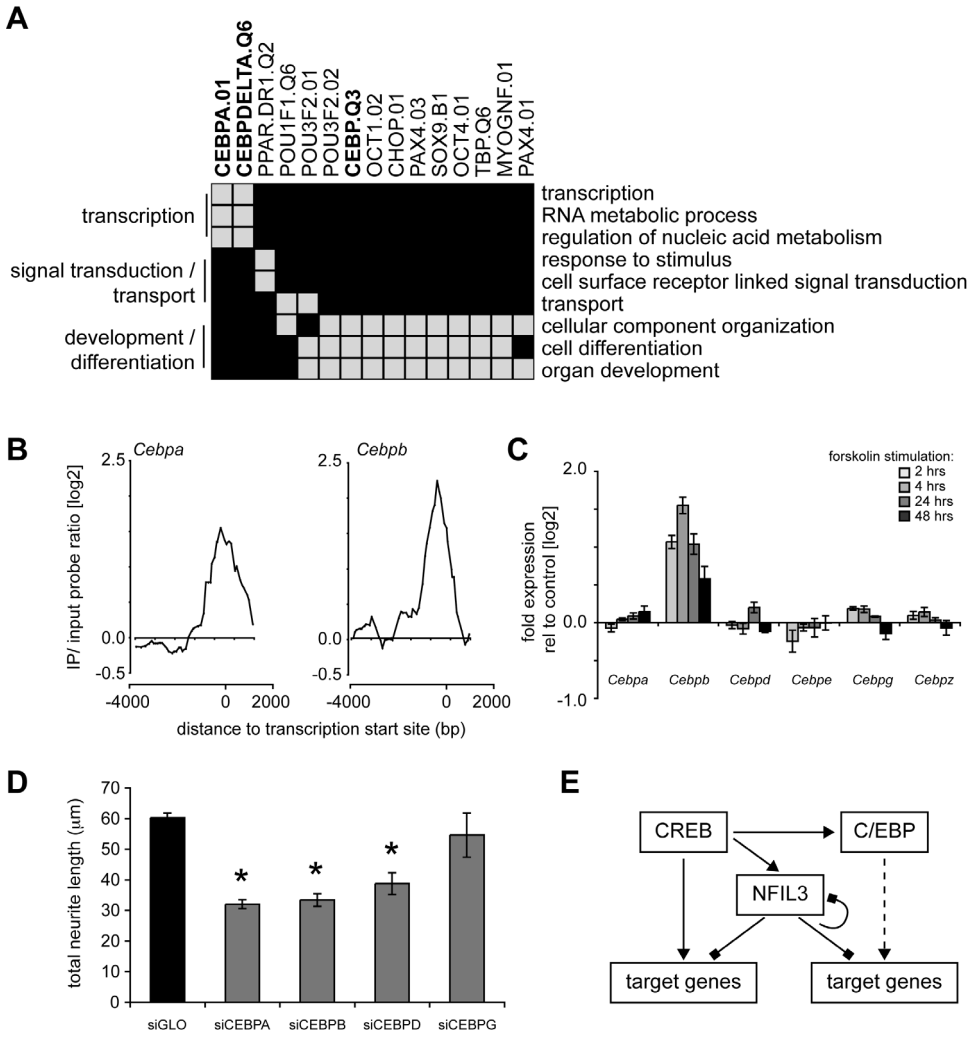

Figure 5. NFIL3 is a general repressor of activating transcription factors.
(A) Matrix showing the 15 most enriched associations between TFBSs (columns) and GO classes (rows) identified by LLM3D in 470 unique NFIL3 target genes identified by ChIP-chip. Green squares indicate a significant enrichment. The three C/EBP motifs are indicated in bold. (B) ChIP-chip enrichment profile of pCREB binding at the *Cebpa* (left) and *Cebpb* (right) promoters. (C) Microarray gene expression data showing specific upregulation of *Cebpb*, and not the other C/EBP isoforms, in forskolin-stimulated F11 cells. Bars represent means ± SEM. (D) Knockdown of C/EBPα, C/EBPβ and C/EBPδ, but not C/EBPγ, significantly reduced forskolin-induced neurite outgrowth in F11 cells. (E) Hypothetical network diagram showing the interactions between the bZIP TFs CREB, NFIL3 and C/EBP. Solid arrow indicate a direct interaction found by ChIP(-chip) analysis. Dashed arrows indicate interactions suggested by computational TFBS predictions.

cupies many promoter regions that are transcriptionally inactive, which confirms the role of NFIL3 as a transcriptional repressor. In contrast, of the 924 promoter regions that bind pCREB, >90% (844 regions) also show H3 acetylation. This indicates that pCREB primarily binds to transcriptionally active genes. Only 46 gene promoters were identified that bind both NFIL3 and pCREB and may thus represent common targets of a CREB-NFIL3 feed-forward loop.

We next wanted to correlate NFIL3 and pCREB enrichment with cAMP-induced gene expression changes. F11 cells were stimulated with forskolin for 0, 2, 4, 24 and 48 hours, and total RNA was isolated, processed and hybridized to rat whole-genome gene expression arrays. The average signal intensity values of the genes whose promoters were found enriched for NFIL3, pCREB or H3Ac were compared. As shown in Figure 4B the mean expression level of genes that show significant enrichment for pCREB and H3Ac are not significantly different from unstimulated control cells ($p = 0.13$), but both are significantly higher than the overall mRNA expression levels in F11 cells 2 hours after forskolin stimulation ($p < 2 \times 10^{-16}$ for both). On the other hand the mean expression level of genes bound by NFIL3 is only slightly higher than the overall expression levels ($p = 9 \times 10^{-7}$), and much lower compared with H3Ac enriched ($p = 3 \times 10^{-12}$) and pCREB enriched regions ($p = 2 \times 10^{-11}$). These results are consistent with the previous observation that NFIL3 predominantly occupies histone H3 hypo-acetylated, transcriptionally silent promoters, whereas pCREB predominantly occupies histone H3 acetylated, active gene promoters.

NFIL3 is a general repressor of predicted C/EBP target genes

The number of target genes that are co-occupied by both NFIL3 and pCREB in forskolin stimulated F11 cells is relatively low (46; see Figure 4A), suggesting that only few genes are co-regulated by CREB and NFIL3. To find other potential activators of NFIL3-repressed genes, we used our previously developed LLM3D algorithm (log-linear modelling for 3D contingency tables) to predict significantly overrepresented TF binding sites in genes that are bound by NFIL3. LLM3D simultaneously uses TF binding site predictions and gene ontology (GO annotations) to detect functional binding sites, and performs significantly better than conventional TF binding site prediction methods (see Chapter 5).

The 526 regions found in the NFIL3 ChIP-chip experiment map to 470 unique Entrez Gene IDs that were used as input for the LLM3D analysis. In total we find 137 TFBSs in combination with 9 GO annotations ($q < 0.1$). The top 15 TFBSs together with their associated GO classes are indicated in Figure 5A. Interestingly, among these most significantly overrepresented TFBSs in NFIL3-bound genes there are three C/EBP (CCAAT/Enhancer binding protein) motifs, together associated with 6 GO classes. Of the 470 NFIL3 target genes, 125 genes (26.6%) have one or more of these C/EBP motifs (Supplementary Table). Interestingly, in our pCREB ChIP-chip data we found evidence that CREB binds the promoters of *Cebpa* and *Cebpb* (Figure 5B), and our microarray data

show a strong increase in *Cebpb* expression in F11 cells after forskolin stimulation (Figure 5C). Finally, knockdown of C/EBPα and C/EBPβ expression in F11 cells significantly reduced forskolin-induced neurite outgrowth (Figure 5D). Together these data suggest that NFIL3 not only represses target genes that are activated by CREB (MacGillavry *et al.,* 2009) but also target genes that are activated by other cAMP/CREB-induced and growth-regulating bZIP TFs, in particular C/EBPs (Figure 5E).

Discussion

This study provides the first genome-wide identification of NFIL3 target genes in neurons using a combined approach of ChIP-chip and microarray gene expression analysis. We identified 526 genomic NFIL3 binding sites, corresponding to 470 unique, known protein-coding genes. On the basis of these *in vivo* NFIL3 binding sites we redefined the NFIL3 consensus DNA binding-site.

We previously showed that NFIL3 and pCREB bind to similar promoter elements (MacGillavry *et al.,* 2009), and we thus expected to find a significant overlap between pCREB and NFIL3 occupied promoter regions. Although we find 46 promoters bound by both pCREB and NFIL3, most NFIL3-bound promoters (>90%) do not show pCREB binding in our ChIP-chip experiments. One possible explanation for this is that binding events are missed because they are below the significance threshold. For instance, we previously showed with qPCR that the *Arg1* promoter is bound by both NFIL3 and pCREB (MacGillavry *et al.,* 2009). Using ChIP-chip analysis we only detect significant NFIL3 binding to the *Arg1* promoter, whereas pCREB binding is detected above background with significant *p*-values, but does not reach our false-discovery (*q*-value) significance threshold.

Alternatively, our results might also indicate that a large number of NFIL3-repressed genes is activated by other transcriptional activators than CREB. Indeed we find evidence that NFIL3 binds to potential C/EBP target genes. Like NFIL3 and CREB, C/EBPs are members of the bZIP family of TFs, and they bind to similar DNA binding sites. We previously showed that NFIL3 can bind to CREB binding sites, and it is tempting to speculate that NFIL3 can also directly bind the C/EBP binding sites. However, our present data cannot confirm this, and only indicate that NFIL3 and C/EBP sites co-occur in promoters, suggesting that both TFs co-regulate a substantial number of target genes.

The family of C/EBPs includes six known members: C/EBPα, β, δ, ε, γ and ζ, and all (except C/EBPζ) recognize the same binding site. C/EBP proteins are expressed in a wide range of tissues including the nervous system and can be upregulated in response to growth factor signalling and axonal injury (Sterneck and Johnson, 1998; Yukawa *et al.,* 1998; Nadeau *et al.,* 2005; Kfoury and Kapatos, 2009). Also, these TFs seem to promote differentiation and neurite outgrowth *in vitro* (Cortes-Canteli *et al.,* 2002). Interestingly, we find pCREB binding at the *Cebpa* and *Cebpb* promoters, and *Cebpb* gene expression is

strongly induced in forskolin-stimulated F11 cells and DRG neurons *in vivo* after peripheral nerve lesion (Chapter 5). These findings are consistent with earlier reports showing that C/EBPs are downstream CREB targets (Impey *et al.,* 2004). Finally, we show that several C/EBPs are involved in regulating neurite outgrowth from F11 cells. Together, our findings suggest a model in which activated CREB induces expression of C/EBPs and of NFIL3, and in which NFIL3 subsequently serves as a general feed-forward repressor of both CREB and C/EBP target genes (Figure 5D).

We find that many NFIL3-bound genes are histone H3 hypo-acetylated, and that their overall expression levels are just above background. This suggests that NFIL3 may also serve to keep genes in a repressed, transcriptionally silent state under basal conditions. Such a mechanism could potentially enhance the response time of target genes upon physiological stimulation. In unstimulated conditions, NFIL3-bound promoters are transcriptionally repressed rather than transcriptionally silent, allowing basal transcription to occur. As a result, stimulus-activated bZIP TFs such as CREB and C/EBP, which bind to the same promoters either or not in direct competition with NFIL3, will then be able to quickly turn on transcription. Indeed, modelling and experimental studies have shown that higher responsiveness of target genes is a general feature of incoherent feed-forward loops (Mangan *et al.,* 2006; Kaplan *et al.,* 2008).

A role for NFIL3 as a general repressor of bZIP TF-activated genes might also explain the diverse functions that NFIL3 has in different biological contexts. Depending on which activating TF is co-expressed or co-activated, context-specific subsets of NFIL3-repressed genes will become transcriptionally active. Possible defects as a consequence of NFIL3 deletion will thus only be revealed under stimulated conditions. Indeed, genetic deletion of NFIL3 has no obvious effects in most tissues other than the immune system, as shown by the recent analysis of three independent NFIL3 knockout mice (Gascoyne *et al.,* 2009; Kamizono *et al.,* 2009). Further analysis of neuron-specific defects in these animals under conditions of nerve injury may help to further elucidate the role of NFIL3 in neuronal regeneration.

Materials and methods

Cell culture

F11 cells were maintained in Dulbeco's Modified Eagle Medium (DMEM; Gibco) supplemented with 10% fetal calf serum and 100U/ml penicillin and 100U/ml streptomycin. Cells were grown at 370C and 5% CO2.

ChIP-chip: array design

Custom rat promoter arrays were designed using Agilent eArray software. The chromosomal locations of the transcription start sites (TSS) of 10,123 RefSeq genes, 8,189 Known Genes and 178 miRNA entries were extracted from the UCSC Genome Browser

(Rattus norvegicus, June 2003 assembly) (Karolchik *et al.,* 2003; Gibbs *et al.,* 2004; Havlak *et al.,* 2004). Based on these locations, 60-mer oligonucleotide DNA probes were selected within a span of 8.5 kb up- and 2.5 kb downstream relative to the TSS. This resulted in a total of 725,098 probes distributed over three 244K arrays.

ChIP-chip: chromatin immunoprecipitation

F11 cells (1 x 10^8 for one ChIP-chip) were grown in five 15 cm culture plates. For NFIL3 ChIP-chip assays, cells were transiently transfected with a Flag-Myc-NFIL3 overexpression construct using the polyethyleneimine (PEI) transfection method. F11 cells were serum starved for three hours and stimulated with 10 μM forskolin for 2 hours. Next, chromatin complexes were cross-linked by adding 37% formaldehyde to a final concentration of 1% for 10 minutes at room temperature. Formaldehyde cross-linking was quenched with 125 mM glycine for 5 minutes. Cells were washed with cold PBS and lysed with SDS lysis buffer (1% SDS, 20 mM EDTA, 20 mM Tris-HCl; pH 8.0), supplemented with protease inhibitor cocktail. Cross-linked chromatin was sheared with 4 pulses of 30 sec on ice water and a 30 sec rest interval on ice. This consistently yielded DNA fragments of 200-600 bp in length. Chromatin samples were diluted 5-10 times with dilution buffer (1% Triton X-1000, 2 mM EDTA, 150 mM NaCl, 20 mM Tris-HCl; pH 8.0). Immunoprecipitation was performed with rabbit anti-acetyl histone H3 (Millipore), mouse anti-Flag-M2 (Sigma) or rabbit anti-phospho-CREB (Cell Signaling) overnight with gentle rotation at 4^0C. Immuno-complexes were then captured with 50 μl protein A/G beads (Santa Cruz Biotechnology) by rotation at 4^0C for 2 hours. Complexes were washed once with low-salt buffer (0.1% SDS, 1% Trition X-100, 2 mM EDTA, 150 mM NaCl in 20 mM Tris-HCl; pH 8.0), once with high-salt buffer (0.1% SDS, 1% Triton X-100, 2 mM EDTA, 500 mM NaCl in 20 mM Tris HCl; pH 8.0), twice with LiCl buffer (1 mM EDTA, 250 mM LiCl, 1% deoxycholate, 1% NP-40 in 20 mM Tris-HCl; pH 8.0) and three times with TE buffer (1 mM EDTA, 10 mM Tris-HCl; pH 8.0), and were then eluted with 400 μl elution buffer (1% SDS, 100 mM $NaHCO_3$). Input and immunoprecipitated chromatin samples were reverse cross-linked by shaking overnight at 65^0C in the presence of proteinase K. DNA was subsequently purified using one phenol/chloroform/isoamyl-alcohol extraction and one chloroform/isoamyl-alcohol extraction, followed by ethanol precipitation.

ChIP-chip: DNA amplification and hybridization

Purified DNA fragments were blunted with T4 DNA polymerase (New England Biolabs) for 20 minutes at 12^0C, and linkers were ligated using T4 ligase (Fermentas) overnight at 16^0C. Fragments were then amplified using two rounds of PCR amplification. Amplified DNA samples were labelled with Cy3-dUTP (input samples) or Cy5-dUTP (IP samples) and purified using the CGH Bioprime random primer labelling and purification kit (Invitrogen). Labelled samples were combined and hybridized to custom Agilent ChIP-on-chip arrays for 40 hours at 65^0C, washed according to the Agilent aCGH array wash

protocol and scanned using an Agilent scanner (Agilent Technologies).

ChIP-chip: data extraction, data normalization and peak detection

Extracted data were processed under R using the Bioconductor packages 'limma' and 'ringo'. Raw probe intensities were background corrected and loess normalized. Resulting log2 probe ratios were averaged using a sliding window of 500 bp, which usually contained three to four probes. For the analysis of the NFIL3 ChIP-chip data a one-sided t-test statistic was computed for each probe location by comparing the sliding window average of the Flag ChIP-chip with the sliding window average of the mock ChIP-chip. Genomic regions containing three adjacent probes with a p-value < 0.01 were collapsed and defined as a bound region.

The pCREB and H3Ac ChIP-chip data were analyzed using the symmetric null-distribution method (Gibbons *et al.,* 2005; Li *et al.,* 2008). Assuming that negative ChIP-chip values are symmetrically distributed around the mean, the null distribution can be estimated from those values that are smaller than the mode of all observed ChIP-chip ratios. From this distribution, p-values are then estimated and corrected for multiple testing using the Storey method (Storey and Tibshirani, 2003). Regions containing three or more probes with a q-value < 0.1 were defined as a bound region. Bound regions were annotated to the TSS that is located closest to the centre of the bound region based on the UCSC Genome Browser annotation (Rattus norvegicus, June 2003 assembly, rn3). All primary ChIP-chip data have been submitted to GEO (http://www.ncbi.nlm.nih.gov/geo/; accession number GSE).

Quantitative analysis of ChIP samples

Quantitative PCR was performed using site-specific primers in duplicate on the ABI 7900HT detection system (Applied Biosystems) with the 2x SYBR green ready reaction mix (Applied Biosystems). Normalized enrichment values were calculated by subtracting the Ct value of the IP sample from the Ct value of the control IP samples, each normalized to the input sample. Regions with a log2 enrichment value >1 were considered as true targets. Specificity of the primers was controlled by inspection of dissociation curves.

De novo motif finding

DNA sequences (300 bp on average) from 17 validated NFIL3-bound regions were extracted and searched for motifs that might represent protein-DNA interaction sites using the motif discovery scan program (MDScan; http://ai.stanford.edu/~xsliu/MDscan/) (Liu *et al.,* 2002). Default settings were used to identify an 8-bp DNA sequence motif. The top-scoring motif is represented as a DNA consensus sequence logo generated by the online WebLogo tool (http://weblogo.berkeley.edu/) (Crooks *et al.,* 2004). The 200 top-scoring ChIP-chip DNA sequences were scanned for the presence of motifs using the Possum *cis*-element detection program (http://zlab.bu.edu/~mfrith/possum/) (Fu *et al.,*

2004). The background set consisted of 200 random genomic sequences of equal lengths. Overrepresentation was analysed using a two-sided Fisher's exact test.

Microarray gene expression analysis

F11 cells were incubated in low-serum medium (DMEM with 0.5% FCS and antibiotics) for three hours and then stimulated with 10 μM forskolin for 0, 2, 4, 24 and 48 hours. Total RNA was isolated using Trizol reagent (Invitrogen). RNA samples were amplified, labelled and hybridized to Agilent 4x44K Rat Whole-Genome expression arrays using standard Agilent protocols. Arrays were scanned using an Agilent scanner and data were read using Agilent Feature Extraction software. Array data were further processed using the R packages 'bioconductor' (Gentleman *et al.,* 2004) and 'limma' (Linear Models for Microarray Data) (Ritchie *et al.,* 2007) for Edward's background subtraction and loess normalization. The microarray gene expression data have been deposited in the Gene Expression Omibus (GEO) database (http://www.ncbi.nlm.nih.gov/geo/; accession number GSE22631).

RNA interference

F11 cells were cultured in 96-well plates and transfected with Dharmacon siGENOME siRNA SMARTpools as previously described (MacGillavry *et al.,* 2009). Two negative controls were included: siGLO RISC-free siRNA and transfection without siRNA. Outgrowth was induced 4 hours after transfection by replacing the medium with DMEM containing 0.5% FCS and 10 μM forskolin. After 2 days cells were fixed and stained. Neurite outgrowth was quantified using a Cellomics ArrayScan HCS Reader and the Neuronal Profiling Bioapplication. Per well 100-500 cells were analyzed and neurite total length per cell was calculated.

References

Acharya A, Rishi V, Moll J, Vinson C (2006) Experimental identification of homodimerizing B-ZIP families in Homo sapiens. J Struct Biol 155:130-139.

Bernstein BE, Kamal M, Lindblad-Toh K, Bekiranov S, Bailey DK, Huebert DJ, McMahon S, Karlsson EK, Kulbokas EJ, 3rd, Gingeras TR, Schreiber SL, Lander ES (2005) Genomic maps and comparative analysis of histone modifications in human and mouse. Cell 120:169-181.

Boland LM, Dingledine R (1990) Expression of sensory neuron antigens by a dorsal root ganglion cell line, F-11. Brain Res Dev Brain Res 51:259-266.

Chen WJ, Lewis KS, Chandra G, Cogswell JP, Stinnett SW, Kadwell SH, Gray JG (1995) Characterization of human E4BP4, a phosphorylated bZIP factor. Biochim Biophys Acta 1264:388-396.

Cortes-Canteli M, Pignatelli M, Santos A, Perez-Castillo A (2002) CCAAT/enhancer-binding protein beta plays a regulatory role in differentiation and apoptosis of neuroblastoma cells. J Biol Chem 277:5460-5467.

Cowell IG, Hurst HC (1994) Transcriptional repression by the human bZIP factor E4BP4: definition of a minimal repression domain. Nucleic Acids Res 22:59-65.

Cowell IG, Hurst HC (1996) Protein-protein interaction between the transcriptional repressor E4BP4 and the TBP-binding protein Dr1. Nucleic Acids Res 24:3607-3613.

Cowell IG, Skinner A, Hurst HC (1992) Transcriptional repression by a novel member of the bZIP family of transcription factors. Mol Cell Biol 12:3070-3077.

Crooks GE, Hon G, Chandonia JM, Brenner SE (2004) WebLogo: a sequence logo generator. Genome Res 14:1188-1190.

Francel PC, Harris K, Smith M, Fishman MC, Dawson G, Miller RJ (1987) Neurochemical characteristics of a novel dorsal root ganglion X neuroblastoma hybrid cell line, F-11. J Neurochem 48:1624-1631.

Fu Y, Frith MC, Haverty PM, Weng Z (2004) MotifViz: an analysis and visualization tool for motif discovery. Nucleic Acids Res 32:W420-423.

Gascoyne DM, Long E, Veiga-Fernandes H, de Boer J, Williams O, Seddon B, Coles M, Kioussis D, Brady HJ (2009) The basic leucine zipper transcription factor E4BP4 is essential for natural killer cell development. Nat Immunol 10:1118-1124.

Gentleman RC et al. (2004) Bioconductor: open software development for computational biology and bioinformatics. Genome Biol 5:R80.

Gibbons FD, Proft M, Struhl K, Roth FP (2005) Chipper: discovering transcription-factor targets from chromatin immunoprecipitation microarrays using variance stabilization. Genome Biol 6:R96.

Gibbs RA et al. (2004) Genome sequence of the Brown Norway rat yields insights into mammalian evolution. Nature 428:493-521.

Havlak P, Chen R, Durbin KJ, Egan A, Ren Y, Song XZ, Weinstock GM, Gibbs RA (2004) The Atlas genome assembly system. Genome Res 14:721-732.

Ikushima S, Inukai T, Inaba T, Nimer SD, Cleveland JL, Look AT (1997) Pivotal role for the NFIL3/E4BP4 transcription factor in interleukin 3-mediated survival of pro-B lymphocytes. Proc Natl Acad Sci U S A 94:2609-2614.

Impey S, McCorkle SR, Cha-Molstad H, Dwyer JM, Yochum GS, Boss JM, McWeeney S, Dunn JJ, Mandel G, Goodman RH (2004) Defining the CREB regulon: a genome-wide analysis of transcription factor regulatory regions. Cell 119:1041-1054.

Inostroza JA, Mermelstein FH, Ha I, Lane WS, Reinberg D (1992) Dr1, a TATA-binding protein-associated phosphoprotein and inhibitor of class II gene transcription. Cell 70:477-489.

Junghans D, Chauvet S, Buhler E, Dudley K, Sykes T, Henderson CE (2004) The CES-2-related transcription factor E4BP4 is an intrinsic regulator of motoneuron growth and survival. Development 131:4425-4434.

Kamizono S, Duncan GS, Seidel MG, Morimoto A, Hamada K, Grosveld G, Akashi K, Lind EF, Haight JP, Ohashi PS, Look AT, Mak TW (2009) Nfil3/E4bp4 is required for the development and maturation of NK cells *in vivo*. J Exp Med.

Kaplan S, Bren A, Dekel E, Alon U (2008) The incoherent feed-forward loop can generate non-monotonic input functions for genes. Mol Syst Biol 4:203.

Karolchik D, Baertsch R, Diekhans M, Furey TS, Hinrichs A, Lu YT, Roskin KM, Schwartz M, Sugnet CW, Thomas DJ, Weber RJ, Haussler D, Kent WJ (2003) The UCSC Genome Browser Database. Nucleic Acids Res 31:51-54.

Kfoury N, Kapatos G (2009) Identification of neuronal target genes for CCAAT/enhancer binding proteins. Mol Cell Neurosci 40:313-327.

Li XY et al. (2008) Transcription factors bind thousands of active and inactive regions in the Drosophila blastoderm. PLoS Biol 6:e27.

Liu XS, Brutlag DL, Liu JS (2002) An algorithm for finding protein-DNA binding sites with applications to chromatin-immunoprecipitation microarray experiments. Nat Biotechnol 20:835-839.

MacGillavry HD, Stam FJ, Sassen MM, Kegel L, Hendriks WT, Verhaagen J, Smit AB, van Kesteren RE (2009) NFIL3 and cAMP response element-binding protein form a transcriptional feedforward loop that controls neuronal regeneration-associated gene expression. J Neurosci 29:15542-15550.

Mangan S, Itzkovitz S, Zaslaver A, Alon U (2006) The incoherent feed-forward loop accelerates the response-time of the gal system of Escherichia coli. J Mol Biol 356:1073-1081.

Mitsui S, Yamaguchi S, Matsuo T, Ishida Y, Okamura H (2001) Antagonistic role of E4BP4 and PAR proteins in the circadian oscillatory mechanism. Genes Dev 15:995-1006.

Nadeau S, Hein P, Fernandes KJ, Peterson AC, Miller FD (2005) A transcriptional role for C/EBP beta in the neuronal response to axonal injury. Mol Cell Neurosci 29:525-535.

Platika D, Boulos MH, Baizer L, Fishman MC (1985) Neuronal traits of clonal cell lines derived by fusion of dorsal root ganglia neurons with neuroblastoma cells. Proc Natl Acad Sci U S A 82:3499-3503.

Ritchie ME, Silver J, Oshlack A, Holmes M, Diyagama D, Holloway A, Smyth GK (2007) A comparison of background correction methods for two-colour microarrays. Bioinformatics 23:2700-2707.

Sterneck E, Johnson PF (1998) CCAAT/enhancer binding protein beta is a neuronal transcriptional regulator activated by nerve growth factor receptor signaling. J Neurochem 70:2424-2433.

Storey JD, Tibshirani R (2003) Statistical significance for genomewide studies. Proc Natl Acad Sci U S A 100:9440-9445.

Vinson C, Acharya A, Taparowsky EJ (2006) Deciphering B-ZIP transcription factor interactions in vitro and in vivo. Biochim Biophys Acta 1759:4-12.

Yukawa K, Tanaka T, Tsuji S, Akira S (1998) Expressions of CCAAT/Enhancer-binding proteins beta and delta and their activities are intensified by cAMP signaling as well as Ca2+/calmodulin kinases activation in hippocampal neurons. J Biol Chem 273:31345-31351.

Zhang W, Zhang J, Kornuc M, Kwan K, Frank R, Nimer SD (1995) Molecular cloning

and characterization of NF-IL3A, a transcriptional activator of the human interleukin-3 promoter. Mol Cell Biol 15:6055-6063.

Supplementary Table

List of NFIL3-bound genes in which C/EBP binding sites are detected.

Symbol	Name	GeneID
Aard	alanine and arginine rich domain containing protein	246323
Acan	aggrecan	58968
Adamts1	ADAM metallopeptidase with thrombospondin type 1 motif, 1	79252
Adrm1	NA	NA
Anp32a	acidic (leucine-rich) nuclear phosphoprotein 32 family, member A	25379
Arhgap5	Rho GTPase activating protein 5	299012
Asb2	ankyrin repeat and SOCS box-containing 2	299266
Asb6	ankyrin repeat and SOCS box-containing 6	296627
Ascl2	achaete-scute complex homolog 2 (Drosophila)	24209
Atg7	ATG7 autophagy related 7 homolog (S. cerevisiae)	312647
Bcl2	B-cell CLL/lymphoma 2	24224
Bid	BH3 interacting domain death agonist	64625
Bub3	budding uninhibited by benzimidazoles 3 homolog (S. cerevisiae)	361662
Casp3	caspase 3	25402
Cby1	chibby homolog 1 (Drosophila)	246768
Ccnd1	cyclin D1	58919
Cdk9	cyclin-dependent kinase 9	362110
Cebpg	CCAAT/enhancer binding protein (C/EBP), gamma	25301
Cfl1	cofilin 1, non-muscle	29271
Chkb	choline kinase beta	29367
Chm	choroideremia (Rab escort protein 1)	24942
Cir	NA	NA
Cit	citron	83620
Cltc	clathrin, heavy chain (Hc)	54241
Creb3l2	cAMP responsive element binding protein 3-like 2	362339
Cxcl12	chemokine (C-X-C motif) ligand 12 (stromal cell-derived factor 1)	24772
Dcn	decorin	29139
Dlat	dihydrolipoamide S-acetyltransferase	81654
Dlg1	discs, large homolog 1 (Drosophila)	25252
Dmbt1	deleted in malignant brain tumors 1	170568
Dnah12	NA	NA
Efna5	ephrin A5	116683
Emcn	endomucin	295490
Emp3	epithelial membrane protein 3	81505
Fastkd2	FAST kinase domains 2	301463
Fat1	FAT tumor suppressor homolog 1 (Drosophila)	83720
Fez2	fasciculation and elongation protein zeta 2 (zygin II)	94269
Fgf22	fibroblast growth factor 22	170579
Fgfr2	fibroblast growth factor receptor 2	25022
Foxa2	forkhead box A2	25099

Symbol	Name	GeneID
Gfpt1	glutamine fructose-6-phosphate transaminase 1	297417
Ghrhr	growth hormone releasing hormone receptor	25321
Gtf2a1l	general transcription factor IIA, 1-like	316711
Hip1r	huntingtin interacting protein 1 related	81917
Hlx	H2.0-like homeobox	364069
Hnrnpf	heterogeneous nuclear ribonucleoprotein F	64200
Hoxa5	homeo box A5	79241
Htra2	HtrA serine peptidase 2	297376
Igfbp2	insulin-like growth factor binding protein 2	25662
Il1rap	interleukin 1 receptor accessory protein	25466
Il8rb	interleukin 8 receptor, beta	29385
Insl3	insulin-like 3	114215
Isy1	ISY1 splicing factor homolog (S. cerevisiae)	362394
Itga7	integrin alpha 7	81008
Kcna2	potassium voltage-gated channel, shaker-related subfamily, 2	25468
Kcnip2	Kv channel-interacting protein 2	56817
LOC312831	NA	NA
Mapk8	mitogen-activated protein kinase 8	116554
Mmd2	monocyte to macrophage differentiation-associated 2	304301
Mrs2	MRS2 magnesium homeostasis factor homolog	79032
Mterf	mitochondrial transcription termination factor	85261
Mtl5	metallothionein-like 5, testis-specific (tesmin)	309142
Mustn1	musculoskeletal, embryonic nuclear protein 1	290553
Mxi1	MAX interactor 1	25701
Myf6	myogenic factor 6	25714
Myh9	myosin, heavy chain 9, non-muscle	25745
Myog	myogenin	29148
Nab1	Ngfi-A binding protein 1	64824
Nap1l5	nucleosome assembly protein 1-like 5	688843
Nfib	nuclear factor I/B	29227
Ngef	neuronal guanine nucleotide exchange factor	246217
Nolc1	nucleolar and coiled-body phosphoprotein 1	64896
Nradd	neurotrophin receptor associated death domain	246143
Nubp1	nucleotide binding protein 1	287042
Nup210	nucleoporin 210	58958
Palm	paralemmin	170673
Pax6	paired box 6	25509
Pdlim1	PDZ and LIM domain 1	54133
Phrf1	PHD and ring finger domains 1	245925
Pmp22	peripheral myelin protein 22	24660

Symbol	Name	GeneID
Pou6f1	POU class 6 homeobox 1	116545
Prdm4	PR domain containing 4	170820
Prkar1b	protein kinase, cAMP dependent regulatory, type I, beta	25521
Prpf6	PRP6 pre-mRNA processing factor 6 homolog (S. cerevisiae)	366276
Pus1	pseudouridylate synthase 1	304567
Rhox7	reproductive homeobox 7	298353
Runx3	runt-related transcription factor 3	156726
Sart1	squamous cell carcinoma antigen recognized by T cells	29678
Sfrs5	splicing factor, arginine/serine-rich 5	29667
Skap2	src kinase associated phosphoprotein 2	155183
Slc22a17	solute carrier family 22, member 17	305886
Slc25a15	solute carrier family 25, member 15	306574
Snap25	synaptosomal-associated protein 25	25012
Snd1	NA	NA
Snip1	Smad nuclear interacting protein 1	313588
Spna2	alpha-spectrin 2	64159
Sptbn2	spectrin, beta, non-erythrocytic 2	29211
Spz1	spermatogenic leucine zipper 1	499510
Srp54a	signal recognition particle 54a	116650
Ssrp1	structure specific recognition protein 1	81785
Star	steroidogenic acute regulatory protein	25557
Stx6	syntaxin 6	60562
Syn1	synapsin I	24949
Synj1	synaptojanin 1	85238
Tbce	tubulin folding cofactor E	361255
Tgfb1	transforming growth factor, beta 1	59086
Tle3	transducin-like enhancer of split 3 (E(sp1) homolog, Drosophila)	84424
Tmbim6	transmembrane BAX inhibitor motif containing 6	24822
Tmem176b	transmembrane protein 176B	171411
Tnp1	transition protein 1	24839
Treh	trehalase (brush-border membrane glycoprotein)	60576
Trim69	tripartite motif-containing 69	311373
Trpc4	transient receptor potential cation channel, subfamily C, 4	84494
Trpv2	transient receptor potential cation channel, subfamily V, 2	29465
Tsc22d3	TSC22 domain family, member 3	83514
Tubb2b	tubulin, beta 2b	291081
Txnrd2	thioredoxin reductase 2	50551
Ucp2	uncoupling protein 2 (mitochondrial, proton carrier)	54315
Ucp3	uncoupling protein 3 (mitochondrial, proton carrier)	25708
Unc5a	unc-5 homolog A (C. elegans)	60629

Symbol	Name	GeneID
Vegfa	vascular endothelial growth factor A	83785
Vegfc	vascular endothelial growth factor C	114111
Vps45	vacuolar protein sorting 45 homolog (S. cerevisiae)	64516
Zfp61	zinc finger protein 61	499094
Znf467	zinc finger protein 467	500110

Chapter 5

LLM3D: a log-linear modeling-based method to predict functional gene regulatory interactions from genome-wide expression data

Geert Geeven[1,4], Harold D MacGillavry[2,4], Ruben Eggers[3], Marion M Sassen[2], Joost Verhaagen[3], August B Smit[2], Mathisca CM de Gunst[1] and Ronald E van Kesteren[2]

[1]Department of Mathematics, Faculty of Sciences, VU University, De Boelelaan 1081, 1081 HV Amsterdam, The Netherlands
[2]Department of Molecular and Cellular Neurobiology, Center for Neurogenomics and Cognitive Research, Neuroscience Campus Amsterdam, VU University, De Boelelaan 1085, 1081 HV Amsterdam, The Netherlands
[3]Laboratory for Neuroregeneration, Netherlands Institute for Neuroscience, Meiberg-dreef 47, 1105 BH Amsterdam, The Netherlands
[4]These authors contributed equally to this work

manuscript under review

Abstract

Condition-specific and time-dependent transcriptional regulatory networks underlie the coordinated expression of genes involved in biological processes. We demonstrate a new method that uses log-linear modeling of three-dimensional contingency tables (LLM3D), and show it successfully predicts transcriptional regulators in cellular systems with different levels of regulatory complexity. LLM3D combines gene expression data, gene ontology (GO) annotation and computationally predicted transcription factor binding sites (TFBSs) in a single statistical analysis, and offers a methodological improvement over existing enrichment-based methods. LLM3D allowed us to identify potential novel transcriptional regulators of genes in the yeast metabolic cycle, and to correctly infer a role for known key regulators of mouse embryonic stem cell self-renewal, whereas existing methods did not. Moreover, in a clinically relevant *in vivo* injury model of mammalian neurons, LLM3D identified peroxisome proliferator-activated receptor γ (PPARγ) as a novel transcriptional regulator of regenerative axon growth.

Introduction

Insight into gene regulatory networks is crucial for the understanding of biological systems under normal and pathological conditions. An important step in the analysis of gene networks is the prediction of functional transcription factor binding sites (TFBSs) within gene regulatory sequences. Recently, advanced methods have been developed to predict TFBSs *in silico* (Wasserman and Sandelin, 2004; Hannenhalli, 2008). Public databases containing large collections of experimentally validated binding sites can be used to derive probabilistic models of TFBSs and software algorithms can subsequently be employed to scan potential gene regulatory sequences for the prediction of new sites. However, in contrast to simple model organisms such as yeast, mammalian gene regulatory sequences are often large and can be located up to several thousands of base pairs away from transcription start sites. Consequently, mammalian TFBS predictions are usually less accurate and more likely to contain false positives. A reduction in false positive TFBS predictions can be achieved by improving the quality of the biological input data, for instance by considering TF binding affinities (Roider *et al*., 2007; Ward and Bussemaker, 2008), TF cooperativity at *cis*-regulatory modules (Warner *et al*., 2008; Zinzen *et al*., 2009) or evolutionary conservation of binding sites across species (Wasserman and Sandelin, 2004; Xie *et al*., 2005), or by improving the way in which computational methods make use of these data.

A common method to reduce false positive TFBS predictions at the computational level involves the identification of TFBSs that are enriched in subsets of related genes compared to a control (background) set of genes (Nam and Kim, 2008; Huang *et al*., 2009b). Co-regulation and co-functionality are often used as criteria to define gene

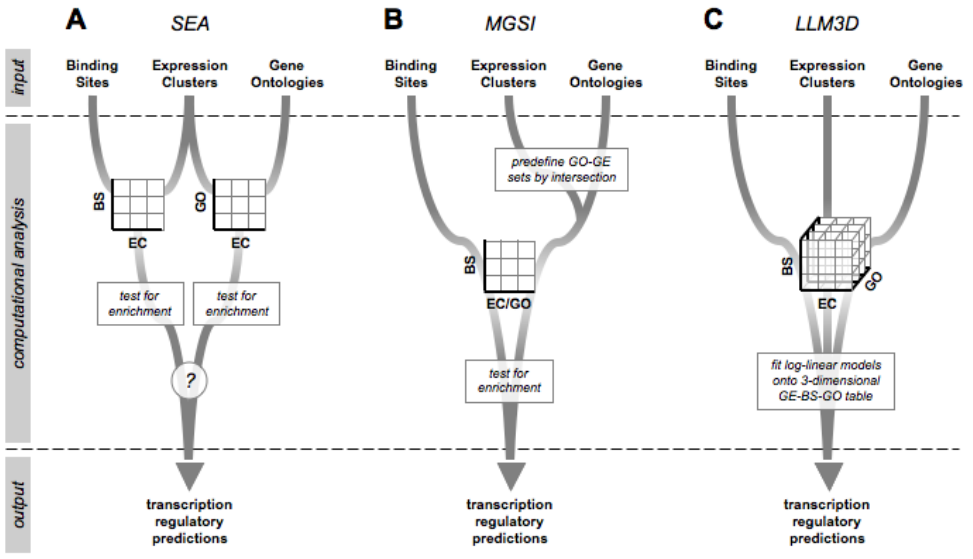

Figure 1. Comparison of LLM3D with other gene set enrichment analysis approaches.
(A) In singular enrichment analysis (SEA), gene expression clusters (EC) are independently tested for enrichment of binding sites (BS) and gene ontology (GO) terms using two two-dimensional contingency tables. It is not clear how meaningful relationships between the two should be inferred. (B) In multi gene set intersection (MGSI), multiple gene sets are predefined based on intersecting sets of co-expressed genes with sets of genes sharing GO terms. MGSI considers all three variables in a single two-dimensional contingency table in which gene expression and GO data are collapsed into a single combined variable. (C) In LLM3D, gene expression, binding site data and GO annotations are used as separate input variables in a single three-dimensional contingency table. To this table, log-linear models are fitted in order to test the joint dependence of all three variables simultaneously.

sets of interest. In order to study enrichment of both TFBSs and gene function in co-expressed genes, two different computational approaches can be used. The first approach, referred to as singular enrichment analysis (SEA) (Huang *et al.*, 2009b), allows separate quantification of gene ontology (GO) term and TFBS enrichment in sets of co-expressed genes (Figure 1A). SEA typically returns separate lists of enriched GO terms and TFBSs (Reimand *et al.*, 2007; Huang *et al.*, 2009a), but is not designed to predict transcriptional targets using gene expression, TFBS and GO data simultaneously. The second approach, which we will refer to as the multi-gene-set-by-intersection (MGSI) approach, predefines multiple sets of co-expressed genes sharing the same GO term, and subsequently tests each set for TFBS enrichment (Figure 1B). MGSI-based methods provide a significant improvement over SEA and perform better in predicting functional TFBSs (Carmona-Saez *et al.*, 2007; Nogales-Cadenas *et al.*, 2009). However, MGSI collapses gene expression and GO annotation into a single combined variable. As a result, important information about the joint dependence of all three variables (i.e., gene expression, GO association, and TFBS presence) is lost.

We present a novel method that uses log-linear modeling of three-dimensional contingency tables (LLM3D), to identify experiment-specific associations between gene expression, TFBS presence and gene function (Figure 1C). We show that LLM3D provides a significant improvement over existing methods. We validate our method using published genome-wide gene expression and transcription factor binding data, and demonstrate that the gene regulatory predictions made by LLM3D have significantly higher predictive value compared with MGSI, and are biologically relevant, both in yeast and in mammals. Finally, we showcase LLM3D by performing and analyzing a genome-wide expression profiling study in a clinically relevant animal model for the functional regeneration of injured neurons. *Post hoc* experimental validation shows that in this case LLM3D is able to identify functional gene regulatory interactions that remain undetected using existing methodologies.

Results

LLM3D: a methodological and statistical improvement in gene set enrichment analysis

Input to the main statistical analysis in LLM3D is a defined set of gene expression clusters, TFBSs and GO terms. For each TFBS-GO pair of interest, LLM3D cross-classifies all genes according to GO annotation, TFBS presence, and gene expression to obtain a three dimensional contingency table (Figure 1C). The main statistical analysis of LLM3D consists of finding the best model that describes the observed counts in this table. The most basic model, i.e., the model that assumes that gene expression, GO annotation and TFBS presence are mutually independent, is referred to as the null model. The underlying hypothesis of mutual independence is tested using a likelihood ratio test statistic (Christensen, 1997). When this hypothesis is rejected, LLM3D considers eight alternative models that differ in the dependence relationships they imply between gene expression, GO annotation, TFBS presence, and selects the best model using the Akaike information criterion (AIC) (Akaike, 1974). The enrichment of TFBSs in functionally homogenous and co-expressed genes implied by the selected model is then used to predict functional gene regulatory interactions. Because we consider all three variables jointly, we expect LLM3D to perform better in comparison with existing enrichment-based methods.

Identification of functional gene regulatory interactions in yeast

We used both LLM3D and MGSI to predict gene regulatory interactions controlling the yeast metabolic cycle. It is estimated that approximately half of all yeast genes show periodic expression during the metabolic cycle. These genes can be divided into three large expression clusters of tightly co-regulated genes: oxidative (Ox; 1,023 genes), reductive/building (Rb; 977 genes) cluster, and reductive/charging (Rc; 1,510 genes) (Tu *et al*., 2005) (Figure 2A). The principle difference between LLM3D and MGSI is depicted in Figure

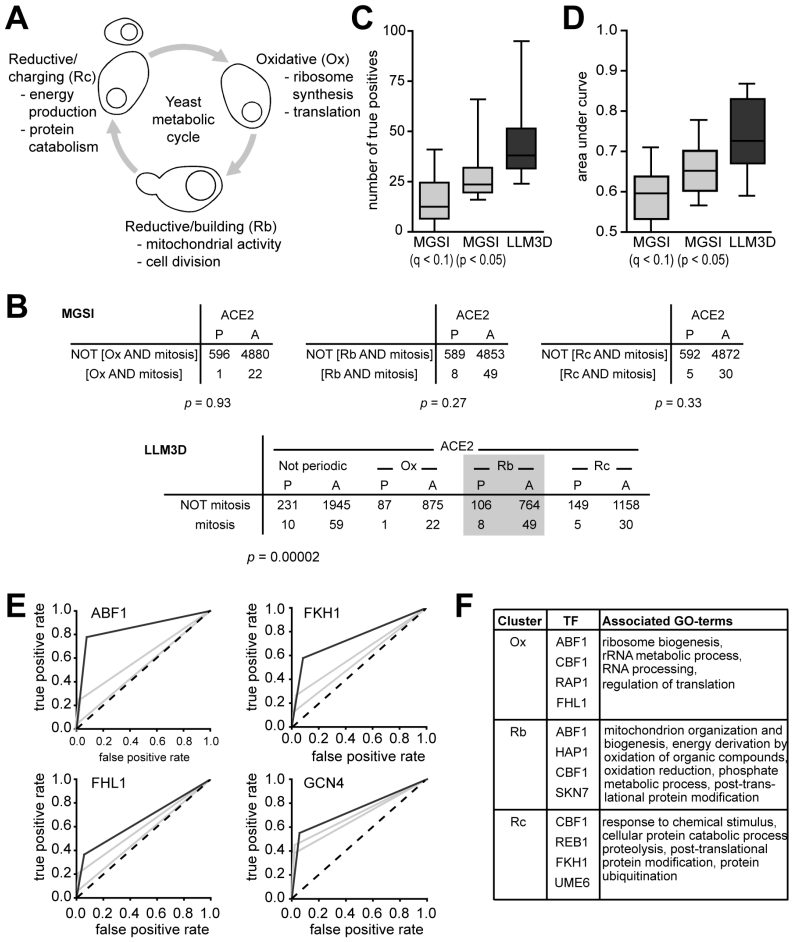

Figure 2. LLM3D correctly infers gene regulatory interactions from yeast metabolic cycle gene expression data. (A) Schematic representation of the yeast metabolic cycle. The three phases of the cycle (Ox, Rb and Rc) are indicated together with the biological processes that dominate each phase. (B) Example contingency tables demonstrating the LLM3D approach. LLM3D detects a significant interaction of ACE2 binding sites with 'mitosis' GO genes in yeast metabolic cycle gene expression clusters, whereas MGSI does not (P: present; A: absent; see text for details). The highest enrichment of ACE2/'mitosis' genes is observed in the Rb expression cluster (grey box), which corresponds with the mitotic phase of the cycle. (C) Number of true positive target gene predictions for top-20 TFs identified by both LLM3D and MGSI in the yeast metabolic cycle expression clusters. LLM3D identifies more true targets than MGSI, even when the stringency of the latter is reduced to a *p*-value cut-off of 0.05 without correction for multiple testing. (D) LLM3D also produces higher AUC values than MGSI, even when the stringency of the latter is reduced to a *p*-value cut-off 0.05 without correction for multiple testing. (E) Example ROC curves for four TFs (LLM3D in dark grey; MGSI in light grey), indicating that LLM3D has better predictive performance. (F) List of the top-four LLM3D-predicted TFs per expression cluster for which at least five additional true positive targets are predicted compared with MGSI, together with their associated GO-terms.

Figure 3. LLM3D correctly infers gene regulatory interactions from mouse ES cell self-renewal gene expression data. (A) Schematic representation of ES cell self-renewal and differentiation. Indicated are the four gene expression clusters (ES up, ES down, Uniform high, and Uniform low) identified by Ouyang *et al.* (2009) together with the biological processes that dominate each cluster. (B) Number of true positive target gene predictions for 9 TFs identified by both LLM3D and MGSI ($p < 0.05$) in the mouse ES cell gene expression clusters. LLM3D identifies more true targets than MGSI, even when the stringency of the latter is reduced to a *p*-value cut-off of 0.05 without correction for multiple testing. (C) LLM3D also produces slightly higher AUC values than MGSI, even when the stringency of the latter is reduced to a *p*-value cut-off 0.05 without correction for multiple testing. (D) Example ROC curves for three TFs (LLM3D in dark grey; MGSI in light grey), indicating that LLM3D has better predictive performance. (E) In contrast to MGSI, LLM3D correctly inferred a role for Nanog and Oct4 and provided a significant improvement of Essrb target gene predictions. The associated GO terms overlap for the three TFs but differ per expression cluster.

2B. In the given example, ACE2 binding sites are not detected in association with 'mitosis' genes in the three yeast metabolic cycle expression clusters separately by MGSI, whereas LLM3D reveals a significant association of ACE2 binding sites with 'mitosis' genes considering all expression clusters simultaneously. The enrichment of ACE2/'mitosis' genes is highest in the Rb cluster, which is consistent with the fact that cell division is initiated during the Rb phase of the cycle (see Figure 2A).

To compare MGSI and LLM3D performance, we only considered the top-20 TFs for which both methods predicted significant TF-target gene associations. We next used *in vivo* yeast TF-target gene interactions reported in the MacIsaac refined regulatory map (MRM) (MacIsaac *et al.*, 2006) to determine whether these predictions are either true or false. Under the assumption that MRM contains true TF-target gene interactions, predictive performance can be measured using receiver operating characteristic (ROC) curves in which the true positive rate (i.e., the number of true positives divided by the sum of the true positives and false negatives) is plotted against false positive rate (i.e., the number of false positives divided by the sum of false positives and true negatives). The area under curve (AUC) is used as a summary statistic to compare different curves; a higher AUC indicates better predictive performance.

On average, LLM3D achieved a 3-fold increase in the number of true positive TF-target gene predictions compared with MGSI at an equivalent false discovery rate of 10% (Figure 2C). LLM3D consistently performed better, even when the original and less stringent MGSI p-values were used ($p < 0.05$) without correction for multiple testing. This increase in the number of true positive predictions did not simply result from an overall increase in TF-target gene predictions, because the observed AUC values were also consistently higher (0.74 for LLM3D compared to only 0.59 ($q < 0.1$) or 0.66 ($p < 0.05$) for MGSI; Figure 2D). Example ROC curves are plotted in Figure 2E, and an overview of all 20 TFs tested is provided in Supplementary Table 1. Results reported in Figure 2 and in Supplementary Table 1 were obtained using MRM as the repository of true in-

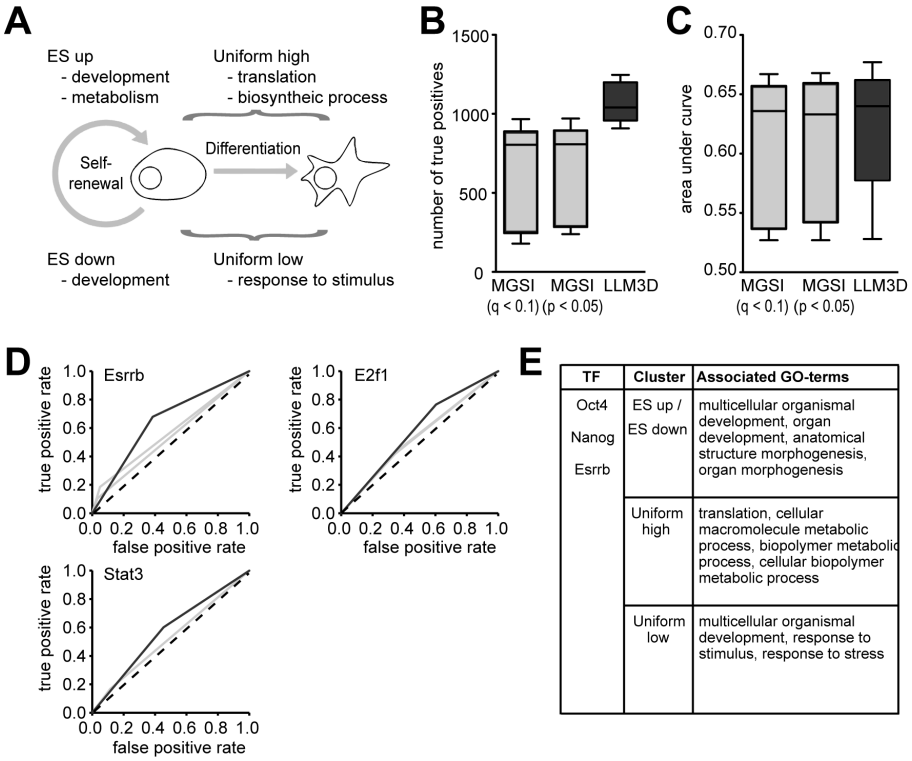

E

TF	Cluster	Associated GO-terms
Oct4 Nanog Esrrb	ES up / ES down	multicellular organismal development, organ development, anatomical structure morphogenesis, organ morphogenesis
	Uniform high	translation, cellular macromolecule metabolic process, biopolymer metabolic process, cellular biopolymer metabolic process
	Uniform low	multicellular organismal development, response to stimulus, response to stress

teractions. Similar results were obtained using the YEASTRACT bibliographic repository of true TF-target gene interactions (Teixeira *et al.*, 2006) (data not shown).

To evaluate LLM3D performance from a functional perspective, we next selected for each expression cluster the four TFs that have the largest contribution to the increase in true positive TF-target gene predictions compared with MGSI. In addition to well-known key regulators of the metabolic cycle (e.g., SKN7 and FKH1) (Lee *et al.*, 2002), this list contains several potential novel cluster-specific regulators, such as RAP1, FHL1, HAP1, REB1 and UME6 (Figure 2F). Importantly, the GO terms that are associated with these TFs all correspond with the biological processes that characterize each cluster (see Figure 2A). Interestingly, both RAP1 and FHL1 were recently implicated in growth-rate dependent changes in ribosome synthesis (Fazio *et al.*, 2008), which confirms their predicted relative importance in the Ox cluster. In conclusion, LLM3D achieves a significant gain in statistical power and improved predictive performance compared with existing methods with respect to the detection of functional TF-target gene interactions in yeast.

Identification of functional gene regulatory interactions in mouse embryonic stem cells

We next wanted to test LLM3D performance on mammalian gene expression data. We used both LLM3D and MGSI to predict the transcriptional regulation of genes that are

involved in controlling self-renewal and differentiation of mouse embryonic stem (ES) cells. Ouyang and colleagues (Ouyang *et al.*, 2009) defined four clusters of genes with characteristic expression patterns in ES cells. These clusters are based on combined RNA-Seq data (Cloonan *et al.*, 2008) and gene expression microarray data (Zhou *et al.*, 2007). The first two clusters include genes that are either induced (Uniform high; 668 genes) or repressed (Uniform low; 838 genes) in both ES cells and differentiated cells. The other two clusters include genes that are either upregulated (Es up; 782 genes) or downregulated (Es down; 831 genes) in ES cells only (Figure 3A). We restricted our analysis to 12 TFs that are known to play a role in ES cell biology and for which genome-wide ChIP-Seq binding profiles are available (Chen *et al.*, 2008). This allowed us to define true targets and to benchmark LLM3D predictive performance as we did for the yeast metabolic cycle data.

LLM3D consistently predicted more TF-target gene interactions than MGSI (Figure 3B), and the average AUC values of LLM3D predictions are slightly higher than obtained with MGSI (Figure 3C; Supplementary Table 2). The modest increase in overall AUC is primarily due to a significant increase for a subset of TFs (e.g., Esrrb, E2f1 and Stat3; Figure 3D). More importantly, however, LLM3D predicted a significant role for two key regulators of ES cell self-renewal, Oct4 and Nanog, whereas MGSI did not.

In addition to Oct4 and Nanog, the highest increase in true positive predictions was observed for Esrrb. For these three TFs, LLM3D predicted similar cluster-specific associations with GO terms that reflect the biological processes underlying each cluster, i.e., 'developmental' and 'morphogenesis' in the ES up and ES down clusters, 'translation' and 'metabolism' in the Uniform high cluster, and 'response to stimulus' in the Uniform low cluster (see Figure 3A). These findings corroborate earlier reports that Oct4, Nanog and Esrrb regulate ES cell gene expression in a combinatorial manner, and that they can either activate or repress genes depending on the context (Ouyang *et al.*, 2009). Thus, LLM3D provides improved detection of functional gene regulatory interactions in mammalian gene expression data.

Identification of novel transcriptional regulators of neuronal regeneration

We next used LLM3D to predict transcriptional regulatory interactions underlying neuronal regeneration. We first generated genome-wide expression profiles of dorsal root ganglion (DRG) neurons following nerve damage (Figure 4A). DRG neurons extend one peripheral axon into the spinal nerve and one central axon into the dorsal root. The peripheral axon regenerates vigorously, while in contrast the central axon has little regenerative capacity. For this study, two groups of animals were subjected either to sciatic nerve (SN) or dorsal root (DR) crush, and at 12, 24, 72 hours and 7 days after the crush, lumbar DRGs L4, L5 and L6 were dissected and total RNA was extracted. Samples were then processed and hybridized to Agilent 44K rat whole-genome arrays. Bayesian Analysis of Time-Series (BATS) (Angelini *et al.*, 2007b; Angelini *et al.*, 2007a) was used

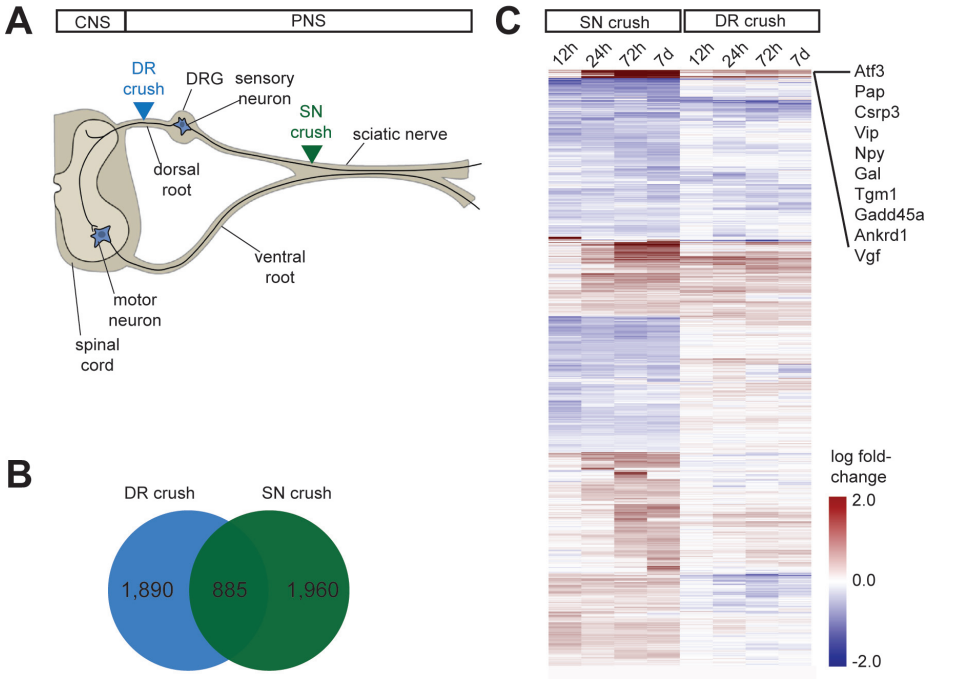

Figure 4. Genome-wide identification of regeneration-associated genes.
(A) Schematic representation of the sensory-motor neuron circuitry and the location of the DRG. A dorsal root crush injures the central projections of DRG sensory neurons, whereas a peripheral nerve crush injures the peripheral projections of the same neurons. (B) Venn diagram showing the number of significantly regulated genes identified in each crush paradigm. The relatively small overlap indicates that SN and DR crush elicit distinct gene responses in DRG neurons. (C) Heat map showing expression profiles of all significantly regulated genes after SN or DR crush.

to identify 2,845 genes that are significantly regulated after SN crush and 2,775 genes that are significantly regulated after DR crush relative to control. Out of the 4,735 regulated genes in total, only 885 genes were regulated in both crush paradigms and 3,850 were regulated in a paradigm-specific manner (Figure 4B), which confirms the notion that SN crush and DR crush elicit very distinct gene expression responses in DRG neurons (Stam *et al.*, 2007). In line with previous gene expression studies (Costigan *et al.*, 2002; Schmitt *et al.*, 2003; Stam *et al.*, 2007; Szpara *et al.*, 2007), we find a strong and SN crush-specific upregulation of regeneration-associated genes, including *Atf3, Pap, Vip, Npy, Gal, Tgm1, Csrp3 and Ankrd1, Gadd45a* and *Vgf* (Figure 4C).

We separated all 4,735 regulated genes into two distinct expression clusters; one cluster of genes that are higher expressed after SN crush than after DR crush (named SN>DR), and one cluster of genes that are higher expressed after DR crush than after SN crush (named DR>SN) (Figure 5A). We next used MGSI and LLM3D to predict transcriptional regulatory interactions underlying each gene expression cluster. After correction for multiple testing, MGSI identified 37 significantly enriched TFBSs whereas

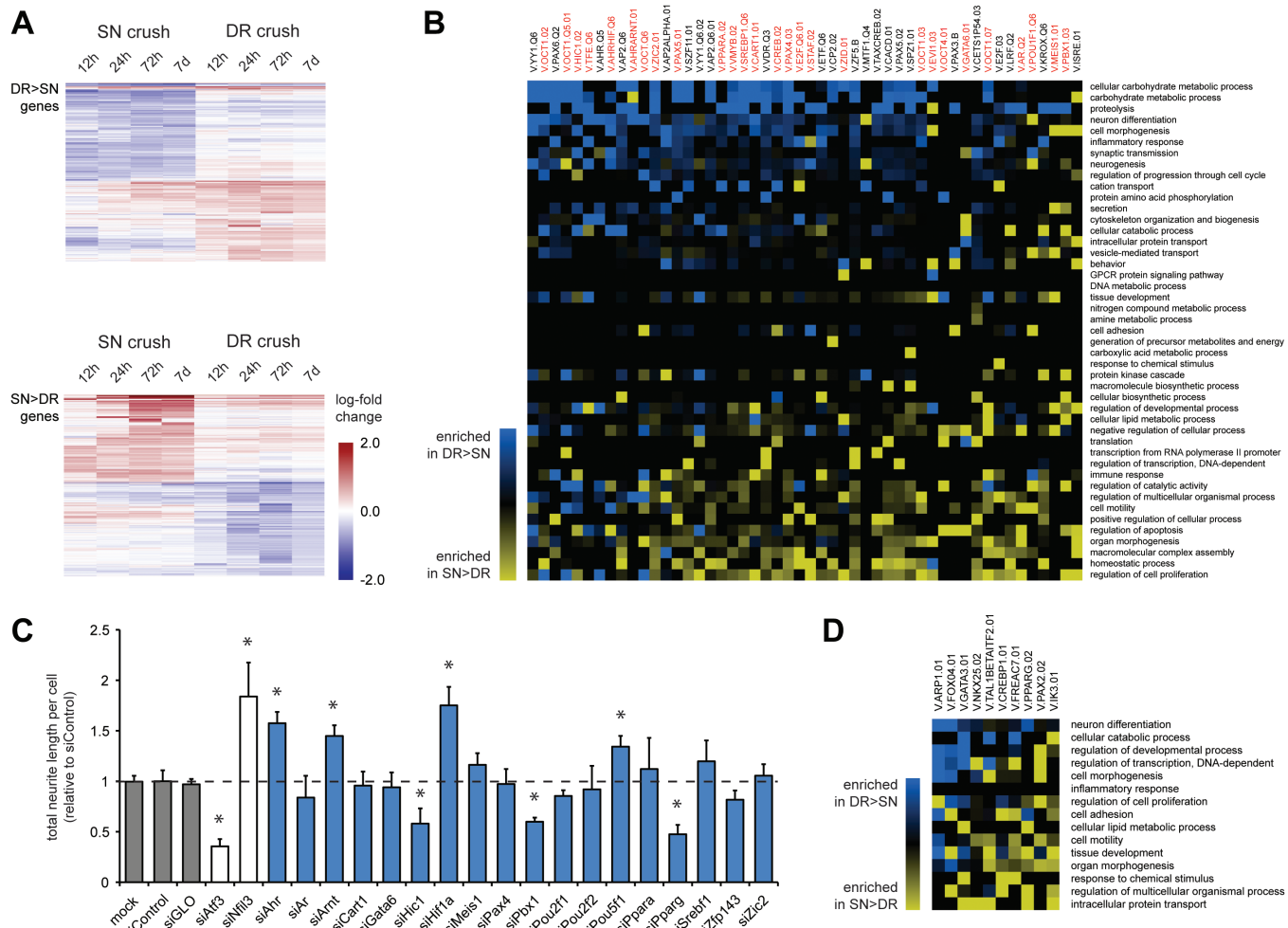
A
SN crush
DR crush
12h
24h
72h
7d
DR>SN genes
SN>DR genes
log-fold change
2.0
0.0
-2.0
B
enriched in DR>SN
enriched in SN>DR
cellular carbohydrate metabolic process
carbohydrate metabolic process
proteolysis
neuron differentiation
cell morphogenesis
inflammatory response
synaptic transmission
neurogenesis
regulation of progression through cell cycle
cation transport
protein amino acid phosphorylation
secretion
cytoskeleton organization and biogenesis
cellular catabolic process
intracellular protein transport
vesicle-mediated transport
behavior
GPCR protein signaling pathway
DNA metabolic process
tissue development
nitrogen compound metabolic process
amine metabolic process
cell adhesion
generation of precursor metabolites and energy
carboxylic acid metabolic process
response to chemical stimulus
protein kinase cascade
macromolecule biosynthetic process
cellular biosynthetic process
regulation of developmental process
cellular lipid metabolic process
negative regulation of cellular process
translation
transcription from RNA polymerase II promoter
regulation of transcription, DNA-dependent
immune response
regulation of catalytic activity
regulation of multicellular organismal process
cell motility
positive regulation of cellular process
regulation of apoptosis
organ morphogenesis
macromolecular complex assembly
homeostatic process
regulation of cell proliferation
C
total neurite length per cell (relative to siControl)
2.5
2
1.5
1
0.5
0
mock
siControl
siGLO
siAtf3
siNfil3
siAhr
siAr
siArnt
siCart1
siGata6
siHic1
siHif1a
siMeis1
siPax4
siPbx1
siPou2f1
siPou2f2
siPou5f1
siPpara
siPparg
siSrebf1
siZfp143
siZic2
D
enriched in DR>SN
enriched in SN>DR
neuron differentiation
cellular catabolic process
regulation of developmental process
regulation of transcription, DNA-dependent
cell morphogenesis
inflammatory response
regulation of cell proliferation
cell adhesion
cellular lipid metabolic process
cell motility
tissue development
organ morphogenesis
response to chemical stimulus
regulation of multicellular organismal process
intracellular protein transport

LLM3D identified 157. We next used a relative enrichment scoring method to select the 50 TFBSs with the highest gene cluster-specific regulatory potential. This method is based on ranking all predicted TFBSs according to the observed variance in enrichment per TFBS-GO association in each of the two expression clusters, and assumes that more variance is indicative of more expression cluster-specific TFBS-GO associations. The 50 TFBSs that were thus selected include 27 that were only identified by LLM3D (Figure 5B).

In the absence of a repository for true positive TF-target gene interactions, we decided to test whether any of the TFBSs that were identified exclusively by LLM3D could reflect functional gene regulatory interactions in the context of regenerative axon growth. We used F11 cells as an *in vitro* model. F11 cells are neuroblastoma cells derived from rat embryonic DRG neurons (Platika *et al.*, 1985). They express many DRG neuron markers (Francel *et al.*, 1987; Boland and Dingledine, 1990) and display cAMP-induced neurite outgrowth (Ghil *et al.*, 2000). We previously showed that DRG regeneration-associated TFs also are important for F11 neurite outgrowth (Stam *et al.*, 2007; MacGillavry *et al.*, 2009). For the 27 TFBSs that were exclusively identified by LLM3D we could unequivocally identify 17 corresponding rat TFs. RNAi-mediated knockdown of 7 these TFs in F11 cells resulted in a significant increase or decrease in neurite outgrowth (Figure 5C). These findings demonstrate that LLM3D identified functional gene regulatory interactions that remained undetected by MGSI.

Another approach to select for functional TFBS predictions is to consider only evolutionary conserved TFBSs (Xie *et al.*, 2005). We included an option in LLM3D to use only human/mouse/rat (HMR)-conserved binding sites in the analysis. Using this option in the analysis of the SN>DR and DR>SN expression clusters, MGSI identified 167 significantly enriched TFBSs compared to 254 identified by LLM3D. Peroxisome proliferator-activated receptor γ (PPARγ) binding sites were identified in combination with 'neuron differentiation' GO genes as one of the highest ranked TFBS-GO associations in the DR>SN expression cluster (Figure 5D). Together with the functional data presented

Figure 5. LLM3D identifies more functional gene regulatory interactions in regeneration-associated genes than MGSI.

(A) All genes that are significantly regulated after SN or DR injury were subdivided into two clusters: DR>SN and SN>DR (see text for details). (B) Heat map showing the top-50 TFBS-GO associations detected in DR>SN genes (blue) and in SN>DR genes (yellow). TRANSFAC binding sites are on the horizontal axis (binding sites indicated in red were only detected with LLM3D, binding sites indicated in black were also identified with MGSI); GO terms are on the vertical axis. (C) siRNA-mediated knockdown of TF expression in F11 cells shows that 8 out of 18 TFs predicted by LLM3D but not by MGSI significantly increase or decrease forskolin-induced neurite outgrowth. Grey and white bars represent negative and positive controls respectively. Bars represent mean neurite total length per cell ± SD; * $p < 0.01$. (D) Heat map as in panel B, showing the top-10 TFBS with their top-15 GO associations as detected by LLM3D using the HMR-conserved TFBSs selection.

in Figure 5C, these findings suggest an important role for PPARGγ in the regulation of regeneration-associated genes.

PPARγ is a repressor of neuronal regeneration-associated genes

Because PPAR binding sites were consistently detected in 'neuron differentiation' GO genes (Figures 5B and 5D) and knockdown of PPARγ significantly reduced neurite outgrowth in F11 cells (Figure 5C), we decided to study the role of PPAR TFs in neuronal regeneration in more detail. Most predicted PPAR target genes are expressed in neurons (Supplementary Table 3), which suggests that PPAR TFs may enhance regeneration by regulating the expression of neuron-intrinsic regeneration-associated genes. Therefore, we tested the effects of different PPAR agonists and antagonists on neurite outgrowth from F11 cells and from primary adult DRG neurons. Stimulation of PPARγ, but not PPARα, stimulated neurite outgrowth from primary DRG neurons and from F11 cells, whereas blocking PPARγ, but not PPARα, inhibited neurite outgrowth in both cell types (Figure 6A-D). These findings show that activation of PPARγ in primary adult DRG neurons, which closely resemble the *in vivo* DRG regeneration paradigm (Stam *et al*., 2007; MacGillavry *et al*., 2009), stimulates neurite outgrowth. Primary DRG cultures are however mixed neuron/glia cultures, and the effects of PPARγ activation or inhibition on DRG neuron outgrowth might be indirectly mediated by glial cells. F11 cell cultures on the other hand contain no glia, and the fact that we could replicate our results in F11 cells indicates that PPARγ is a neuron-intrinsic stimulator of neurite outgrowth.

To test whether PPARγ binds directly to the promoters of predicted target genes, we next performed quantitative chromatin immunoprecipitation (ChIP). F11 cells were stimulated with the PPARγ agonist ciglitazone or with DMSO (control) and chromatin complexes were cross-linked after 24 hours and subjected to ChIP using an antibody specific for PPARγ. Immunoprecipitated DNA was then analyzed using quantitative PCR.

Figure 6. Experimental validation of PPARγ binding sites in regeneration-associated genes. (A) F11 cells treated with PPARγ agonist ciglitazone show increased neurite outgrowth, whereas cells treated with PPARγ antagonists GW9662 show decreased neurite outgrowth. (B) Similar results were obtained for cultured primary adult DRG neurons. (C) Quantification of the effects of ciglitazone and GW9662 on F11 cell neurite outgrowth. (D) Quantification of the effects of ciglitazone and GW9662 on primary DRG neurite outgrowth. Note that PPARα agonist Wy-14643 and antagonist GW6471 do not affect neurite outgrowth. (E) PPARγ binds to the promoters of predicted 'neuron differentiation' target genes. Anti-PPARγ immunoprecipitated chromatin from F11 cells treated with DMSO (negative control; white bars) or PPARγ agonist ciglitazone (blue bars) was quantified by PCR using site-specific primers. *Icer* and *JunD* were included as negative control genes. All predicted target genes tested, except *Pick1* and *Ptpn11*, show PPARγ binding above background (dashed line), and for most genes this binding was strongly enhanced by ciglitazone. (F) Three out of the top-5 PPARγ-binding genes show a significant reduction in expression after ciglitazone treatment (blue bars) compared with DMSO treatment (white bars). PPARα agonist Wy-14643 did not affect gene expression levels (green bars), nor did ciglitazone or Wy-14643 affect the expression levels of PPARγ. Bars represent means ± SD; * $p < 0.01$.

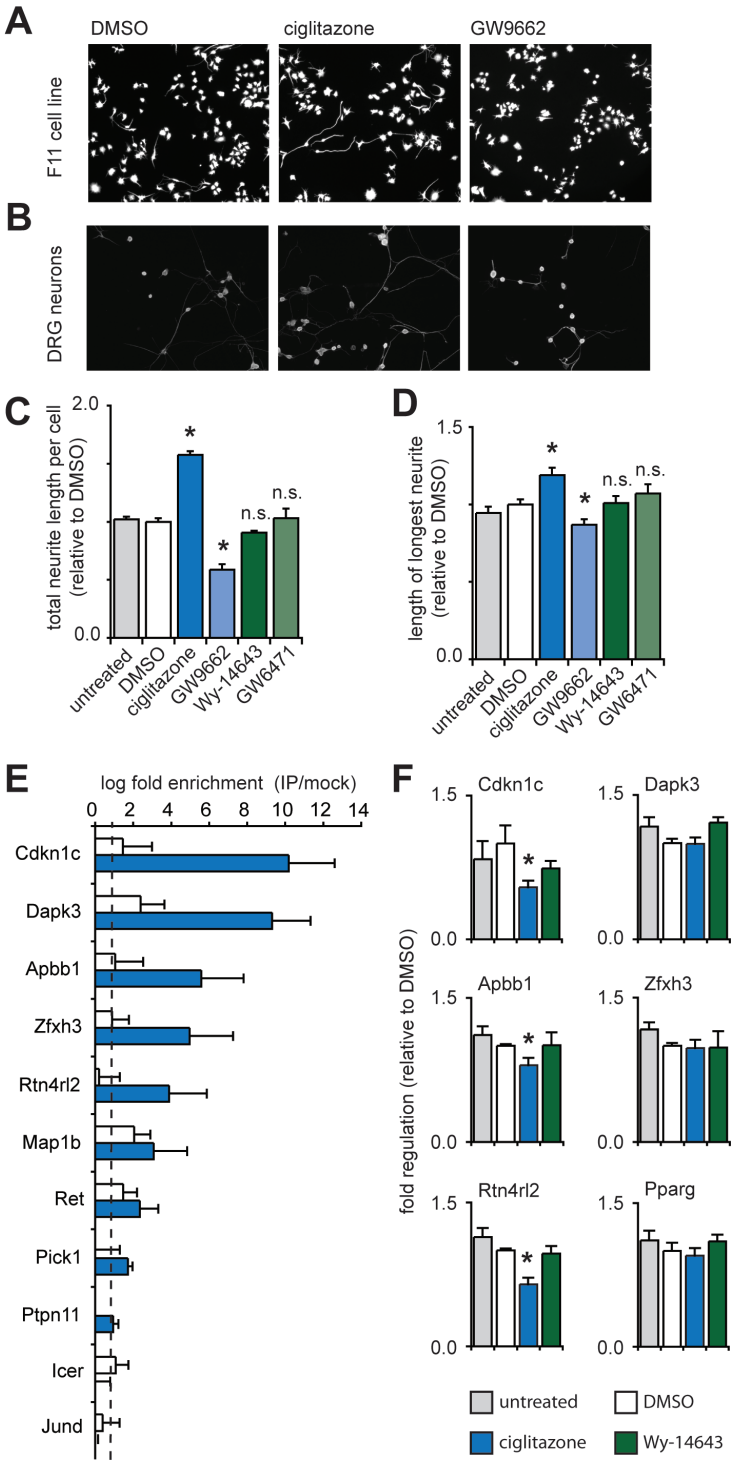
A
DMSO
ciglitazone
GW9662
F11 cell line
B
DRG neurons
C
total neurite length per cell (relative to DMSO)
2.0
0.0
*
*
n.s.
n.s.
untreated
DMSO
ciglitazone
GW9662
Wy-14643
GW6471
D
length of longest neurite (relative to DMSO)
1.5
0.0
*
*
n.s.
n.s.
untreated
DMSO
ciglitazone
GW9662
Wy-14643
GW6471
E
log fold enrichment (IP/mock)
0 2 4 6 8 10 12 14
Cdkn1c
Dapk3
Apbb1
Zfxh3
Rtn4rl2
Map1b
Ret
Pick1
Ptpn11
Icer
Jund
F
fold regulation (relative to DMSO)
Cdkn1c
Dapk3
Apbb1
Zfxh3
Rtn4rl2
Pparg
1.5
0.0
*
untreated
DMSO
ciglitazone
Wy-14643

PCR primers were designed to recognize ~100 base pair promoter regions containing the predicted PPAR binding sites for nine randomly chosen predicted target genes. As negative controls we used primers recognizing promoter regions of *Icer* and *JunD* that lack PPAR binding sites. For seven promoter regions tested, we found a specific interaction with PPARγ, which in most cases was further induced by ciglitazone (Figure 6E). These findings indicate that LLM3D predicts within a given functional context (i.e., neuron differentiation) PPARγ target gene interactions with an accuracy of >75%.

We finally measured the effect of ciglitazone on the expression of the six predicted target genes that show the highest PPARγ-binding. Quantitative PCR measurements indicate that activation of PPARγ with ciglitazone significantly reduces the expression of three of these genes (Figure 6F), which demonstrates that PPARγ acts as a ligand-dependent repressor of gene expression. Importantly, PPARα agonist Wy-14643 did not affect gene expression levels, nor did any of the pharmacons affect the expression levels of PPARγ (Figure 6F).

Discussion

Reverse engineering transcriptional regulatory networks from experimental data presents great challenges, particularly in higher organisms. As more genome-wide gene expression and functional data sets become available, there is a growing need for computational methods to analyze these data and accurately infer regulatory relationships from them. Of particular interest are those methods that automatically generate experimentally testable hypotheses regarding the direct regulation of genes by DNA-binding TFs. Combining heterogeneous sources of information, including genome-wide gene expression, DNA sequence and functional annotation, may prove to be essential to accurately predict true regulatory relationships. Here, we present a new method that offers a significant improvement over currently used enrichment-based methods, and show that this method can be applied to predict novel, condition-specific sets of transcriptional targets in the context of the complexity of the mammalian genome.

The main problem associated with existing methods is that they do not model the joint dependence between gene expression, TFBS presence and gene function. SEA-based methods for instance produce lists in which enriched TFBS and GO terms occur separately. From such lists it is unclear how GO terms and TFBS are jointly related to the gene sets of interest, and thus it is not possible to directly use SEA results to predict functionally homogenous sets of TF target genes. MGSI-based methods on the other hand try to circumvent this problem by using pre-defined GO-expression gene sets, and subsequently test these sets for enrichment of TFBSs. Although it makes sense to search for TFBS enrichment in functionally homogeneous sets of co-expressed genes, there are important conceptual problems with this approach that compromise the analysis and adversely affect the power to detect biologically meaningful associations. For instance,

MGSI does not really consider gene expression, TFBS presence and GO annotation jointly, but rather collapses gene expression and GO annotation into a single combined variable before computational analysis. Thus, important information about the joint dependence of all three variables is lost. Moreover, by analyzing multiple disjoint gene expression clusters, MGSI aggravates the multiple-testing problem because separate tests are performed for each cluster. LLM3D efficiently deals with both problems; it allows modeling of the joint distribution between all variables and reduces the number of tests to be performed.

We validated LLM3D performance using published yeast and mammalian gene expression and TF binding data sets. In yeast metabolic cycle gene expression clusters, LLM3D detects experimentally validated TFBSs that remain undetected using MGSI. Moreover, for most of these TFBSs, the true positive target gene prediction rates are significantly higher than found with MGSI. A similar increase in performance of LLM3D compared with MGSI was observed for mouse ES cell gene expression data. Although true positive rates did not increase as much as in the yeast example, LLM3D was uniquely able to identify target gene interactions for classical key regulators of the cell cycle (i.e., Nanog and Oct4) and showed significantly improved target gene detection for several other TFs (e.g., Esrrb, E2f1 and Stat3). Importantly, in both the yeast metabolic cycle data and the mouse ES cell data, LLM3D identified known and novel TFs in association with GO terms that reflect the biological processes underlying each expression cluster. We conclude that LLM3D not only provides a significant computational improvement over MGSI, but it also detects biologically relevant TF-target gene interactions, both in yeast and in mammals.

We next used LLM3D to identify gene regulatory interactions underlying neuronal regeneration. We first used microarray analysis to define two clusters of genes with differential expression in DRGs during either successful or unsuccessful axonal regeneration. Out of 50 LLM3D-predicted TFBSs that showed the highest gene cluster-specific enrichment, 27 were identified exclusively by LLM3D. For these 27 TFBSs, we could identify 17 corresponding rat TFs, seven of which significantly increased or decreased neurite outgrowth after siRNA-mediated knockdown in F11 cells. Most notably, knockdown of AHR, ARNT and HIF1α, which are structurally related bHLH TFs involved in the cellular response to hypoxia (Bracken *et al.*, 2003), all strongly enhanced neurite outgrowth, whereas knockdown of PBX1, HIC1 and PPARγ strongly reduced neurite outgrowth. Thus, LLM3D identified potential novel TFs and transcriptional regulatory pathways involved in neurite outgrowth.

We decided to focus on one of these newly identified TFs, i.e., PPARγ. Previous work showed that activation of PPARγ in spinal cord injury models has beneficial effects on the functional outcome (McTigue *et al.*, 2007; Park *et al.*, 2007), but it is not clear whether these effects are directly on the damaged neurons, or whether PPARγ reduces the secondary inflammatory response (McTigue, 2008). Our findings show that PPARγ,

but not PPARα, stimulates neurite outgrowth of DRG neurons. Moreover, this effect of PPARγ is neuron-intrinsic since we also observe it in DRG-like F11 cells, which in the presence of forskolin acquire a neuronal phenotype. Activated PPARγ binds to promoters of predicted target genes and reduces their expression. Importantly, several predicted PPARγ target genes are known inhibitors of neurite outgrowth (e.g., *Rtn4rl2, Slit1, Hes5*; see Supplementary Table 3), which suggests that PPARγ promotes neurite outgrowth by repressing growth-inhibitory genes. At this moment we can only speculate about the relevance of these findings for neuronal regeneration *in vivo*. The primary ligands of PPARγ are polyunsaturated fatty acids (Hihi *et al.*, 2002). Following nerve crush and degeneration of the myelin sheath, free myelin lipids are taken up by macrophages and released again as fatty acids to be incorporated into the newly forming myelin sheath (Goodrum *et al.*, 1995). We propose that injured axons might benefit from fatty acid production in the damaged nerve, and that the neuron-intrinsic lipid sensing properties of PPARγ may play an important role in conveying injury signals from the crush site to the nucleus. This hypothesis is supported by several reports showing beneficial effects of fatty acids on neurite outgrowth *in vitro* (Liu *et al.*, 2008; Robson *et al.*, 2008) and on neuronal regeneration *in vivo* (McTigue *et al.*, 2007; Park *et al.*, 2007), and the induction of fatty acid-binding proteins in regenerating axons (De Leon *et al.*, 1996).

One of the challenges left unaddressed in the current implementation of our method is that transcriptional regulation in higher organisms is believed to be highly combinatorial, and that the spatiotemporal expression of genes is influenced by multiple regulatory TFs that form complexes at multiple TFBSs. Although some basic models for the cooperative effect of multiple TFs on the expression of target genes have been suggested (Lee *et al.*, 2002; Shen-Orr *et al.*, 2002; Alon, 2007; Warner *et al.*, 2008), in general the *cis*-regulatory grammar underlying gene regulation is still poorly understood. Moreover, combinatorial models of gene regulation are difficult to validate and the effect of different TFs on target genes is therefore most often studied independently. As soon as reliable and genome-wide descriptions of *cis*-regulatory modules become available, this information can easily be incorporated into LLM3D to allow modeling of *cis*-regulatory modules in addition to individual TFBSs.

In conclusion, LLM3D provides an important improvement over existing computational methods in identifying functional TFBSs from gene expression data. Its unique property of testing the joint association between multiple features (e.g., gene expression, gene function and TFBS occurrence) based on one table allows further generalization to tables with more dimensions including additional relevant gene attributes. The implementation of such multi-dimensional computational methods will be of critical importance in order to extract biologically meaningful information from the increasing number, size and diversity of data sets generated by biologists.

Material and methods

LLM3D

For each TFBS-GO pair of interest, LLM3D cross-classifies all genes according to observed gene expression, GO annotation and TFBS prediction to obtain a three dimensional table (see Figure 2B for an example). The rows of this table correspond to the GO terms, the columns to the TFBSs, and the gene expression clusters define the layers of the table. Let μ_{ijk} denote the observed number of genes in row i, column j and layer k. We let π_{ijk} denote the marginal probability that a gene falls in row i, column j and layer k. Then, for a gene universe of size N and under the null hypothesis of complete independence between rows, columns and layers: $\mu_{ijk} = N_{\pi ijk} = N_{\pi i..\pi .j.\pi ..k}$, or, equivalently, $log\ (\mu_{ijk}) = \eta + \alpha_i + \beta_j + \gamma_k$. Under the assumption that this model holds, the unknown parameters can be estimated using maximum likelihood. Lack of fit can be formally tested using a standard likelihood ratio G^2 statistic. For a three dimensional contingency table, there are 7 other natural models to consider. These models differ in the parameters used to describe the observed counts and the dependence relationships they imply between the rows, columns and layers of the table. For each of these models, we estimated parameters using maximum likelihood and calculated the G^2 statistic. Next, we selected the model that best describes the observed data using Akaike's information criterion (AIC), which can be calculated from G^2 and the degrees of freedom of the model. For re-analysis of yeast data, we considered all models with at least two two-way (first order) interactions, i.e., $M^{(4)}$, $M^{(5)}$, $M^{(6)}$, $M^{(7)}$, and $M^{(S)}$. For analysis of the neuronal regeneration data we only considered models with all pairwise interactions and the saturated model, i.e., $M^{(7)}$ and $M^{(S)}$, since these simultaneously imply (i) enrichment of GO terms in co-regulated genes, (ii) enrichment of TFBSs in co-regulated genes, and (iii) enrichment of TFBSs in genes that share the same GO terms.

MGSI

For any given gene expression cluster and GO term, MGSI first generates a new gene set by intersecting the genes in the expression cluster with the set of genes annotated to the GO term. Enrichment of any TFBS in this new set is tested using a Fisher's exact test (one-sided) for two-dimensional contingency tables. A Benjamini Hochberg correction is applied to the resulting p-values to correct for multiple testing with the aim of controlling the false discovery rate (FDR) at 10%.

Yeast TFBS annotation

Yeast ORF sequences with introns and untranslated regions 1,000 bp immediately upstream of the initial ATG were downloaded from the Saccharomyces Genome Database (SGD) on http://www.yeastgenome.org. Log-odds matrices representing probabilistic

models for binding sites were downloaded from http://fraenkel.mit.edu/improved_map/ and converted to probability matrices to be used with the Motifscanner tool (Aerts *et al.*, 2003). Motifscanner was used to computationally predict binding sites for all TFs on both DNA strands with the "prior probability" parameter set to 0.15. A 3rd order Markov background model was generated, trained on the SGD sequences with the accompanying CreateBackgroundModel tool.

Mammalian TFBS annotation

Gene regulatory sequences (5,000 bp upstream to 2,000 bp downstream of the predicted transcription start site) for all human, mouse and rat genes identifiable by Entrez Gene ID were downloaded using the biomaRt package under R. Potential TFBSs were predicted in silico using all 214 vertebrate non-redundant position weight matrices in the TRANSFAC Professional database (release 11.1) (Matys *et al.*, 2003) and the supplied MATCH-tool (Kel *et al.*, 2003) with parameters set to minimize false positives. The MATCH output was used to create a binary matrix with rows corresponding to regulatory sequences and columns corresponding to TRANSFAC matrices. In this matrix, '1' represents the presence of at least one predicted TFBS, whereas '0' represents the absence of predicted TFBSs. In addition, all human, mouse and rat genes in LLM3D were also annotated with human/mouse/rat (HMR) conserved TFBSs downloaded from http://genome.ucsc.edu/. This allows LLM3D analysis to be limited to evolutionary conserved binding sites only. For the mouse ES cell data analysis, 12 additional TFBS motif models were used that were derived from ChIP-Seq data (Chen *et al.*, 2008). FIMO, part of the MEME software suite (Bailey *et al.*, 2009), was used to predict TFBS occurrences for these 12 TFs in regulatory sequences of all known mouse RefSeq genes (UCSC, NCBI36/mm8 assembly).

GO pre-selection

Yeast GO annotation data were extracted from the R-package 'org.Sc.sgd.db', which was downloaded from http://www.bioconductor.org. GO Biological Process annotations for human, mouse and rat genes were retrieved from http://www.geneontology.org/. Informative GO terms were selected as follows. For any GO term i, let GO(i) be the set of genes whose annotation contains term i and let N(i) be the size of that set. We let Child(i) denote the set of children of i in the directed acyclic Gene Ontology graph. Let M(i) be the maximum over N(r), for terms r in Child(i). For any positive number γ and any term i, we now say that i is the most informative GO term at level γ if $N(i) \geq \gamma$ and $M(i) < \gamma$. For analysis of the yeast metabolic cycle data we considered all most informative GO terms at level 20. For the analysis of the mouse ES cell data and the rat neuronal regeneration data we selected most informative GO terms at level 50.

Selection and visualization of biologically relevant TFBSs

To measure cluster-specific enrichment of TFBSs, LLM3D uses the normalized log-linear

residuals observed in the contingency table. Residuals with a positive sign indicate enrichment, whereas a negative sign indicates depletion. The set of predicted targets for a given TFBS-GO pair is then defined as the union of sets of TFBS-GO genes in all clusters with a positive residual. For any two clusters of interest, relative enrichment is assessed in one cluster with respect to the other using a relative enrichment score. Next, all significant TFBSs predicted by LLM3D are ranked according to the sample variance of their enrichment scores over all associated GO terms, and the top-ranked TFBSs are then selected as the ones with the most cluster-specific regulatory potential.

Yeast metabolic cycle data

For analysis of the yeast metabolic cycle data, we used the original clustering (Tu *et al.*, 2005). The MRM refined regulatory map providing true interactions between TFs and target genes based on ChIP-chip data (MacIsaac *et al.*, 2006) was downloaded from http://fraenkel.mit.edu/improved_map/. True TF-target gene interactions reported in the YEASTRACT database (Teixeira *et al.*, 2006) were downloaded from http://www.yeastract.com. For validation of predicted regulatory interactions we used a 'RegulationMatrix' containing all documented regulatory interactions in eiter MRM or YEASTRACT.

Mouse embryonic stem cell data

For analysis of the mouse ES cell data, we used the gene expression clusters defined by (Ouyang *et al.*, 2009). TF association strength (TFAS) scores as computed by (Ouyang *et al.*, 2009) were used for all RefSeq genes to define target genes for all 12 TFs. Genes with a positive TFAS were defined as true targets.

Animals and surgical procedures

Adult Wistar rats (~220 g; Harlan, The Netherlands) were subjected to either sciatic nerve or dorsal root crush as described previously (Stam *et al.*, 2007) in approval with the KNAW animal experimentation committee for animal welfare. L4-6 DRGs were isolated at 12 h, 24 h, 72 h, and 7 days after surgery. Control DRGs were obtained from three uninjured animals.

Microarray hybridization, normalization and analysis

Total RNA was isolated from L4, 5 and 6 DRGs using Trizol (Invitrogen; Carlsbad, CA). RNA pooled from three control animals served as a common reference sample. RNA samples were amplified, labelled and hybridized to Agilent 44K Rat Whole-Genome expression arrays using standard Agilent protocols (Agilent; Santa Clara, CA). Arrays were scanned using an Agilent scanner and data were read using Agilent Feature Extraction software. Array data were further processed using the R packages Bioconductor (Gentleman *et al.*, 2004) and limma (Linear Models for Microarray Data) (Ritchie *et al.*, 2007) for standard background subtraction and loess normalization. For statistical analyses we

used the Bayesian approach for microarray time course data developed by Angelini *et al.* (Angelini *et al.*, 2007b; Angelini *et al.*, 2007a). This algorithm is implemented in a Matlab executive, termed Bayes Analysis of Time-Series (BATS). Heatmaps and hierarchical clusters were generated using TIGR MeV software (http://www.tm4.org/mev.html). Primary microarray data have been submitted to GEO (http://www.ncbi.nlm.nih.gov/geo/; accession number GSE 21007).

Expression clusters

The log fold gene expression change (relative to control; averaged over three replicates per time point) in both experiments (SN and DR crush) was calculated for each gene. Expression data from significantly regulated genes following SN and DR crush were analyzed separately using a standard principal component analysis algorithm under R. For each gene, we used the coefficient corresponding to the first principal component to further define two homogeneous gene expression clusters: one containing genes that are either upregulated after DR crush or downregulated after SN crush (DR>SN), and one containing genes that are either upregulated after SN crush or downregulated after DR crush (SN>DR). For a small group of genes that were significantly regulated following both crushes and for which the dominant direction of log fold change (i.e. either up- or downregulation) coincided in both experiments, we compared the average log fold change of expression following SN and DR crush directly for classification into (DR>SN) or (SN>DR).

Cell culture and neurite outgrowth assays

F11 cells were maintained as previously described (Stam *et al.*, 2007). For pharmacological stimulations F11 cells were plated in 96-well plates. Medium was replaced with DMEM containing 0.5% FCS, and 1 μM of PPAR agonist (ciglitazone for PPARγ and Wy-14643 for PPARα) or antagonist (GW9662 for PPARγ and GW6471 for PPARα; all from Sigma-Aldrich, St. Louis, MO) was added. Cells were fixed two days later and stained with anti-beta-III-tubulin (Sigma-Aldrich). Neurite outgrowth was quantified using a Cellomics ArrayScan HCS Reader and the Neuronal Profiling 3.5 Bioapplication (Cellomics Inc., Pittsburgh, PA, USA). Per well 500-1,000 cells were analyzed and neurite total length per cell was calculated. For statistical analysis, the average neurite total length for 5 wells was compared between experimental and control conditions and a Student's *t*-test was used to determine significance. Dissection and dissociation of primary adult DRG neurons was carried out as described (Stam *et al.*, 2007). After 40 hours in culture neurons were fixed and immunostained with anti-beta-III-tubulin. The longest neurite of each of 100-200 neurons was measured using the ImageJ Simple Neurite Tracer plugin.

RNA interference

F11 cells were transfected with Dharmacon siGENOME siRNA SMARTpools using the

DharmaFECT 3 transfection reagent as previously described (MacGillavry *et al.*, 2009). Neurite outgrowth was quantified two days later using a Cellomics ArrayScan HCS Reader as decribed above.

Chromatin immunoprecipitation (ChIP) and quantitative (RT-)PCR analysis

F11 cells were plated in 15 cm plates, and stimulated with 10 μM forskolin and 10 μM ciglitazone or DMSO as control for 24 hours. Chromatin of F11 cells was then cross-linked with 1% formaldehyde for 10 minutes and subsequently quenched with 125 mM glycine for 5 minutes. Cells were washed with cold PBS, nuclei were extracted with cell lysis buffer (10 mM EDTA, 10 mM HEPES, 0.25% Triton X-100) and lysed with SDS lysis buffer (1% SDS, 10 mM EDTA in 20 mM Tris-HCl). Cross-linked chromatin was sheared with 4 pulses of 15 sec yielding products of 200-1,000 bp in length. Immunoprecipitation was performed with anti-PPARγ (H-100, Santa Cruz Biotechnology) overnight with rotation at 4^0C. Immuno-complexes were then captured with protein A/G beads (Santa Cruz Biotechnology) pre-incubated with sonicated salmon sperm DNA. Complexes were washed and eluted with elution buffer (1% SDS, 100 mM $NaHCO_3$). The eluates were proteinase K treated (215μg/ml) and incubated at 65^0C for overnight. DNA was purified by phenol/chloroform isolation and subsequent ethanol precipitation. Quantitative PCR was performed using site-specific primers in duplicate on a Roche LightCycler with 2x SYBR green ready reaction mix (Applied Biosystems). Normalized enrichment values were calculated by subtracting the Ct value of the IP sample from the Ct value of the mock IP samples, each normalized to the input sample. Promoter regions with >1.5 log fold enrichment were considered as true targets. For gene expression level measurements, RNA was isolated from F11 cells using Trizol and reverse-transcribed into cDNA as previously described (Stam *et al.*, 2007). Ct values were normalized to *Gapdh* and *Nse* as reference genes. Fold changes were calculated relative to DMSO-treated cells. Specificity of all primers was checked by visual inspection of dissociation curves.

References

Aerts S, Thijs G, Coessens B, Staes M, Moreau Y, De Moor B (2003) Toucan: deciphering the cis-regulatory logic of coregulated genes. Nucleic Acids Res 31:1753-1764.

Akaike H (1974) A new look at the statistical model identification. IEEE Transactions on Automatic Control 19:716-723.

Alon U (2007) Network motifs: theory and experimental approaches. Nat Rev Genet 8:450-461.

Angelini C, De Canditiis D, Mutarelli M, Pensky M (2007a) A Bayesian approach to es-

timation and testing in time-course microarray experiments. Stat Appl Genet Mol Biol 6:Article24.

Angelini C, Cutillo L, De Canditiis D, Mutarelli M, Pensky M (2007b) BATS: A Bayesian user-friendly software for analyzing time series microarray data. Technical Report CNR-IAC 331/07

Bailey TL, Boden M, Buske FA, Frith M, Grant CE, Clementi L, Ren J, Li WW, Noble WS (2009) MEME SUITE: tools for motif discovery and searching. Nucleic Acids Res 37:W202-208.

Boland LM, Dingledine R (1990) Expression of sensory neuron antigens by a dorsal root ganglion cell line, F-11. Brain Res Dev Brain Res 51:259-266.

Bracken CP, Whitelaw ML, Peet DJ (2003) The hypoxia-inducible factors: key transcriptional regulators of hypoxic responses. Cell Mol Life Sci 60:1376-1393.

Carmona-Saez P, Chagoyen M, Tirado F, Carazo JM, Pascual-Montano A (2007) GENECODIS: a web-based tool for finding significant concurrent annotations in gene lists. Genome Biol 8:R3.

Chen X et al. (2008) Integration of external signaling pathways with the core transcriptional network in embryonic stem cells. Cell 133:1106-1117.

Christensen R (1997) Log-linear models and logistic regression, 2nd Edition: Springer.

Cloonan N, Forrest AR, Kolle G, Gardiner BB, Faulkner GJ, Brown MK, Taylor DF, Steptoe AL, Wani S, Bethel G, Robertson AJ, Perkins AC, Bruce SJ, Lee CC, Ranade SS, Peckham HE, Manning JM, McKernan KJ, Grimmond SM (2008) Stem cell transcriptome profiling via massive-scale mRNA sequencing. Nat Methods 5:613-619.

Costigan M, Befort K, Karchewski L, Griffin RS, D'Urso D, Allchorne A, Sitarski J, Mannion JW, Pratt RE, Woolf CJ (2002) Replicate high-density rat genome oligonucleotide microarrays reveal hundreds of regulated genes in the dorsal root ganglion after peripheral nerve injury. BMC Neurosci 3:16.

De Leon M, Welcher AA, Nahin RH, Liu Y, Ruda MA, Shooter EM, Molina CA (1996) Fatty acid binding protein is induced in neurons of the dorsal root ganglia after peripheral nerve injury. J Neurosci Res 44:283-292.

Fazio A, Jewett MC, Daran-Lapujade P, Mustacchi R, Usaite R, Pronk JT, Workman CT, Nielsen J (2008) Transcription factor control of growth rate dependent genes in Saccharomyces cerevisiae: a three factor design. BMC Genomics 9:341.

Francel PC, Harris K, Smith M, Fishman MC, Dawson G, Miller RJ (1987) Neurochemical characteristics of a novel dorsal root ganglion X neuroblastoma hybrid cell line, F-11. J Neurochem 48:1624-1631.

Gentleman RC et al. (2004) Bioconductor: open software development for computational biology and bioinformatics. Genome Biol 5:R80.

Ghil SH, Kim BJ, Lee YD, Suh-Kim H (2000) Neurite outgrowth induced by cyclic AMP can be modulated by the alpha subunit of Go. J Neurochem 74:151-158.

Goodrum JF, Weaver JE, Goines ND, Bouldin TW (1995) Fatty acids from degenerating myelin lipids are conserved and reutilized for myelin synthesis during regeneration in peripheral nerve. J Neurochem 65:1752-1759.

Hannenhalli S (2008) Eukaryotic transcription factor binding sites--modeling and integrative search methods. Bioinformatics 24:1325-1331.

Hihi AK, Michalik L, Wahli W (2002) PPARs: transcriptional effectors of fatty acids and their derivatives. Cell Mol Life Sci 59:790-798.

Huang DW, Sherman BT, Lempicki RA (2009a) Systematic and integrative analysis of large gene lists using DAVID bioinformatics resources. Nat Protoc 4:44-57.

Huang DW, Sherman BT, Lempicki RA (2009b) Bioinformatics enrichment tools: paths toward the comprehensive functional analysis of large gene lists. Nucleic Acids Res 37:1-13.

Kel AE, Gossling E, Reuter I, Cheremushkin E, Kel-Margoulis OV, Wingender E (2003) MATCH: A tool for searching transcription factor binding sites in DNA sequences. Nucleic Acids Res 31:3576-3579.

Lee TI et al. (2002) Transcriptional regulatory networks in Saccharomyces cerevisiae. Science 298:799-804.

Liu JW, Almaguel FG, Bu L, De Leon DD, De Leon M (2008) Expression of E-FABP in PC12 cells increases neurite extension during differentiation: involvement of n-3 and n-6

fatty acids. J Neurochem 106:2015-2029.
MacGillavry HD, Stam FJ, Sassen MM, Kegel L, Hendriks WT, Verhaagen J, Smit AB, van Kesteren RE (2009) NFIL3 and cAMP response element-binding protein form a transcriptional feedforward loop that controls neuronal regeneration-associated gene expression. J Neurosci 29:15542-15550.

MacIsaac KD, Wang T, Gordon DB, Gifford DK, Stormo GD, Fraenkel E (2006) An improved map of conserved regulatory sites for Saccharomyces cerevisiae. BMC Bioinformatics 7:113.

Matys V et al. (2003) TRANSFAC: transcriptional regulation, from patterns to profiles. Nucleic Acids Res 31:374-378.

McTigue DM (2008) Potential therapeutic targets for PPARgamma after spinal cord injury. PPAR Res 2008:517162.

McTigue DM, Tripathi R, Wei P, Lash AT (2007) The PPAR gamma agonist Pioglitazone improves anatomical and locomotor recovery after rodent spinal cord injury. Exp Neurol 205:396-406.

Nam D, Kim SY (2008) Gene-set approach for expression pattern analysis. Brief Bioinform 9:189-197.

Nogales-Cadenas R, Carmona-Saez P, Vazquez M, Vicente C, Yang X, Tirado F, Carazo JM, Pascual-Montano A (2009) GeneCodis: interpreting gene lists through enrichment analysis and integration of diverse biological information. Nucleic Acids Res 37:W317-322.

Ouyang Z, Zhou Q, Wong WH (2009) ChIP-Seq of transcription factors predicts absolute and differential gene expression in embryonic stem cells. Proc Natl Acad Sci U S A 106:21521-21526.

Park SW, Yi JH, Miranpuri G, Satriotomo I, Bowen K, Resnick DK, Vemuganti R (2007) Thiazolidinedione class of peroxisome proliferator-activated receptor gamma agonists prevents neuronal damage, motor dysfunction, myelin loss, neuropathic pain, and inflammation after spinal cord injury in adult rats. J Pharmacol Exp Ther 320:1002-1012.

Platika D, Boulos MH, Baizer L, Fishman MC (1985) Neuronal traits of clonal cell lines derived by fusion of dorsal root ganglia neurons with neuroblastoma cells. Proc Natl Acad Sci U S A 82:3499-3503.

Reimand J, Kull M, Peterson H, Hansen J, Vilo J (2007) g:Profiler--a web-based toolset for functional profiling of gene lists from large-scale experiments. Nucleic Acids Res 35:W193-200.

Ritchie ME, Silver J, Oshlack A, Holmes M, Diyagama D, Holloway A, Smyth GK (2007) A comparison of background correction methods for two-colour microarrays. Bioinformatics 23:2700-2707.

Robson LG, Dyall S, Sidloff D, Michael-Titus AT (2008) Omega-3 polyunsaturated fatty acids increase the neurite outgrowth of rat sensory neurones throughout development and in aged animals. Neurobiol Aging.

Roider HG, Kanhere A, Manke T, Vingron M (2007) Predicting transcription factor affinities to DNA from a biophysical model. Bioinformatics 23:134-141.

Schmitt AB, Breuer S, Liman J, Buss A, Schlangen C, Pech K, Hol EM, Brook GA, Noth J, Schwaiger FW (2003) Identification of regeneration-associated genes after central and peripheral nerve injury in the adult rat. BMC Neurosci 4:8.

Shen-Orr SS, Milo R, Mangan S, Alon U (2002) Network motifs in the transcriptional regulation network of Escherichia coli. Nat Genet 31:64-68.

Stam FJ, MacGillavry HD, Armstrong NJ, de Gunst MC, Zhang Y, van Kesteren RE, Smit AB, Verhaagen J (2007) Identification of candidate transcriptional modulators involved in successful regeneration after nerve injury. Eur J Neurosci 25:3629-3637.

Szpara ML, Vranizan K, Tai YC, Goodman CS, Speed TP, Ngai J (2007) Analysis of gene expression during neurite outgrowth and regeneration. BMC Neurosci 8:100.

Teixeira MC, Monteiro P, Jain P, Tenreiro S, Fernandes AR, Mira NP, Alenquer M, Freitas AT, Oliveira AL, Sa-Correia I (2006) The YEASTRACT database: a tool for the analysis of transcription regulatory associations in Saccharomyces cerevisiae. Nucleic Acids Res 34:D446-451.

Tu BP, Kudlicki A, Rowicka M, McKnight SL (2005) Logic of the yeast metabolic cycle: temporal compartmentalization of cellular processes. Science 310:1152-1158.

Ward LD, Bussemaker HJ (2008) Predicting functional transcription factor binding through alignment-free and affinity-based analysis of orthologous promoter sequences.

Bioinformatics 24:i165-171.
Warner JB, Philippakis AA, Jaeger SA, He FS, Lin J, Bulyk ML (2008) Systematic identification of mammalian regulatory motifs' target genes and functions. Nat Methods 5:347-353.

Wasserman WW, Sandelin A (2004) Applied bioinformatics for the identification of regulatory elements. Nat Rev Genet 5:276-287.

Xie X, Lu J, Kulbokas EJ, Golub TR, Mootha V, Lindblad-Toh K, Lander ES, Kellis M (2005) Systematic discovery of regulatory motifs in human promoters and 3' UTRs by comparison of several mammals. Nature 434:338-345.

Zhou Q, Chipperfield H, Melton DA, Wong WH (2007) A gene regulatory network in mouse embryonic stem cells. Proc Natl Acad Sci U S A 104:16438-16443.

Zinzen RP, Girardot C, Gagneur J, Braun M, Furlong EE (2009) Combinatorial binding predicts spatio-temporal cis-regulatory activity. Nature 462:65-70.

Supplementary Table 1. Comparison of MGSI and LLM3D predictive performance for yeast metabolic cycle gene expression data.

binding site	# true positives			area under curve			Fisher enrichment *p*-value		
	MGSI ($q < 0.1$)	MGSI ($p < 0.05$)	LLM3D	MGSI ($q < 0.1$)	MGSI ($p < 0.05$)	LLM3D	MGSI ($q < 0.1$)	MGSI ($p < 0.05$)	LLM3D
ABF1	4	22	70	0.52	0.61	0.85	0.0013	1.44E-15	8.59E-58
CBF1	34	66	95	0.63	0.76	0.87	1.44E-36	3.74E-75	5.29E-108
FHL1	5	20	35	0.53	0.60	0.65	7.18E-07	3.38E-15	7.83E-19
FKH1	8	17	37	0.56	0.62	0.75	1.43E-06	2.19E-11	3.12E-23
FKH2	13	29	47	0.57	0.66	0.75	4.10E-10	8.03E-21	1.02E-28
GCN4	41	49	60	0.68	0.71	0.75	9.66E-46	4.31E-48	5.79E-43
HAP1	8	18	32	0.55	0.60	0.67	3.34E-08	1.12E-15	1.10E-17
HSF1	15	16	24	0.68	0.69	0.79	2.89E-25	6.37E-23	4.06E-33
MBP1	41	50	65	0.71	0.75	0.81	2.00E-45	2.64E-50	1.36E-52
MCM1	10	25	35	0.61	0.76	0.86	2.34E-13	1.95E-31	1.09E-38
MSN2	26	31	39	0.65	0.68	0.71	1.61E-20	4.66E-22	1.87E-20
RAP1	4	16	34	0.53	0.60	0.71	8.07E-05	8.43E-14	1.75E-22
REB1	0	40	46	0.50	0.65	0.67	1	4.06E-30	9.81E-33
RPN4	11	22	28	0.64	0.78	0.85	1.79E-15	2.37E-26	3.69E-30
SKN7	3	22	27	0.51	0.58	0.59	0.037	5.47E-12	5.65E-12
STE12	12	19	29	0.55	0.57	0.60	1.98E-11	2.08E-12	1.80E-15
SWI4	23	32	43	0.62	0.66	0.71	3.23E-20	5.47E-25	2.57E-26
SWI6	28	32	47	0.62	0.64	0.69	9.85E-24	2.12E-24	8.47E-25
UME6	16	24	56	0.61	0.65	0.86	1.20E-15	3.21E-20	8.12E-54
YAP7	15	23	31	0.59	0.63	0.68	5.91E-18	1.75E-24	1.06E-29

Supplementary Table 2. Comparison of MGSI and LLM3D predictive performance for mouse EC cell gene expression data.

binding site	# true positives			area under curve			Fisher enrichment *p*-value		
	MGSI ($q < 0.1$)	MGSI ($p < 0.05$)	LLM3D	MGSI ($q < 0.1$)	MGSI ($p < 0.05$)	LLM3D	MGSI ($q < 0.1$)	MGSI ($p < 0.05$)	LLM3D
E2f1	536	549	984	0.537	0.543	0.581	0.00148	0.000373	3.29E-12
Mycn	967	971	1017	0.657	0.658	0.662	8.23E-20	4.20E-20	4.97E-21
Zfx	887	901	1112	0.657	0.661	0.662	6.54E-18	8.92E-19	6.40E-19
Myc	811	817	931	0.642	0.642	0.633	1.49E-18	1.65E-18	5.66E-16
Klf4	891	891	1247	0.636	0.633	0.64	4.77E-13	1.35E-12	5.35E-15
Tcfcp2l1	804	808	1235	0.667	0.668	0.677	2.05E-13	1.47E-13	5.13E-14
Esrrb	179	317	1164	0.536	0.568	0.647	0.00401	1.72E-05	1.33E-10
Nanog	0	0	1150	0.5	0.5	0.543	1	1	0.0257
Oct-04	0	0	1117	0.5	0.5	0.531	1	1	0.0344
Sox2	239	239	1040	0.541	0.541	0.528	8.46E-05	8.46E-05	0.0442
Stat3	252	252	908	0.527	0.527	0.574	0.00866	0.00866	8.19E-07
Smad1	0	0	1044	0.5	0.5	0.517	1	1	0.0674

Supplementary Table 3. Predicted PPAR target genes with DR>SN expression and 'neuron differentiation' GO annotation, and predicted by both the non-conserved (rat only) and the HMR-conserved binding site options in LLM3D.

gene symbol	gene name	alternative gene symbol	cellular source	role in neurite outgrowth	supporting literature
Apbb1	amyloid beta (A4) precursor protein-binding, family B, member 1 (Fe65)	FE65	neuron	unknown	
Cdkn1c	cyclin-dependent kinase inhibitor 1C (P57)	p57; Kip2; p57KIP2; MGC112585	neuron	unknown	
Cnp1	2',3'-cyclic nucleotide 3' phosphodiesterase	CNPF; CNPI; CNPII; Cnp	neuron/glia	unknown	
Dapk3	death-associated protein kinase 3	Dapkl	neuron	unknown	
Dpysl3	dihydropyrimidinase-like 3	Crmp4; TUC-4b	neuron	inhibits	Alabed et al., 2007
Fgfr1	fibroblast growth factor receptor 1		neuron	stimulates	Hausott et al., 2008
Galr2	galanin receptor 2		neuron	stimulates	Hobson et al., 2006
Gnao	guanine nucleotide binding protein, alpha O	RATBPGTPC; Gnao1	neuron/glia	unknown	
Hes5	hairy and enhancer of split 5 (Drosophila)			inhibits	Sestan et al., 1999
L1cam	L1 cell adhesion molecule	Hyd; Hsas; NCAML1	neuron	stimulates	Panicker et al., 2003
Map1b	microtubule-associated protein 1B	Mtap1b	neuron/glia	inhibits	Bouquet et al., 2007
Nnat	neuronatin	Peg5; MGC156562	neuron	unknown	
Pgrmc1	progesterone receptor membrane component 1	MPR; 25Dx; VEMA; 25-Dx	neuron	unknown	
Pick1	protein interacting with PRKCA 1	Prkcabp	neuron	stimulates	Bartoe et al., 2006
Ptpn11	protein tyrosine phosphatase, non-receptor type 11	Shp2	neuron	stimulates	Rosario et al., 2007
Ret	ret proto-oncogene		neuron	stimulates	Luo et al., 2007
Rtn4	reticulon 4	r; Vp20; rat N; NI-250; MGC116054; rat NogoA	glia	inhibits	GrandPre et al., 2000; Chen et al., 2000
Rtn4rl2	reticulon 4 receptor-like 2	Ngrh1	neuron	inhibits	Venkatesh et al., 2005
S100a6	S100 calcium binding protein A6		glia	unknown	
Slit1	slit homolog 1 (Drosophila)	MEGF4	glia	inhibits	Brose et al., 1999
Thbs4	thrombospondin 4		neuron	stimulates	Arber and Caroni, 1995
Zfxh3	zinc finger homeobox 3		neuron	unknown	

Alabed YZ, Pool M, Ong Tone S, Fournier AE (2007) Identification of CRMP4 as a convergent regulator of axon outgrowth inhibition. J Neurosci 27:1702-1711

Arber S, Caroni P (1995) Thrombospondin-4, an extracellular matrix protein expressed in the developing and adult nervous system promotes neurite outgrowth. J Cell Biol 131:1083-1094

Bartoe JL, McKenna WL, Quan TK, Stafford BK, Moore JA, Xia J, Takamiya K, Huganir RL, Hinck L (2006) Protein interacting with C-kinase 1/protein kinase Calpha-mediated endocytosis converts netrin-1-mediated repulsion to attraction. J Neurosci 26:3192-3205

Bouquet C, Ravaille-Veron M, Propst F, Nothias F (2007) MAP1B coordinates microtubule and actin filament remodeling in adult mouse Schwann cell tips and DRG neuron growth cones. Mol Cell Neurosci 36:235-247

Brose K, Bland KS, Wang KH, Arnott D, Henzel W, Goodman CS, Tessier-Lavigne M, Kidd T (1999) Slit proteins bind Robo receptors and have an evolutionarily conserved role in repulsive axon guidance. Cell 96:795-806

Chen MS, Huber AB, van der Haar ME, Frank M, Schnell L, Spillmann AA, Christ F, Schwab ME (2000) Nogo-A is a myelin-associated neurite outgrowth inhibitor and an antigen for monoclonal antibody IN-1. Nature 403:434-439

GrandPré T, Nakamura F, Vartanian T, Strittmatter SM (2000) Identification of the Nogo inhibitor of axon regeneration as a Reticulon protein. Nature 403:439-444

Hausott B, Schlick B, Vallant N, Dorn R, Klimaschewski L (2008) Promotion of neurite outgrowth by fibroblast growth factor receptor 1 overexpression and lysosomal inhibition of receptor degradation in pheochromocytoma cells and adult sensory neurons. Neuroscience 153:461-473

Hobson SA, Holmes FE, Kerr NC, Pope RJ, Wynick D (2006) Mice deficient for galanin receptor 2 have decreased neurite outgrowth from adult sensory neurons and impaired pain-like behaviour. J Neurochem 99:1000-1010

Luo W, Wickramasinghe SR, Savitt JM, Griffin JW, Dawson TM, Ginty DD (2007) A hierarchical NGF signaling cascade controls Ret-dependent and Ret-independent events during development of nonpeptidergic DRG neurons. Neuron 54:739-754

Panicker AK, Buhusi M, Thelen K, Maness PF (2003) Cellular signalling mechanisms of neural cell adhesion molecules. Front Biosci 8:900-911

Rosário M, Franke R, Bednarski C, Birchmeier W (2007) The neurite outgrowth multiadaptor RhoGAP, NOMA-GAP, regulates neurite extension through SHP2 and Cdc42. J Cell Biol 178:503-516

Sestan N, Artavanis-Tsakonas S, Rakic P (1999) Contact-dependent inhibition of cortical neurite growth mediated by notch signaling. Science 286:741-746

Venkatesh K, Chivatakarn O, Lee H, Joshi PS, Kantor DB, Newman BA, Mage R, Rader C, Giger RJ (2005) The Nogo-66 receptor homolog NgR2 is a sialic acid-dependent receptor selective for myelin-associated glycoprotein. J Neurosci 25:808-822

Chapter 6

General discussion: deciphering the gene regulatory network underlying neuronal regeneration

Introduction

Axonal injury in the peripheral nervous system (PNS) induces a neuron-intrinsic gene expression program that promotes axonal regeneration. Over the past decades, numerous genes were found to be upregulated during successful axonal regeneration. These genes are commonly referred to as regeneration-associated genes (RAGs), and their protein products as growth-associated proteins (GAPs) (Skene 1984; Tetzlaff *et al*. 1991). Prototypic examples of RAGs are the well-known growth cone protein encoding genes *Gap43* and *Cap23*. RAG expression is generally considered to be beneficial for the regenerative capacity of an injured axon and to facilitate functional recovery. However, recent studies seem to indicate that genes that are induced upon axonal injury are not necessarily growth-promoting genes. In particular, several transcription factors (TFs) that are upregulated during successful regeneration, and are thus considered RAGs themselves, were found to suppress rather than to promote the regenerative response (Miao *et al*. 2006; MacGillavry *et al*. 2009; Smith *et al*. 2009). These unexpected findings raise the question whether the original RAG hypothesis postulated nearly 30 years ago, should be adjusted in the context of contemporary gene network theories. Understanding RAG expression from a gene network perspective may eventually help to identify key transcriptional regulators in the RAG network that provide entry points for improved regeneration-promoting therapies.

Regeneration-associated genes: a historical perspective

The most extensively studied and exemplifying RAG is *Gap43*, encoding the growth-associated protein-43 (GAP-43, also named B-50, F1 or pp46) (Benowitz and Routtenberg 1997). In a search for polypeptides that are transported along the axon during regeneration of the toad optic nerve, Skene and Willard were the first to identify GAP-43 (Skene and Willard 1981b; Skene and Willard 1981a). Studies in several other species showed that GAP-43 is consistently enriched in regenerating axons, but not in injured, non-regenerating axons (Skene 1989). GAP-43 is also present at high levels in developing axons, but its expression declines in fully matured neurons. The strict correlation between the induction of a small group of axonally transported proteins (including GAP43) and periods of axonal growth led to the GAP hypothesis, which postulates that damage to peripheral nerve axons triggers an intrinsic cell body response that includes the expression of a set of GAPs that together promote axon regeneration (Skene 1984). Around the same period, studies by the lab of Aguayo showed that spinal cord neurons, which normally do not regenerate spontaneously, actually could regenerate injured axons into a peripheral nerve graft (David and Aguayo 1981; Richardson *et al.* 1982). This indicated that central neurons do have the intrinsic capacity to regenerate injured axons, but that the expression of a regenerative response needs to be triggered by appropriate extrinsic signals. Later experiments also showed that when dorsal root ganglion (DRG) neurons are pre-

conditioned by a peripheral nerve transection, their central (dorsal root) axons show an enhanced regenerative sprouting response into the spinal cord, even beyond the lesion site (Richardson and Issa 1984; Neumann and Woolf 1999). Importantly, the pre-conditioning lesion effect could be mimicked by injecting cAMP analogues into the DRG, and is transcription dependent (Smith and Skene 1997; Neumann and Woolf 1999; Neumann *et al.* 2002). Together, these findings led to the introduction of the RAG hypothesis, stating that injured neurons need to induce the expression of a set of regeneration-associated genes in order to regenerate damaged axons (Tetzlaff *et al.* 1991; Kobayashi *et al.* 1997).

The RAG hypothesis was further strengthened by the identification of many additional growth-promoting genes using open screening methods such as differential display PCR and sequencing-based methods (Kiryu *et al.* 1995; Su *et al.* 1997; Tanabe *et al.* 1999). By now, genome-wide gene expression profiling studies have provided a near-complete view of the neuronal gene expression changes in diverse PNS and CNS injury paradigms (Costigan *et al.* 2002; Xiao *et al.* 2002; Schmitt *et al.* 2003; Kury *et al.* 2004; Di Giovanni *et al.* 2005; Bosse *et al.* 2006; Stam *et al.* 2007; Stam *et al.* 2008). Meta-analyses of such studies are now starting to reveal the core set of RAGs that is consistently up-regulated following neuronal injury (Szpara *et al.* 2007; Stam *et al.* 2008) and which we might call the regeneration-associated transcriptome or RAT. These studies have further supported the original RAG hypothesis by showing that many genes are strongly upregulated during successful regeneration only, whereas injury alone, which is not followed by regeneration, is insufficient to produce a robust induction of their expression (Stam *et al.* 2007 and Chapter 5 of this thesis).

The identification of RAGs led to the idea that axon regeneration could be promoted by overexpressing specific RAGs in injured neurons. Initial studies using transgenic GAP-43 mice were promising and showed a strong enhancement of long-distance regenerative axon growth in the PNS (Aigner *et al.* 1995). In the CNS, however, overexpression of GAP-43 only induced nerve sprouting, but failed to induce long-distance regeneration (Aigner *et al.* 1995; Buffo *et al.* 1997; Neumann and Woolf 1999), even into growth-promoting peripheral nerve grafts (Mason *et al.* 2000). Also, GAP-43 knockout mice have no gross axonal growth deficits, but show profound defects in axonal guidance (Strittmatter *et al.* 1995; Sretavan and Kruger 1998; Maier *et al.* 1999; Zhu and Julien 1999). A study on double-transgenic mice overexpressing both GAP-43 and CAP-23 did show enhanced DRG regeneration into the spinal cord (Bomze *et al.* 2001). Other RAGs that promote successful regeneration in the PNS include *Sprr1a*, *Itga7* and *c-Jun* (Werner *et al.* 2000; Bonilla *et al.* 2002; Raivich *et al.* 2004). Although these findings demonstrate that overexpression of (combinations of) individual RAGs can promote neuronal regeneration in the PNS, the observed effects were much less robust in the CNS. Therefore, research started to focus on transcriptional regulators that could affect the expression of multiple RAGs jointly.

Regeneration-associated transcription factors

In the late 1980's and early 1990's it was recognized that neuronal gene expression changes in response to environmental conditions occur in a precise temporal order. Physiological stimuli produce an initial wave of so-called immediately early genes (IEGs), which then trigger a second wave of late gene expression (Herdegen and Leah 1998; Hughes *et al.* 1999). Interestingly, following nerve transection, a rapid upregulation of c-Jun and JunD was observed, while JunB, c-Fos or FosB proteins remained undetected (Herdegen *et al.* 1991; Jenkins and Hunt 1991; Leah *et al.* 1991; Leah *et al.* 1993). The consistent upregulation of c-Jun in diverse injury paradigms was exciting as it implied that c-Jun might control the expression of down-stream RAGs. However, the precise function of c-Jun in neuronal regeneration remained controversial as it was also linked to neuronal cell death and degeneration (Herdegen *et al.* 1997). Analysis of a conditional knockout mouse that lacks c-Jun expression in the CNS finally showed that c-Jun plays an important role in the successful regeneration of facial nerve motorneurons (Raivich *et al.* 2004).

Additional studies demonstrated the specific upregulation and/or activation of other TFs during successful neuronal regeneration, including ATF3, SOX11, CREB, p53 and STAT3 (Schwaiger *et al.* 2000; Tsujino *et al.* 2000; Gao *et al.* 2004; Di Giovanni *et al.* 2006; Jankowski *et al.* 2006; Seijffers *et al.* 2006). Later, gene expression profiling studies have significantly expanded this set of regeneration-associated TFs (Tanabe *et al.* 1999; Stam *et al.* 2007; Moore *et al.* 2009; Zou *et al.* 2009), and TF genes were soon recognized as potentially important RAGs because they appear to regulate multiple RAGs simultaneously. For instance, c-Jun induces expression of *Itga7*, *Cd44* and *Gal* (Raivich *et al.* 2004), and ATF3 induces *c-Jun*, *Hsp27* and *Sprr1a* expression (Seijffers *et al.* 2007).

Surprisingly, recent studies show that the relation between the expression of a TF and its apparent role in regeneration can be paradoxical. At least four studies have now shown examples of TFs that are upregulated after peripheral nerve lesion, but are actually repressors of neurite outgrowth. The first example was provided by a study of Miao *et al* (2006) showing that SOCS3 (suppressor of cytokine signaling-3) is induced by peripheral nerve lesion, but represses neurite outgrowth by inhibiting the growth-promoting TF STAT3. Moreover, the regeneration-promoting effects of cAMP on injured retinal ganglion cells appear to be mediated by a downregulation of SOCS3 (Park *et al.* 2009) and genetic deletion of SOCS3 promotes optic nerve regeneration (Smith *et al.* 2009). Another study demonstrated that NFAT-3 is a transcriptional repressor of GAP-43 expression (Nguyen *et al.* 2009). This was unexpected, as it is long known that NFAT TFs are activated in response to growth factors and mediate axon outgrowth and presynaptic differentiation (Graef *et al.* 2003). We recently identified several TFs that are either up- or downregulated during successful regeneration, but that affect regenerative neurite outgrowth in an opposite and paradoxical manner. One of these TFs is NFIL3, which is upregulated in DRG sensory neurons by peripheral nerve injury, and inhibits neurite outgrowth by suppressing CREB target genes such as *Arg1* and *Gap43* (MacGil-

lavry *et al.* 2009). Finally, Moore *et al.* (2009) showed that KLF4 is a repressor of retinal ganglion cell axon growth, and although KLF4 expression is not upregulated after injury, *in vivo* deletion of KLF4 does enhance optic nerve regeneration. Together, these findings challenge the original RAG concept, and demonstrate that RAGs operate in the context of gene regulatory networks in which multiple TFs act in concert to regulate their expression. Consequently, RAG expression is also constrained by gene network characteristics that probably evolved for other reasons than to promote regenerative axon growth. A better understanding of the transcriptional regulation of regeneration thus requires more insight into the architecture of the gene regulatory network that underlies RAG expression.

Regeneration-associated gene regulatory network motifs

The finding that several TFs that are activated during successful regeneration in fact suppress regenerative axon growth asks for a reinterpretation of the RAG concept. Apparently not all RAGs promote regeneration, and we need to find explanations for the paradoxical nature of some regeneration-associated TFs. Studies on transcriptional regulatory mechanisms in simple organisms demonstrated that TFs and their target genes are organized in small-scale network motifs, the basic architecture of which seems to recur often in nature (Lee *et al.* 2002; Milo *et al.* 2002; Shen-Orr *et al.* 2002). In order to understand the paradoxical role of NFIL3 in peripheral axon regeneration of injured DRG sensory neurons, we determined whether NFIL3 might be part of such a TF-target gene network motif (Chapter 2).

Network motifs consist of several TFs that together regulate target gene expression in a coordinated fashion. We observed that the induction of NFIL3, either following a nerve crush or in neurons stimulated with cAMP, is preceded by a rapid activation of CREB (MacGillavry *et al.* 2009). We could also show that CREB is recruited to the *Nfil3* promoter after peripheral nerve crush, indicating that NFIL3 is a direct CREB target. Both CREB and NFIL3 are members of the bZIP family of TFs, and recognize similar DNA binding sites. We found that CREB and NFIL3 compete for binding to promoters of several RAGs (e.g. *Gap43* and *Arg1*), but that they have opposite effects on gene transcription; CREB activates and NFIL3 represses RAG expression. Thus, NFIL3 is upregulated as a consequence of CREB activation, and acts as a repressor of CREB target genes during neuronal regeneration. Such a transcriptional network motif, in which a TF activates a gene response that includes a downstream transcriptional repressor of that gene response, is named a type 1 incoherent feed-forward loop (Mangan and Alon 2003). Experimental and computational modeling studies showed that these loops are conserved throughout evolution and are important to generate pulses of target gene expression and to accelerate the response time of target genes (Mangan *et al.* 2006; Alon 2007). Thus, the CREB/NFIL3 feed-forward loop probably serves to control temporal RAG expression during axon regeneration.

Genome-wide identification of CREB and NFIL3 target genes during cAMP-induced neuronal outgrowth showed that only a small fraction of NFIL3-bound genes are also CREB target genes (Chapter 4). Instead, many NFIL3-bound genes appear to be co-regulated by C/EBPs. C/EBPs are activating bZIP TFs that can act downstream of CREB (Impey *et al.* 2004) and seem to be involved in the regulation of neuronal outgrowth (Cortes-Canteli *et al.* 2002; Nadeau *et al.* 2005). Thus, in addition to CREB target genes, NFIL3 probably also represses C/EBP target genes, suggesting that NFIL3 may be a general feed-forward repressor of bZIP TF-activated gene expression. The transcriptional interactions between CREB, C/EBP and NFIL3 provide the first example of a RAG transcriptional regulatory network motif, and a first glimpse at the RAG regulatory network as a whole (see Chapter 4, Figure 5E).

Studies on transcriptional repressors such as SOCS3, NFAT, KLF7 and NFIL3 highlight the importance of understanding the temporal regulation of RAG expression from a gene network perspective, and may explain why many RAGs only partially promote regeneration *in vivo*. Seijffers *et al.* (2007) for instance showed that ATF3, which is strongly upregulated by a peripheral nerve lesion, can indeed promote peripheral nerve regeneration, but fails to induce axon growth after a central nerve lesion. Also, overexpression of constitutive-active CREB, which *in vitro* robustly overcomes myelin-induced growth inhibition, induces a limited central nerve sprouting response (Gao *et al.* 2004). We believe that these results can in part be explained by the fact that ATF3 and CREB induce a RAG program that includes intrinsic downstream feed-forward repressors such as SOCS3 and NFIL3, which in turn suppress the activated growth response. Thus, although activating TFs can cause an initial activation of the RAG program, intrinsic gene network design triggers subsequent transcriptional repressors that prevent the RAG response from being maximally effective. Interestingly, the degree to which such intrinsic repressive mechanisms are active seems to differ depending on the growth conditions (i.e. *in vivo* versus *in vitro* and peripheral versus central). Although transcriptional repressive mechanisms probably evolved for good reasons (see the NFIL3 feed-forward loop described earlier), we argue that temporal relieve from transcriptional repression might help to boost the initial regenerative response (Chapter 3), making transcriptional repressors interesting novel targets for regeneration therapy.

The regeneration-associated gene network

The examples described above show how gene regulatory network motifs may regulate the dynamics of target gene expression and constrain target gene expression within physiological limits. A major challenge is now to reconstruct the entire RAG network, and to predict the key transcriptional regulators that would maximally affect the network as a whole. Gene networks can be described as directed graphs in which genes are represented by nodes (formally named vertices), and transcriptional regulatory interactions by arrows (formally named arcs). Gene network graphs give better insight into the gene

regulatory mechanisms underlying biological processes, and allow researches to model the effects of network perturbations and predict the key elements in the network that would be maximally sensitive to network perturbation (Almaas 2007). To reconstruct a gene regulatory network graph, we need to systematically assemble biological data gene expression, gene function and gene interaction into a single regulatory network. Pioneering work in simple organisms, including bacteria and yeast, has guided the development of new computational and high-throughput quantitative experimental techniques to reconstruct gene networks from biological data. The application of these methods in more complex biological systems such the as nervous system is not trivial, but is progressively evolving.

A first step towards the construction of the RAG network is the experimental identification of genes that are functionally involved in regenerative axon outgrowth and thus form the nodes in the network. Recent developments in automated (fluorescence) microscopy and the availability of (genome-wide) siRNA libraries enable researchers to conduct high-throughput functional assays (Echeverri and Perrimon 2006). The success of these methods in the field of neuroregeneration has recently been demonstrated by screening large gene sets for effects on neurite outgrowth and/or survival (Saito *et al.* 2005; MacGillavry *et al.* 2009; Moore *et al.* 2009; Ossovskaya *et al.* 2009). Although these studies often rely on *in vitro* cell systems, and results do not necessarily reflect *in vivo* gene function, they do enable the pre-selection of candidate genes from larger gene expression data sets for further in-depth analysis.

The next step is the identification of TF-gene interactions. With the completion of the whole-genome sequence, new computational methods that reliably predict functional TF binding sites (TFBSs) in gene promoters are emerging. Overrepresentation of TFBSs in sets of co-regulated genes can predict TFs that coordinately regulate these genes. However, these methods critically depend on the accuracy of TFBS predictions, while the identification of these generally short and degenerate sequences often results in high numbers of false-positives. Therefore, we developed a new method, named LLM3D or log-linear modeling using 3D-contingency tables, which simultaneously tests the interaction between gene expression, the presence of TFBSs and gene ontology annotation. LLM3D performs better in predicting transcription regulatory mechanisms from temporal gene expression data, both in yeast and in mammals (Chapter 5). We applied this method to gene expression data from DRGs subjected to either peripheral (sciatic) nerve crush or central (dorsal root) crush. This resulted in the identification of several TFs that might regulate RAG expression and promote successful regeneration. One of these predicted TFs, PPARγ, promotes neurite outgrowth *in vitro*. Interestingly, PPARγ expression is not changed after injury or during regeneration, which demonstrates the importance of computational TFBS predictions in identifying transcriptional regulators that are not revealed using gene expression-based methods only.

Computational predictions of TF-gene interactions result hypotheses that can

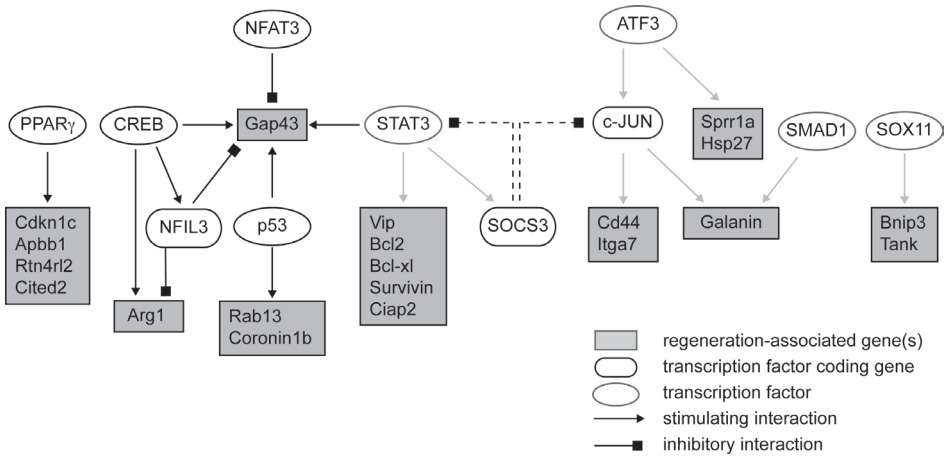

Figure 1. An initial blueprint for the gene regulatory network that underlies successful neuronal regeneration.
TF-target gene interactions described in the literature are indicated with solid black lines (direct interactions identified with ChIP), or a solid gray line (interactions inferred by other means). Non-transcriptional interactions are indicated with dashed lines.

subsequently be validated experimentally. Chromatin immunoprecipitation (ChIP) is often used to determine the direct interaction of a TF with a gene's promoter. ChIP is a powerful method to confirm individual TF-target gene interactions, and we used it for instance to show that NFIL3 and CREB bind to the same RAG promoters *in vivo* (Chapter 2), and that PPARγ binds to target genes that were computationally predicted by LLM3D (Chapter 5). ChIP methods become even more powerful when combined with DNA array (ChIP-chip) or deep-sequencing (ChIP-Seq) technologies, allowing genome-wide identification of TF-gene interactions (Chapter 4). In principle, ChIP-chip or ChIP-Seq data could directly be integrated with genome-wide gene expression data in order to infer gene regulatory networks. However, ChIP analysis still requires high amounts of input chromatin and ChIP results thus necessarily reflect the average level of TF binding at a certain gene promoter in the entire cell population. Interpretation of these data is further complicated by the heterogeneous nature of mammalian nervous tissue, and the power of genome-wide ChIP approaches to directly reconstruct gene networks in mammalian neurons still needs to be demonstrated.

Future perspectives

One critical feature of gene regulatory networks, and of biochemical interaction networks in general, is that they have a scale-free topology in which the connectivity distribution follows a power law. This means that many nodes in the network have a low degree of connectivity, whereas few nodes are highly connected and are also called network hubs.

Scale-free networks are by nature highly resistant against random perturbation, but also very sensitive to targeted attacks at critical hubs. The wealth of data that has been gathered over the years on RAG expression has led to important insights in the transcriptional regulation of regeneration. Although the outlines of the gene regulatory network for regeneration are slowly emerging (Figure 1), we still have to determine what the critical hubs in the network are. In the future, additional data from computational and experimental studies will undoubtedly start to accumulate, resulting in a more complete view of the network's connectivity. Eventually this will lead to the identification of the critical nodes and pinpoint targets for therapy. The development of viral vectors to deliver (modified) genes to injured neurons or the surrounding glia (Hendriks *et al.* 2004; Tannemaat *et al.* 2008) will greatly aid in the study of new targets and holds great promise to be used as therapy in the damaged nervous system.

References

Aigner L, Arber S, Kapfhammer JP, Laux T, Schneider C, Botteri F, Brenner HR, Caroni P (1995) Overexpression of the neural growth-associated protein GAP-43 induces nerve sprouting in the adult nervous system of transgenic mice. Cell 83:269-278.

Almaas E (2007) Biological impacts and context of network theory. J Exp Biol 210:1548-1558.

Alon U (2007) Network motifs: theory and experimental approaches. Nat Rev Genet 8:450-461.

Benowitz LI, Routtenberg A (1997) GAP-43: an intrinsic determinant of neuronal development and plasticity. Trends Neurosci 20:84-91.

Bomze HM, Bulsara KR, Iskandar BJ, Caroni P, Skene JH (2001) Spinal axon regeneration evoked by replacing two growth cone proteins in adult neurons. Nat Neurosci 4:38-43.

Bonilla IE, Tanabe K, Strittmatter SM (2002) Small proline-rich repeat protein 1A is expressed by axotomized neurons and promotes axonal outgrowth. J Neurosci 22:1303-1315.

Bosse F, Hasenpusch-Theil K, Kury P, Muller HW (2006) Gene expression profiling reveals that peripheral nerve regeneration is a consequence of both novel injury-dependent and reactivated developmental processes. J Neurochem 96:1441-1457.

Buffo A, Holtmaat AJ, Savio T, Verbeek JS, Oberdick J, Oestreicher AB, Gispen WH, Ver-

haagen J, Rossi F, Strata P (1997) Targeted overexpression of the neurite growth-associated protein B-50/GAP-43 in cerebellar Purkinje cells induces sprouting after axotomy but not axon regeneration into growth-permissive transplants. J Neurosci 17:8778-8791.

Cortes-Canteli M, Pignatelli M, Santos A, Perez-Castillo A (2002) CCAAT/enhancer-binding protein beta plays a regulatory role in differentiation and apoptosis of neuroblastoma cells. J Biol Chem 277:5460-5467.

Costigan M, Befort K, Karchewski L, Griffin RS, D'Urso D, Allchorne A, Sitarski J, Mannion JW, Pratt RE, Woolf CJ (2002) Replicate high-density rat genome oligonucleotide microarrays reveal hundreds of regulated genes in the dorsal root ganglion after peripheral nerve injury. BMC Neurosci 3:16.

David S, Aguayo AJ (1981) Axonal elongation into peripheral nervous system "bridges" after central nervous system injury in adult rats. Science 214:931-933.

Di Giovanni S, De Biase A, Yakovlev A, Finn T, Beers J, Hoffman EP, Faden AI (2005) In vivo and in vitro characterization of novel neuronal plasticity factors identified following spinal cord injury. J Biol Chem 280:2084-2091.

Di Giovanni S, Knights CD, Rao M, Yakovlev A, Beers J, Catania J, Avantaggiati ML, Faden AI (2006) The tumor suppressor protein p53 is required for neurite outgrowth and axon regeneration. EMBO J 25:4084-4096.

Echeverri CJ, Perrimon N (2006) High-throughput RNAi screening in cultured cells: a user's guide. Nat Rev Genet 7:373-384.

Gao Y, Deng K, Hou J, Bryson JB, Barco A, Nikulina E, Spencer T, Mellado W, Kandel ER, Filbin MT (2004) Activated CREB is sufficient to overcome inhibitors in myelin and promote spinal axon regeneration in vivo. Neuron 44:609-621.

Graef IA, Wang F, Charron F, Chen L, Neilson J, Tessier-Lavigne M, Crabtree GR (2003) Neurotrophins and netrins require calcineurin/NFAT signaling to stimulate outgrowth of embryonic axons. Cell 113:657-670.

Hendriks WT, Ruitenberg MJ, Blits B, Boer GJ, Verhaagen J (2004) Viral vector-mediated gene transfer of neurotrophins to promote regeneration of the injured spinal cord. Prog Brain Res 146:451-476.

Herdegen T, Leah JD (1998) Inducible and constitutive transcription factors in the mam-

malian nervous system: control of gene expression by Jun, Fos and Krox, and CREB/ATF proteins. Brain Res Brain Res Rev 28:370-490.

Herdegen T, Skene P, Bahr M (1997) The c-Jun transcription factor--bipotential mediator of neuronal death, survival and regeneration. Trends Neurosci 20:227-231.

Herdegen T, Kummer W, Fiallos CE, Leah J, Bravo R (1991) Expression of c-JUN, JUN B and JUN D proteins in rat nervous system following transection of vagus nerve and cervical sympathetic trunk. Neuroscience 45:413-422.

Hughes PE, Alexi T, Walton M, Williams CE, Dragunow M, Clark RG, Gluckman PD (1999) Activity and injury-dependent expression of inducible transcription factors, growth factors and apoptosis-related genes within the central nervous system. Prog Neurobiol 57:421-450.

Impey S, McCorkle SR, Cha-Molstad H, Dwyer JM, Yochum GS, Boss JM, McWeeney S, Dunn JJ, Mandel G, Goodman RH (2004) Defining the CREB regulon: a genome-wide analysis of transcription factor regulatory regions. Cell 119:1041-1054.

Jankowski MP, Cornuet PK, McIlwrath S, Koerber HR, Albers KM (2006) SRY-box containing gene 11 (Sox11) transcription factor is required for neuron survival and neurite growth. Neuroscience 143:501-514.

Jenkins R, Hunt SP (1991) Long-term increase in the levels of c-jun mRNA and jun protein-like immunoreactivity in motor and sensory neurons following axon damage. Neurosci Lett 129:107-110.

Kiryu S, Yao GL, Morita N, Kato H, Kiyama H (1995) Nerve injury enhances rat neuronal glutamate transporter expression: identification by differential display PCR. J Neurosci 15:7872-7878.

Kobayashi NR, Fan DP, Giehl KM, Bedard AM, Wiegand SJ, Tetzlaff W (1997) BDNF and NT-4/5 prevent atrophy of rat rubrospinal neurons after cervical axotomy, stimulate GAP-43 and Talpha1-tubulin mRNA expression, and promote axonal regeneration. J Neurosci 17:9583-9595.

Kury P, Abankwa D, Kruse F, Greiner-Petter R, Muller HW (2004) Gene expression profiling reveals multiple novel intrinsic and extrinsic factors associated with axonal regeneration failure. Eur J Neurosci 19:32-42.

Leah JD, Herdegen T, Bravo R (1991) Selective expression of Jun proteins following axotomy and axonal transport block in peripheral nerves in the rat: evidence for a role in the regeneration process. Brain Res 566:198-207.

Leah JD, Herdegen T, Murashov A, Dragunow M, Bravo R (1993) Expression of immediate early gene proteins following axotomy and inhibition of axonal transport in the rat central nervous system. Neuroscience 57:53-66.

Lee TI et al. (2002) Transcriptional regulatory networks in Saccharomyces cerevisiae. Science 298:799-804.

MacGillavry HD, Stam FJ, Sassen MM, Kegel L, Hendriks WT, Verhaagen J, Smit AB, van Kesteren RE (2009) NFIL3 and cAMP response element-binding protein form a transcriptional feedforward loop that controls neuronal regeneration-associated gene expression. J Neurosci 29:15542-15550.

Maier DL, Mani S, Donovan SL, Soppet D, Tessarollo L, McCasland JS, Meiri KF (1999) Disrupted cortical map and absence of cortical barrels in growth-associated protein (GAP)-43 knockout mice. Proc Natl Acad Sci U S A 96:9397-9402.

Mangan S, Alon U (2003) Structure and function of the feed-forward loop network motif. Proc Natl Acad Sci U S A 100:11980-11985.

Mangan S, Itzkovitz S, Zaslaver A, Alon U (2006) The incoherent feed-forward loop accelerates the response-time of the gal system of Escherichia coli. J Mol Biol 356:1073-1081.

Mason MR, Campbell G, Caroni P, Anderson PN, Lieberman AR (2000) Overexpression of GAP-43 in thalamic projection neurons of transgenic mice does not enable them to regenerate axons through peripheral nerve grafts. Exp Neurol 165:143-152.

Miao T, Wu D, Zhang Y, Bo X, Subang MC, Wang P, Richardson PM (2006) Suppressor of cytokine signaling-3 suppresses the ability of activated signal transducer and activator of transcription-3 to stimulate neurite growth in rat primary sensory neurons. J Neurosci 26:9512-9519.

Milo R, Shen-Orr S, Itzkovitz S, Kashtan N, Chklovskii D, Alon U (2002) Network motifs: simple building blocks of complex networks. Science 298:824-827.

Moore DL, Blackmore MG, Hu Y, Kaestner KH, Bixby JL, Lemmon VP, Goldberg JL

(2009) KLF family members regulate intrinsic axon regeneration ability. Science 326:298-301.

Nadeau S, Hein P, Fernandes KJ, Peterson AC, Miller FD (2005) A transcriptional role for C/EBP beta in the neuronal response to axonal injury. Mol Cell Neurosci 29:525-535.

Neumann S, Woolf CJ (1999) Regeneration of dorsal column fibers into and beyond the lesion site following adult spinal cord injury. Neuron 23:83-91.

Neumann S, Bradke F, Tessier-Lavigne M, Basbaum AI (2002) Regeneration of sensory axons within the injured spinal cord induced by intraganglionic cAMP elevation. Neuron 34:885-893.

Nguyen T, Lindner R, Tedeschi A, Forsberg K, Green A, Wuttke A, Gaub P, Di Giovanni S (2009) NFAT-3 is a transcriptional repressor of the growth-associated protein 43 during neuronal maturation. J Biol Chem 284:18816-18823.

Ossovskaya VS, Dolganov G, Basbaum AI (2009) Loss of function genetic screens reveal MTGR1 as an intracellular repressor of beta1 integrin-dependent neurite outgrowth. J Neurosci Methods 177:322-333.

Park KK, Hu Y, Muhling J, Pollett MA, Dallimore EJ, Turnley AM, Cui Q, Harvey AR (2009) Cytokine-induced SOCS expression is inhibited by cAMP analogue: impact on regeneration in injured retina. Mol Cell Neurosci 41:313-324.

Raivich G, Bohatschek M, Da Costa C, Iwata O, Galiano M, Hristova M, Nateri AS, Makwana M, Riera-Sans L, Wolfer DP, Lipp HP, Aguzzi A, Wagner EF, Behrens A (2004) The AP-1 transcription factor c-Jun is required for efficient axonal regeneration. Neuron 43:57-67.

Richardson PM, Issa VM (1984) Peripheral injury enhances central regeneration of primary sensory neurones. Nature 309:791-793.

Richardson PM, McGuinness UM, Aguayo AJ (1982) Peripheral nerve autografts to the rat spinal cord: studies with axonal tracing methods. Brain Res 237:147-162.

Saito S, Honma K, Kita-Matsuo H, Ochiya T, Kato K (2005) Gene expression profiling of cerebellar development with high-throughput functional analysis. Physiol Genomics 22:8-13.

Schmitt AB, Breuer S, Liman J, Buss A, Schlangen C, Pech K, Hol EM, Brook GA, Noth J, Schwaiger FW (2003) Identification of regeneration-associated genes after central and peripheral nerve injury in the adult rat. BMC Neurosci 4:8.

Schwaiger FW, Hager G, Schmitt AB, Horvat A, Streif R, Spitzer C, Gamal S, Breuer S, Brook GA, Nacimiento W, Kreutzberg GW (2000) Peripheral but not central axotomy induces changes in Janus kinases (JAK) and signal transducers and activators of transcription (STAT). Eur J Neurosci 12:1165-1176.

Seijffers R, Allchorne AJ, Woolf CJ (2006) The transcription factor ATF-3 promotes neurite outgrowth. Mol Cell Neurosci 32:143-154.

Seijffers R, Mills CD, Woolf CJ (2007) ATF3 increases the intrinsic growth state of DRG neurons to enhance peripheral nerve regeneration. J Neurosci 27:7911-7920.

Shen-Orr SS, Milo R, Mangan S, Alon U (2002) Network motifs in the transcriptional regulation network of Escherichia coli. Nat Genet 31:64-68.

Skene JH (1984) Growth-associated proteins and the curious dichotomies of nerve regeneration. Cell 37:697-700.

Skene JH (1989) Axonal growth-associated proteins. Annu Rev Neurosci 12:127-156.
Skene JH, Willard M (1981a) Changes in axonally transported proteins during axon regeneration in toad retinal ganglion cells. J Cell Biol 89:86-95.

Skene JH, Willard M (1981b) Characteristics of growth-associated polypeptides in regenerating toad retinal ganglion cell axons. J Neurosci 1:419-426.

Smith DS, Skene JH (1997) A transcription-dependent switch controls competence of adult neurons for distinct modes of axon growth. J Neurosci 17:646-658.

Smith PD, Sun F, Park KK, Cai B, Wang C, Kuwako K, Martinez-Carrasco I, Connolly L, He Z (2009) SOCS3 deletion promotes optic nerve regeneration in vivo. Neuron 64:617-623.

Sretavan DW, Kruger K (1998) Randomized retinal ganglion cell axon routing at the optic chiasm of GAP-43-deficient mice: association with midline recrossing and lack of normal ipsilateral axon turning. J Neurosci 18:10502-10513.

Stam FJ, Mason MR, Smit AB, Verhaagen J (2008) A meta-analysis of large-scale gene

expression studies of the injured PNS: toward the genetic networks that govern successful regeneration. In: Neural degeneration and repair: expression profiling, proteomics, glycomics, and systems biology.

Stam FJ, MacGillavry HD, Armstrong NJ, de Gunst MC, Zhang Y, van Kesteren RE, Smit AB, Verhaagen J (2007) Identification of candidate transcriptional modulators involved in successful regeneration after nerve injury. Eur J Neurosci 25:3629-3637.

Strittmatter SM, Fankhauser C, Huang PL, Mashimo H, Fishman MC (1995) Neuronal pathfinding is abnormal in mice lacking the neuronal growth cone protein GAP-43. Cell 80:445-452.

Su QN, Namikawa K, Toki H, Kiyama H (1997) Differential display reveals transcriptional up-regulation of the motor molecules for both anterograde and retrograde axonal transport during nerve regeneration. Eur J Neurosci 9:1542-1547.

Szpara ML, Vranizan K, Tai YC, Goodman CS, Speed TP, Ngai J (2007) Analysis of gene expression during neurite outgrowth and regeneration. BMC Neurosci 8:100.

Tanabe K, Nakagomi S, Kiryu-Seo S, Namikawa K, Imai Y, Ochi T, Tohyama M, Kiyama H (1999) Expressed-sequence-tag approach to identify differentially expressed genes following peripheral nerve axotomy. Brain Res Mol Brain Res 64:34-40.

Tannemaat MR, Verhaagen J, Malessy M (2008) The application of viral vectors to enhance regeneration after peripheral nerve repair. Neurol Res 30:1039-1046.

Tetzlaff W, Alexander SW, Miller FD, Bisby MA (1991) Response of facial and rubrospinal neurons to axotomy: changes in mRNA expression for cytoskeletal proteins and GAP-43. J Neurosci 11:2528-2544.

Tsujino H, Kondo E, Fukuoka T, Dai Y, Tokunaga A, Miki K, Yonenobu K, Ochi T, Noguchi K (2000) Activating transcription factor 3 (ATF3) induction by axotomy in sensory and motoneurons: A novel neuronal marker of nerve injury. Mol Cell Neurosci 15:170-182.

Werner A, Willem M, Jones LL, Kreutzberg GW, Mayer U, Raivich G (2000) Impaired axonal regeneration in alpha7 integrin-deficient mice. J Neurosci 20:1822-1830.

Xiao HS, Huang QH, Zhang FX, Bao L, Lu YJ, Guo C, Yang L, Huang WJ, Fu G, Xu SH, Cheng XP, Yan Q, Zhu ZD, Zhang X, Chen Z, Han ZG, Zhang X (2002) Identification of

gene expression profile of dorsal root ganglion in the rat peripheral axotomy model of neuropathic pain. Proc Natl Acad Sci U S A 99:8360-8365.

Zhu Q, Julien JP (1999) A key role for GAP-43 in the retinotectal topographic organization. Exp Neurol 155:228-242.

Zou H, Ho C, Wong K, Tessier-Lavigne M (2009) Axotomy-induced Smad1 activation promotes axonal growth in adult sensory neurons. J Neurosci 29:7116-7123.

Nederlandse Samenvatting

Zenuwschade en regeneratie

Het centrale zenuwstelsel, de hersenen en het ruggenmerg, staat in verbinding met de organen en zintuigen via het perifere zenuwstelsel. Zenuwcellen (neuronen) zenden elkaar en hun doelorganen elektrische signalen via lange uitlopers, axonen. Motorneuronen sturen zo de spieren aan, en sensorische neuronen geven zo de gevoelsprikkels door naar de hersenen. Bij beschadiging van de zenuwbanen die deze axonen bevatten, kan dus verlies van beweging en gevoel optreden. De gevolgen van een beschadiging kunnen echter sterk verschillen. In het perifere zenuwstelsel vindt vaak vrij goed herstel, of regeneratie, van axonen plaats, terwijl beschadiging van axonen in het centrale zenuwstelsel meestal permanent is. De reactie van op perifere zenuwschade is dus fundamenteel anders dan de reactie op schade in het centrale zenuwstelsel. Dit verschil is enerzijds een gevolg van de directe omgeving van de beschadigde axonen. In het centrale zenuwstelsel vindt vaak een sterke ontstekingsreactie plaats, wat samen met de vorming van littekenweefsel de regeneratie van axonen sterk remt. In het perifere zenuwstelsel gebeurt dit niet en zijn er lokaal cellen aanwezig die de teruggroei van axonen stimuleren. Anderzijds is dit verschil een gevolg van de intrinsieke respons van het beschadigde neuron. Een neuron in het perifere zenuwstelsel is in staat om in reactie op de beschadiging specifieke groepen eiwitten aan te maken die de regeneratie van het axon bevorderen. De aanmaak van eiwitten in een cel is een strikt gereguleerd proces dat begint bij het activeren van een gen dat codeert voor het eiwit. Dit proces, het reguleren van genen die betrokken zijn bij axonregeneratie, is het onderwerp van mijn promotieonderzoek.

Van gen tot eiwit; de regulatie van genexpressie

De kern van elke cel in ons lichaam bevat dezelfde genetische code, opgeslagen in het DNA. Over de lange DNA strengen verspreid, liggen ongeveer 23.000 losse gebieden, de genen, die ieder voor een ander eiwit coderen. Eiwitten zijn nodig voor de opbouw en onderhoud van de cel. Dit betekent dat tijdens de ontwikkeling in verschillende celtypen specifieke eiwitten moeten worden aangemaakt. Een levercel heeft bijvoorbeeld andere eiwitten nodig dan een neuron. Niet alleen tijdens de ontwikkeling, maar ook als een cel beschadigd raakt of signalen van buitenaf krijgt, worden specifieke genen geactiveerd om de benodigde eiwitten te produceren. Van een actief gen wordt dan een kopie gemaakt, een “messenger RNA” (mRNA), wat de celkern verlaat, alwaar de informatie op het mRNA wordt afgelezen en het juiste eiwit wordt geproduceerd. Dit hele proces wordt ook wel genexpressie genoemd. Genexpressie wordt heel nauwkeurig gereguleerd door een speciale groep eiwitten, transcriptiefactoren. Deze eiwitten binden aan het DNA om genen te kunnen reguleren. Naast de code om eiwitten te kunnen maken (genen), bevat het DNA dus ook de code die de activiteit van genen reguleert. Als een transcriptiefactor

aan het DNA vlak voor het begin van een gen (dit gebied heet de "promotor") bindt, kan het de productie van mRNA, ofwel de expressie van dat gen stimuleren, maar ook remmen.

Transcriptionele netwerken

Elke transcriptiefactor kan hele groepen genen reguleren. Omgekeerd, kan een gen door een verschillend aantal transcriptiefactoren worden gereguleerd. Deze interacties tussen genen en transcriptiefactoren wordt beschreven in "transcriptionele netwerken". Mijn promotieonderzoek was gericht op het identificeren van genen die betrokken zijn bij de regulatie van axonregeneratie na schade én de transcriptiefactoren die deze genen reguleren. Uiteindelijk willen we het volledige netwerk van transcriptiefactoren en genen in kaart brengen dat succesvolle axonregeneratie reguleert. Als je weet welke genen in een proces betrokken zijn en hoe die genen worden gereguleerd krijg je beter inzicht in het verloop van het proces. Ook kun je dan beter de knelpunten in de regulatie aanwijzen. Samen zouden deze inzichten kunnen leiden tot een strategie om herstel na zenuwschade in het centrale zenuwstelsel te bevorderen.

Het meten van genexpressie na zenuwschade

Voor het in kaart brengen van zo'n netwerk is het allereerst belangrijk te weten welke genen er gereguleerd worden, ofwel tot expressie komen. Dit kan met behulp van "microarrays" gemeten worden. Microarrays zijn glaasjes waar kopieën van genen op gespot zijn. Door uit cellen onder een bepaalde conditie de mRNAs te isoleren en op zo'n glaasje aan te brengen kan afgeleid worden welke mRNAs blijven binden aan de spots en dus aanwezig waren in die cellen. Door verschillende condities te vergelijken kan zo ook gekeken worden of genen na b.v. celschade meer of minder tot expressie komen.

Op deze manier hebben we in de rat genen geïdentificeerd die geactiveerd ofwel geremd worden na zenuwschade. We hebben hiervoor de neuronen in de dorsale wortel ganglion bestudeerd. Deze, naast het ruggenmerg gelegen zenuwknoop, bevat sensorische neuronen die gevoelsprikkels van de zintuigen doorgeven naar de hersenen. Interessant aan dit model is dat deze neuronen zowel een perifeer axon hebben dat na beschadiging goed herstelt, als een centraal axon, dat niet herstelt na beschadiging. Met behulp van microarrays hebben we bestudeerd welke genen geactiveerd of geremd worden in deze sensorische zenuwcellen na zenuwschade. We hebben dit bestudeerd na een perifere zenuwbeschadiging én na een centrale zenuwbeschadiging. Deze studie geeft een volledig inzicht in welke genen geactiveerd (of opgereguleerd) zijn en welke genen geremd zijn na succesvolle en niet-succesvolle zenuwregeneratie. We zien bijvoorbeeld genen opgereguleerd waarvan al bekend is dat ze betrokken zijn bij zenuw uitgroei, maar ook genen waarvan de functie onbekend is, en die wellicht een rol spelen in het proces van zenuwregeneratie. Op basis van deze studie hebben we vervolgens op verschillende manieren geprobeerd inzicht te krijgen in de functie en regulatie van deze genen.

Het identificeren van transcriptiefactoren die zenuwregeneratie bevorderen of remmen

Omdat we geïnteresseerd zijn in transcriptiefactoren, hebben we eerst gekeken welke van de gevonden genen coderen voor transcriptiefactoren en een rol kunnen spelen in zenuwregeneratie (Hoofdstuk 2). Van de paar honderd genen die gereguleerd zijn na zenuwschade, vinden we er ongeveer 70 die coderen voor transcriptiefactoren. In kweekexperimenten hebben we ieder van deze 70 transcriptiefactoren uitgeschakeld en het effect daarvan op de neuriet uitgroei van deze cellen getest. Als een model voor axonregeneratie, maken we hier gebruik van zenuwcellen die gemakkelijk gekweekt kunnen worden en gestimuleerd kunnen worden om "neurieten" te groeien. We spreken hier van "neurieten" omdat deze zenuwuitlopers op dit moment nog geen volgroeide, functionele axonen zijn. Van de 70 door ons geteste transcriptiefactoren zijn er 10 die neuriet uitgroei stimuleren of remmen. Tot onze verassing ontdekten wij dat er ook factoren zijn die worden geactiveerd tijdens succesvolle regeneratie, maar een remmend effect hebben op neuriet uitgroei. Dit betekent dus dat het proces van succesvolle zenuwregeneratie ook factoren activeert die remmend werken op datzelfde herstelproces. Een voorbeeld van zo'n transcriptiefactor die deze paradox duidelijk illustreert en waar een groot deel van mijn onderzoek zich op gericht heeft is NFIL3.

NFIL3 en CREB vormen samen een transcriptioneel netwerk dat zenuwregeneratie reguleert

Uit de eerste experimenten bleek dat van alle 70 transcriptiefactoren NFIL3 het sterkste remmend werkt op neuriet uitgroei. Echter, we hadden eerder gevonden dat als we de perifere zenuw van de rat beschadigen en dus zenuwregeneratie induceren, NFIL3 verhoogt tot expressie komt. Ook in diverse celmodellen zien we een sterke toename in NFIL3 expressie, wanneer neuriet uitgroei wordt gestimuleerd. Wanneer we nu deze toename in NFIL3 expressie voorkomen of we blokkeren de werking van NFIL3, wordt de neuriet uitgroei van deze cellen nog verder gestimuleerd. Kortom, NFIL3 expressie neemt toe tijdens neuriet uitgroei, maar remt dit proces vervolgens. Om deze paradox te kunnen verklaren zijn we gaan bestuderen hoe NFIL3 samen werkt met andere transcriptiefactoren, welke genen het reguleert, en dus hoe het transcriptionele netwerk rondom NFIL3 eruit ziet. We hebben ons daarbij gebaseerd op voorgaand werk van andere laboratoria. Het was bijvoorbeeld al bekend dat een aan NFIL3 verwante transcriptiefactor, CREB, een stimulerende werking heeft op genen die zenuwregeneratie bevorderen. In tegenstelling tot CREB is NFIL3 echter een remmende transcriptiefactor. Wij hebben nu kunnen aantonen dat deze twee transcriptiefactoren in principe dezelfde genen kunnen reguleren, maar dus in tegengestelde richting. Deze vindingen hebben geleid tot het identificeren van een eerste transcriptionele (sub-) netwerk dat betrokken is bij de regulatie van genen die zenuwregeneratie bevorderen. Dit netwerk bevat dus zowel een

positieve (CREB) als een negatieve (NFIL3) component die samen de regulatie van een groep genen controleren.

Is NFIL3 een target voor gentherapie?

Deze resultaten illustreren dat het proces van zenuwregeneratie misschien wel versneld kan worden als we negatieve componenten zoals NFIL3 kunnen remmen. Dit is belangrijk als we denken aan een therapie die zenuwregeneratie bevordert. Een veelbelovende techniek die de laatste jaren in het medische biologisch onderzoek steeds verder is ontwikkeld is gentherapie. Hierbij wordt een (gemodificeerd) gen ingebracht als behandeling van een aandoening. Dit wordt bijvoorbeeld ontwikkeld voor de behandeling van aangeboren ziektes waarbij een gen mist of door een mutatie niet of minder werkt. Voor het inbrengen van het genetisch materiaal wordt vaak gebruik gemaakt van gemodificeerde virussen. Virussen zijn van nature in staat cellen binnen te dringen en zo ziekmakende genen in te brengen bij hun gastheer. Voor het doel van gentherapie zijn er nu virus varianten gemaakt die de ziekmakende genen missen en zich ook niet meer kunnen vermenigvuldigen. Door nu het gen naar keuze in te bouwen bij zo'n virus, kan dit virus gebruikt worden om een gen in cellen te brengen. Wij hebben gebruik gemaakt van virusdeeltjes om een gemodificeerde vorm van het NFIL3 gen in zenuwcellen van volwassen ratten te brengen (Hoofdstuk 3). Deze gemodificeerde vorm van het NFIL3 gen die wij ontwikkeld hebben werkt remmend op NFIL3 in zenuwcellen in kweek en bevordert daardoor neuriet uitgroei (Hoofdstuk 2). Met de virusdeeltjes die deze vorm dragen, zijn we nu dus in staat te testen of we door het remmen van NFIL3 zenuwregeneratie in de rat kunnen bevorderen. We hebben deze virussen geïnjecteerd in de sensorische zenuwcellen van de rat en vervolgens de perifere zenuw beschadigd, precies zoals in voorgaande experimenten. Zoals verwacht vinden we inderdaad meer regenererende axonen in de ratten behandeld met de remmende NFIL3 variant dan in de controle groep. Deze experimenten zijn bemoedigend, maar nog preliminair en worden herhaald om in meer detail te bestuderen wat de effecten zijn op de regeneratie van perifere en centrale axonen en het functioneel herstel van de gevoelsprikkels.

Het identificeren van NFIL3 target genen

In Hoofdstuk 2 hebben we laten zien dat NFIL3 en CREB samen een groep genen reguleert dat betrokken is bij zenuwregeneratie. Om dit transcriptionele netwerk uit te breiden wilden we weten welke genen nog meer door NFIL3, CREB of door NFIL3 en CREB samen worden gereguleerd. We hebben hiervoor een techniek gebruikt die "chromatin immunoprecipitation", ofwel ChIP wordt genoemd (Hoofdstuk 4). Met behulp van ChIP kun je de interacties van een transcriptiefactor met zijn target genen vastleggen en vervolgens identificeren. We hebben dit gedaan in gekweekte zenuwcellen voor zowel NFIL3 als CREB. Voor beide factoren hebben we zo de target genen kunnen identificeren en dus het netwerk kunnen uitbreiden.

Het voorspellen van transcriptiefactoren die zenuwregeneratie reguleren

In het gebied vlak voor het begin van een eiwitcoderende gen bevindt zich de "promotor". Deze promotor bevat elementen die herkend worden door transcriptiefactoren. Elke transcriptiefactor herkent een specifieke DNA code en de aanwezigheid van deze code, of bindingsplaats in de promotor van een gen bepaalt dus of een transcriptiefactor kan binden of niet. Uit de promotor code van een gen kan dus worden afgeleid welke bindingsplaatsen er zijn en dus welke transcriptiefactoren effect kunnen hebben op dat gen. Uit de voorgaande beschreven microarray studie weten we precies welke genen geactiveerd of geremd worden tijdens succesvolle en niet-succesvolle zenuwregeneratie. Wij hebben de promotor regio's van al deze genen bestudeerd om te voorspellen welke transcriptiefactoren deze genen reguleren en welke transcriptiefactoren dus een rol kunnen spelen in zenuwregeneratie (Hoofdstuk 5). Voor dit werk is een nieuw wiskundig algorithme ontwikkeld door Geert Geeven van de afdeling Wiskunde aan de Vrije Universiteit wat heeft geleid tot betere en nieuwe voorspellingen die wij in het lab hebben getest. Op deze manier hebben we transcriptiefactoren geïdentificeerd die nog niet eerder in verband zijn gebracht met zenuwregeneratie.

Conclusies

De vindingen in mijn proefschrift geven meer inzicht in de transcriptionele regulatie van genen die betrokken zijn bij zenuwregeneratie. Door diverse invalshoeken en technieken te combineren hebben we nu een aantal transcriptiefactoren geïdentificeerd die betrokken zijn bij axonregeneratie. Daarnaast hebben we de eerste connecties tussen deze transcriptiefactoren en hun target genen kunnen blootleggen. Kortom, we beginnen inzicht te krijgen in het transcriptionele netwerk dat zenuwregeneratie reguleert. Een van de belangrijkste en nieuwe conclusies uit dit werk is dat het proces van succesvolle, perifere axonregeneratie gereguleerd wordt door zowel positieve als negatieve componenten. Niet alleen het stimuleren van positieve componenten, maar ook het wegnemen of remmen van zulke negatieve componenten zou wel eens net zo belangrijk kunnen zijn voor de ontwikkeling van een succesvolle (gen)therapie die de regeneratie van axonen na zenuwschade bevordert.

Dankwoord

Het is af. Alle experimenten, al het schrijfwerk, en nu ook het lay-outen van het uiteindelijke boekje liggen achter me. Vanaf de andere kant van de oceaan kijk ik terug op een geweldige tijd in Amsterdam. Ik wil graag een heleboel mensen bedanken die de afgelopen jaren hebben bijgedragen aan het plezier dat ik heb gehad in mijn werk op het lab en daarbuiten. Samen vormen jullie het netwerk dat mijn succesvol promoveren heeft gestimuleerd.

Guus, mijn "core" promotor, vlak voor de "start site" heb jij mij de mogelijkheid gegeven mijn werk te kunnen initiëren. Jouw enthousiasme, doortastendheid en vrijwel oneindige kennis van de neurobiologie hebben mij altijd erg geïnspireerd. Jij wist me altijd weer te motiveren om "even door te pakken" als er nog een "paar" experimenten gedaan moesten worden om de "boel hoog weg te kunnen zetten"!

Ronald, mijn co-promotor, of misschien is "enhancer" een beter woord, jij wist mij altijd precies de goede begeleiding te geven; nooit teveel controle en nooit te weinig aandacht, gecombineerd met een gelijkgestemd gevoel voor humor, creëerde voor mij de perfecte werksfeer. Ik heb veel bewondering voor jouw vakkennis, redeneringsvermogen en logisch inzicht. Ik heb daar enorm veel van kunnen leren en hoop veel van deze opgedane vaardigheden mee te nemen in de toekomst.

Joost, mijn "distal" promotor, je was letterlijk verder weg, maar daarom niet minder waardevol voor dit werk. Jouw oneindige kennis over neuronale regeneratie en virale vectoren zijn onmisbaar geweest voor dit werk. Ik heb veel van jou precieze en concrete manier van werken geleerd en waardeer je oprechtheid en enthousiasme voor degelijke wetenschap.

Alle collega's van MCN; Floor, 'single-malt' Pim, 'ren-maatje' Maarten, 'stelling-broeders' Michel, Michiel, 'bierkanon' Yvonne, Eisuke, Sabine, Ka Wan, 'surf-dude' Mark, Brigitte, Marion, 'maldi-TOFfe' Roel, 'dokter' Jeroen, Iris, Remco, 'king-of-maxi' William, Priyanka, 'bbq' Tariq, Jorn, Ning, René, Marlene, 'brabo' Pieter, 'madlab' Jochem, Eva, Nutabi, Bart, Andrea, Ruud, Loek, Rolinka, Nelleke, Patricia, bedankt voor alle zinnige discussies, dagelijkse pret en gezelligheid binnen en buiten het lab! Daarnaast hebben Joost, Robbie en Désirée en andere 'buren' veel bijgedragen aan de gezelligheid na het werk in de stelling of basket, bedankt!

Michel, laten we op de komende SfN meeting de 'women in neuroscience social' weer eens bezoeken. Ik ben blij dat je mijn paranimf wilt zijn!

Floor, op jouw reuzenschouders heb ik het regeneratie project dat jij begonnen bent mogen voortzetten, ik hoop dat ik je niet teleurgesteld heb. Dankjewel voor alle support in het begin, maar ook toen je verderop zat. Loek, aan jou geef ik het stokje door, ik heb er alle vertrouwen in dat NFIL3 bij jou in goede handen is!

Beste Jan, het heeft niet zo mogen zijn dat ik aan ribosomen ging werken, maar dan toch nog wel aan axonen. Ik ben je erg dankbaar voor je enthousiasme en begeleiding tijdens mijn stage. Jij hebt bijgedragen aan mijn enthousiasme voor de celbiologie en microscopie; kijk waar ik nu weer terecht ben gekomen!

Brigitte, altijd wist ik wel weer een smoes te verzinnen om even bij je langs te kunnen gaan... Bedankt voor al je praktische hulp, maar ook je gezelligheid en goede gesprekken.

Verschillende stagestudenten hebben een belangrijke bijgedrage geleverd aan dit werk, Eva, Linde, Mark, Linda en Loek, ik heb met veel plezier met jullie samengewerkt.

Het regeneratielab op het NIN, Gerard, Martijn, Koen, Kasper, Asia, Freddy, Ruben, Erich, Tam, Bas, Elske, Martijn, Matt, Nitish, Ruben, ik was niet vaak op het NIN, maar jullie wetenschappelijke bijdragen en gezelligheid waren van onschatbare waarde!

Ruben, ik had altijd een erg leuke tijd met jou in de ok, bedankt voor alle voorbereidingen, (nachtelijke) operaties en zorgen, geweldig!

Mathisca, Geert, samenwerken met jullie heeft onder meer geleid tot hoofdstuk 5 van dit boekje, ik ben jullie erg gaan waarderen als collega's en wiskundigen, en heb het samenwerken met jullie altijd erg leuk, leerzaam en uitdagend gevonden. Geert, ik hoop nog vaak onder het genot van een biertje verhalen te horen over de verzamelingenleer van Cantor en de paradox van Russell.

Een groot deel van mijn werk berust op microarray data, Bauke, Paul, Danielle, bedankt voor al jullie hulp bij mijn werk op de MAL (of MAF natuurlijk), zonder jullie hulp zouden hoofdstukken 4 en 5 er niet zijn geweest.

Niels, topgozer, bedankt voor je eeuwige interesse en vriendschap!

Lieve Anda, Guillaume en Michel, ik voel me altijd erg thuis bij jullie en ik ben erg dankbaar voor jullie interesse, steun en gezelligheid.

Lieve, grote broer en paranimf, Edward, je hebt me altijd onvoorwaardelijk gesteund en

geholpen waar nodig. Marielle, Julian en Elin, wat ben ik blij met jullie!

Lieve papa en mama, jullie hebben mij groot gebracht in alle vrijheid en met onbegrensde liefde en steun, jullie hebben mij gebracht waar ik nu ben. Bedankt voor alle mogelijkheden die jullie me geboden hebben.

Lieve Daantje, jij bent een van de weinige mensen die echt weet wat er in mij omgaat, ik prijs mezelf gelukkig dat ik elke dag weer mag genieten van jouw vrolijkheid, jouw mooie lach en jouw liefde, voor altijd.

Harold, Baltimore, 2010.

Curriculum Vitae

Harold Duncan Mac Gillavry werd geboren 30 augustus 1981 te Gouda. In 1994 begon hij aan het Christelijk Lyceum in Gouda, waar hij in 2000 zijn VWO diploma behaalde. In september dat jaar begon hij zijn studie Medische Biologie aan de Universiteit van Amsterdam. Vanuit zijn interesse naar de kanker biologie heeft hij 6 maanden een onderzoeksstage gedaan bij de afdeling Pathologie in het Amsterdam Medisch Centrum onder begeleiding van dr. Marcel Spaargaren. Dit project over signaaleiwitten in multiple myeloma (ziekte van Kahler) maakte hem nog enthousiaster voor het wetenschappelijk onderzoek. Zijn interesse begon vanaf dat moment echter te verschuiven richting neurobiologie en door het schrijven van een scriptie over de rol van calcium signalering in leren en geheugen processen onder begeleiding van dr. Wim Ghijssen aan de Universiteit van Amsterdam was hij volledig om. Daarom viel de keuze voor een tweede onderzoeksstage op de afdeling Moleculaire en Cellulaire Neurobiologie aan de Vrije Universiteit, Amsterdam. Onder begeleiding van prof. dr. Jan van Minnen werkte hij daar 9 maanden aan een project over de overdracht van ribosomen (eiwitproducerende organellen) van Schwann cellen naar axonen. Aansluitend aan dit project begon hij op dezelfde afdeling met zijn promotieonderzoek onder begeleiding van dr. Ronald van Kesteren, prof. dr. Guus Smit en prof. dr. Joost Verhaagen, waarvan dit boekje het resultaat is. Momenteel werkt Harold in het lab van dr. Thomas Blanpied aan de University of Maryland Baltimore, waar hij met superresolutie imaging technieken localisatie en mobiliteit van eiwitten in de synapse onderzoekt. Hij woont samen met Danielle Counotte in Baltimore in de Verenigde Staten.

List of publications

MacGillavry HD, Stam FJ, Sassen MM, Kegel L, Hendriks WT, Verhaagen J, Smit AB, van Kesteren RE (2009) NFIL3 and cAMP response element-binding protein form a transcriptional feedforward loop that controls neuronal regeneration-associated gene expression. J Neurosci 29: 15542-15550.

Court FA, Hendriks WT, **MacGillavry HD**, Alvarez J, van Minnen J (2008) Schwann cell to axon transfer of ribosomes: toward a novel understanding of the role of glia in the nervous system. J Neurosci 28: 11024-11029.

Stam FJ, **MacGillavry HD**, Armstrong NJ, de Gunst MC, Zhang Y, van Kesteren RE, Smit AB, Verhaagen J (2007) Identification of candidate transcriptional modulators involved in successful regeneration after nerve injury. Eur J Neurosci 25: 3629-3637.

Derksen PW, Tjin E, Meijer HP, Klok MD, **MacGillavry HD**, van Oers MH, Lokhorst HM, Bloem AC, Clevers H, Nusse R, van der Neut R, Spaargaren M, Pals ST (2004) Illegitimate WNT signaling promotes proliferation of multiple myeloma cells. Proc Natl Acad Sci U S A 101: 6122-6127.